Modified biopolymers for removal of organic dyes from aqueous solution

by

Nompumelelo Malatji

DISSERTATION

Submitted in fulfilment of the requirements for the degree of

Master of Science

in

Chemistry

in the

FACULTY OF SCIENCE AND AGRICULTURE

(School of Physical and Mineral Sciences)

at the

UNIVERSITY OF LIMPOPO

Supervisor: Prof M.J. Hato

Co-Supervisors: Prof K.D. Modibane

Prof A. Maity (CSIR)

2020

DECLARATION

I declare that the Modified biopolymers for removal of organic dyes from aqueous solution hereby submitted to the University of Limpopo, for the degree of Master of Science in Chemistry has not previously been submitted by me for a degree at this or any other university; that it is my work in design and in execution, and that all material contained herein has been duly acknowledged.

_____ _____

Malatji, N **Date**

DEDICATION

To my beautiful daughter

Busisiwe Sharon Malatji

ACKNOWLEDGEMENTS

Firstly, I would like to extend my profound gratitude and appreciations to my supervisor Prof M.J. Hato for his constant motivation, guidance, remarkable support and encouragement throughout my master's degree studies. Prof has believed in my capabilities by allowing me to register under his supervision and equipped me with problem-solving skills and being innovative. I really appreciate your precious time and invaluable advice (both academic and social) throughout the studies. I also thank you, Prof, for your patience. I also want to thank Prof A. Maity (CSIR) for constructive discussions regarding the study of modified biopolymers and their application in wastewater treatment. I would like to pass my sincere acknowledgement to Prof K.D Modibane for his support and encouragement throughout my master's degree. I really appreciate your constant motivation and assistance with my academics. My heartfelt gratitude goes to Mr K.E Ramohlola and Dr E. Makhado for their constant guidance, academic support and encouragement. I gratefully thank Dr Makhado for helping me understand the concepts of hydrogels in adsorption applications, assisting me in the laboratory and for analysis of my samples on my behalf at the CSIR using various techniques such as X-ray diffraction, scanning electron microscopy, high-resolution transmission microscopy, and dynamic mechanical analysis.

I would like to thank the University of Limpopo, Department of Chemistry especially the Nanotechnology Research Group at the University of Limpopo (NanoRG@UL) led by Prof Hato for their support. Thanks to Maponya T.C, Teffu D.M, Ramaripa P.S, Somo, T.R, Mashao, G, Makhafola, M.D, Moichela, E, Matsabe, N.T, Morudu, T.C, and Jonker, M.P.

I would like to give special thanks to Sasol bursary and the National Research Foundation (NRF) of South Africa for financial support.

My greatest thanks go to my mother Nomsombuluko Joyce Malatji for her love, support, encouraging me and being by my side every step in my life especially encouraging me to persevere even in difficult times. I thank my Father Isaac Maribe Malatji for his

support and constant love. I would like to also thank the Matsepe Family, Mokono family, my late aunt Pauline Matsepe, my aunts Sabina Mogane, Agnes Mosito, and uncle Dan Malatji for their constant encouragement and support throughout my academic journey. I am grateful to my friend Mangana Berel Rampheri for her constant support and encouragement. I would also like to thank my siblings Sanele, Samukelisiwe, Sandile, Nosipho, Ayanda, Siyanda and Wandile for being my motivation in life to work hard. I give special thanks to my closest friend Andries Manganye for the constant support and encouragement.

I would like to present my heartfelt appreciations to my daughter, Busisiwe Sharon Malatji for her love and motivation for me to be the best mother I can be to her and motivating me to work even harder in life.

ABSTRACT

An extensive search for a highly efficient, reusable, and non-toxic adsorbent materials for the removal of organic dyes from wastewater continues to be of great importance to the world. Activated carbon is the most widely used adsorbent material for treating dye contaminants from water owing to its high removal capacity and large surface area. However, activated carbon is expensive and not easy to regenerate. Hence, the use of biodegradable, non-toxic, and cost-effective biopolymer-based hydrogel adsorbents has attracted great attention. These adsorbents have high swelling capacity and number of adsorptive functional groups to allow adsorption of methylene blue dye. Hence in this work, we present carboxymethyl cellulose crosslinked with poly (acrylic acid) incorporated with magnetic cloisite 30B clay (CMC-cl-pAA/Fe_3O_4-C30B) and sodium alginate crosslinked with poly (acrylic acid) incorporated with zinc oxide (SA-cl-pAA/ZnO) hydrogel nanocomposites (HNCs) for the removal of methylene blue from aqueous solution. The hydrogel nanocomposites were synthesised through in situ free-radical polymerisation.

The structural properties of the prepared materials were studied using Fourier transform infrared (FTIR), X-ray diffraction (XRD), scanning electron microscopy (SEM), transmission electron microscopy (TEM), thermogravimetric analysis (TGA), and dynamic mechanical analysis (DMA). The FTIR and XRD confirmed the successful synthesis of the CMC-cl-pAA and SA-cl-pAA hydrogels, Fe_3O_4-C30B and ZnO nanoparticles (NPs) and their hydrogel nanocomposites. Furthermore, the co-existence of the metal oxide nanoparticles in the CMC-cl-pAA and SA-cl-pAA hydrogel matrices was confirmed by XRD. The SEM revealed that upon the incorporation of the Fe_3O_4-C30B NPs onto CMC-cl-pAA, the resulting material showed spherical particles of the magnetite nanoparticles on the irregular shaped hydrogel structure. As well as on the SA-cl-pAA after modification by ZnO nanoparticles, the spherical ZnO particles were embedded on the hydrogel surface. The successful modification with metal oxide nanoparticles was also confirmed by the presence of characteristic elements of the

incorporated materials on the EDS. The TEM coupled with selected area electron diffraction (SAED) confirmed the presence of Fe_3O_4-C30B on the hydrogel structure, in which circular bright dotted lines were observed corresponding to light diffracted by the lattice planes of different energies on the Fe_3O_4 structure. The thermogravimetric analysis was conducted to study the thermal stability of the materials, the results showed that the incorporation of Fe_3O_4-C30B and ZnO nanoparticles on CMC-cl-pAA and SA-cl-pAA hydrogels, respectively improved their thermal stability. Furthermore, DMA was used to study the mechanical stability of the prepared hydrogels and their composites. In the case of CMC-cl-pAA hydrogel, the storage modulus of CMC-cl-pAA/Fe_3O_4-C30B nanocomposite was higher than of the hydrogel, indicating improved mechanical stability, and on SA-cl-pAA hydrogel the storage modulus decreased, indicating a decrease in mechanical stability on the SA-cl-pAA/ZnO HNC. Consequently, the swelling studies revealed that the SA/AA/ZnO HNC was highly efficient for water uptake in comparison to SA/AA hydrogel. Whereas, CMC-cl-pAA/Fe_3O_4-C30B had lower swelling capacity than CMC-cl-pAA hydrogel.

Various factors influencing the adsorption of adsorbents were systematically investigated. The kinetics, isotherms, and thermodynamics of adsorption were examined, and results showed that equilibrium data fitted the Langmuir isotherm model, and the adsorption kinetics of MB followed pseudo-second-order model in both the CMC-based HNC and SA-based HNC. Maximum adsorption capacities of 1129 and 1529.6 mg/g were achieved for SA/AA hydrogel and SA/AA/ZnO HNC, respectively, in 0.25 g/L MB solution at pH 6.0 within 40 min. Whereas maximum capacities of 1165 mg/g (pH 5) and 806.51 mg/g (pH 7) for CMC-cl-pAA hydrogel and CMC-cl-pAA/Fe_3O_4-C30B HNC, respectively. Thermodynamic parameters for SA/AA and CMC-cl-pAA hydrogels exhibited exothermic adsorption processes and their nanocomposites SA/AA/ZnO and CMC-cl-pAA/Fe_3O_4-C30B exhibited endothermic nature of the adsorption processes, respectively. Moreover, the CMC-cl-pAA/Fe_3O_4-C30B NCH showed improved mechanical and thermal properties as compared to CMC-cl-pAA hydrogel. In contrast, the SA/AA/ZnO HNC presented outstanding reusability with relatively better adsorption efficiencies than SA/AA hydrogel.

RESEARCH OUTPUT

PRESENTATIONS

- **Nompumelelo Malatji**, Mpitloane J. Hato, Kwena D. Modibane, Thabiso C, Maponya, Edwin Makhado. PREPARATION OF CARBOXYMETHYL CELLULOSE-CROSSLINKED-POLY (ACRYLIC ACID) HYDROGEL NANOCOMPOSITE INCORPORATED WITH MAGNETIC C30B FOR ADSORPTION OF METHYLENE BLUE FROM AQUEOUS SOLUTION. Oral Presentation. Faculty of Science and Agriculture Research Day, Protea hotel (The ranch), Polokwane, South Africa on the 20th September 2019.
- **Nompumelelo Malatji**, Mpitloane J. Hato, Kwena D. Modibane, Thabiso C, Maponya, Edwin Makhado. PREPARATION OF CARBOXYMETHYL CELLULOSE-CROSSLINKED-POLY (ACRYLIC ACID) HYDROGEL NANOCOMPOSITE INCORPORATED WITH MAGNETIC C30B FOR ADSORPTION OF METHYLENE BLUE FROM AQUEOUS SOLUTION. Poster Presentation. South African Young Scientists Symposium, University of Venda, Thohoyandou, South Africa on the 31st October 2019.

PUBLICATIONS

- **Nompumelelo Malatji**, Edwin Makhado, Kabelo E. Ramohlola, Thabiso C, Maponya, Gobeng R. Monama, Mpitloane J. Hato, Kwena D. Modibane, REMOVAL OF METHYLENE BLUE FROM WASTEWATER USING HYDROGEL NANOCOMPOSITES. A REVIEW. Submitted as a Review article for possible publication in the International Journal of Water (Appendix 1).
- **Nompumelelo Malatji**, Kabelo E. Ramohlola, Thabiso C. Maponya, Gobeng R. Monama, Mpitloane J. Hato, Kwena D. Modibane, Edwin Makhado. SYNTHESIS OF CARBOXYMETHYL CELLULOSE CROSSLINKED-POLY (ACRYLIC ACID) HYDROGEL BASED MAGNETIC C30B NANOCOMPOSITE AND ITS ADSORPTION EFFICIENCY TOWARDS METHYLENE BLUE. Submitted as

Research article for possible publication in the International Journal of Biological Macromolecules (Appendix 2).

TABLE OF CONTENTS

LIST OF FIGURES

LIST OF SCHEMES

LIST OF TABLES

LIST OF ABBREVIATIONS

AA: Acrylic acid

APS: Ammonium persulfate

CNTs: Carbon nanotubes

CMC: Carboxymethyl cellulose

C30B: Cloisite 30B

EDS, EDX: Energy dispersive X-ray spectroscopy

FTIR: Fourier transform infrared

GO: Graphene oxide

HR-TEM: High-Resolution Transmittance Electron Microscope

HNC: Hydrogel nanocomposite

IR: Infra-red

MMT: Montmorillonite

MWNT: Multi-walled nanotube

MNPs: Magnetic nanoparticles

NPs: Nanoparticles

PAA: Poly (Acrylic acid)

rGO: Reduced graphene oxide

SEM: Scanning electron microscope

SA: Sodium alginate

SDS: Sodium dodecyl sulphate

SWNT: Single-walled nanotube

TEM: Transmission electron microscope

TGA: Thermogravimetric analysis

UV: Ultraviolet

UV-vis: Ultraviolet-visible

WHO: World health organisation

XRD: X-ray diffraction

LIST OF SYMBOLS

A	: Absorbance
a	: Absorptivity constant
b	: Path-length
C	: Molar concentration
C_{ads}	: Adsorbed concentration
C	: Speed of light and concentration of analyte
C_o	: Initial concentration
C_e	: Equilibrium concentration
C_t	: Concentration at specific time
MB	: Methylene blue
d	: Interplanar spacing
E	: Energy
ε	: Molar absorptivity
$\Delta G°$	: Free Gibbs energy change
$\Delta H°$	: Enthalpy change
K_{eq}	: Equilibrium constant
K_F	: Freundlich adsorption constant
K_L	: Langmuir adsorption constant
k_1	: First order rate coefficient
k_2	: Second order rate coefficient
S%	: Swelling capacity
q_e	: Equilibrium adsorption capacity

q_m	: Maximum adsorption capacity
q_t	: Adsorption capacity at a specific time
$\Delta S°$	: Entropy change
T	: Temperature
$\%T$	: Percentage transmittance
Θ	: Diffraction angle
Λ	: wavelength

CHAPTER ONE

INTRODUCTION

1.1 BACKGROUND

The demand for clean water continues to be a global concern as this affects the quality of the life of humans, animals and the environment. South Africa is amongst countries in the world that depend on groundwater and surface water as the main sources of water supply [1]. It has been reported that the decrease in water quality in South Africa is mainly due to increasing pollution and the destruction of water catchments [2]. Pollutants that threaten the water supply include insecticides, domestic wastes, food processing waste, chemical waste, heavy metals, and volatile organic compounds (VOCs) [2]. Among water pollutants mentioned, chemical pollutants such as inorganics and organics are the major contributor of water contaminants [3]. For example, the textile industry is reported to be the major source of organic dye pollutants such as methyl orange, acid blue, brilliant green, methylene blue, and vat blue [4]. The most widely used dye in the industries is methylene blue (MB). MB is known to cause various health problems such as vomiting, shock, tissue necrosis, cancer, dermatitis and mutation in humans [4,5]. Its accumulation in water may block light from penetrating through water, therefore, disturbing the photosynthetic processes in water, which may lead to the death of some aquatic animals [6]. To resolve these problems, various techniques namely; biological treatment, oxidation, flocculation, electrolysis, ultrafiltration, and adsorption have been used to remove MB from wastewater [4,5,7]. Despite their success in dye removal, these methods suffer major drawbacks, for example; membrane filtration suffers from membrane fouling and concentrated sludge production [8]. The problem of the ion-exchange method is that it does not remove all dye types, adsorption by activated carbon applies for a wide range of dyes but is very expensive [9,10]. The photochemical method leads to the production of by-products [8]. During electrochemical destruction, relatively high flow rates reduce the amount of dye removed [8]. Anaerobic bioremediation systems lead to the production of methane and hydrogen sulfide which are harmful [10,11]. Amongst these methods, adsorption technique is most preferred [12]. The process in which molecules attach on the solid

surface through the formation of bonds or via physical force such as van der Waals interactions is called adsorption [13]. Due to its cheap synthesis, operation costs, easy design and fast removal of dye, adsorption is the most used technique [11-14].

1.2 PROBLEM STATEMENT

As explained above, the adsorption technique is the most efficient technique for removing MB from solution and it depends mostly on the type of adsorbent material used [12]. An ideal adsorbent material must have high adsorption capacity, be environmentally friendly, cost-effective, have an easy recovery, be re-usable, and thermally stable [15]. The decolourisation of water by adsorption occurs either through sorption or ion exchange. Factors that affect the efficiency of adsorption include the surface area of the adsorbent, its particle size, dye-adsorbent interaction, temperature, adsorbent dose, dye concentration, pH, and contact time [16]. Examples of adsorbent materials used for dye removal include activated carbon (435 mg/g), fly ash (13.42 mg/g), graphene oxide (714 mg/g), and clay (6.3 mg/g) [17-19]. However, these materials suffer from disadvantages such as high costs (activated carbon, disposal measure after use are expensive and are not environmentally friendly (fly ash),non-degradable (GO), and low removal capacity (clay) [17-19]. Recently, biopolymer-based adsorbents have been widely explored for use in dye treatment. This is due to their availability, environmental friendliness and cost-effective properties [15]. Examples of these biopolymers include; starch, chitosan, sodium alginate, chitin, cellulose, etc [20]. The literature reports Carboxymethyl cellulose (CMC) and sodium alginate (SA) as the most attractive polysaccharides for preparing adsorbents for MB removal owing to their non-toxic nature, easy modification, and low cost [20-22]. Begum *et al.* [23]. removed 606 mg/g MB using CMC as their adsorbent at pH 5. In the removal of MB using SA, the removal capacity was reported to be 213.7 mg/g [24]. The major drawback of these biopolymers is their poor mechanical stability [25]. Therefore, chemical or physical modification by incorporation of synthetic polymers or inorganic components may improve stability and enhance the removal capacity [25].

1.3 RATIONALE

The realisation of CMC and SA as adsorbents for removing methylene blue, there is a need to improve the properties or limitations they suffer. Most researchers have reported the crosslinking with a synthetic polymer such as acrylic acid using N, N' methylene bis-acrylamide (MBA) crosslinker [7, 11]. In this case, hydrophobic networks of 3D structures called hydrogels are formed and the gel does not dissolve in water [11, 16]. Other examples of synthetic polymers are; polyvinylpyrrolidone (PVP), polyvinyl alcohols (PVA), acrylamide (AM), etc. [25, 26]. Hydrogels are crosslinked polymer networks with the ability to trap fluids for a longer period [27]. For this reason, hydrogels have found their use in agriculture to trap water for plants, use in making contact lenses, drug delivery, diapers, and recently as adsorbents [25]. Although the incorporation of the acrylic acid monomer onto the biopolymer backbone may improve adsorption through its adsorptive groups (carboxylic groups) and enhance mechanical stability, it is not easy to recover the material after removing contaminants [26-29]. It has been reported that the incorporation of inorganic materials such as metal oxides (Fe_3O_4 and ZnO) to form hydrogel composites and/or nanocomposites improves the mechanical stability and other physical properties of the hydrogels [30,31]. Taking advantage of the ferromagnetic properties of magnetic nanoparticles (Fe_3O_4), its incorporation into the hydrogel chain will allow easy recovery of the adsorbent using an external magnetic force [30,32]. The problem with magnetic particles is that they tend to form aggregates, hence the incorporation of cloisite 30B (C30B) clay allows homogeneous dispersion of magnetic nanoparticles with the polymer matrix to avoid agglomeration [33,34]. Hence, this study focuses on the preparation of CMC-based hydrogel modified with magnetic C30B clay nanoparticles and SA-based hydrogel coated with zinc oxide (ZnO) nanoparticles to produce hydrogel nanocomposites with enhanced properties.

1.4. AIM AND OBJECTIVES

1.4.1 RESEARCH AIM

This study aimed to synthesise biopolymer-based acrylic hydrogels incorporated with metal oxides for removing methylene blue from aqueous solution.

1.4.2 OBJECTIVES

The objectives of the study were to:

I. synthesise carboxymethyl cellulose crosslinked with poly (acrylic acid) (CMC-cl-pAA) hydrogel, magnetic cloisite 30B (Fe_3O_4-C30B) nanoparticles, and CMC-cl-pAA modified with Fe_3O_4-C30B nanoparticles hydrogel nanocomposite for removing methylene blue from aqueous solution.

II. synthesise sodium alginate crosslinked with poly (acrylic acid) (SA/AA) hydrogel, zin oxide (ZnO) nanoparticles, and SA-pAA modified with zinc oxide (ZnO) (SA/AA/ZnO) nanoparticles for removing methylene blue from aqueous solution.

III. characterise all the synthesised materials using various analytical techniques.

IV. apply adsorption kinetics, isotherms, and thermodynamics to understand the adsorption processes.

1.5 DISSERTATION OUTLINE

This dissertation attempts to investigate the efficiency of adsorption of dyes on various biopolymer-based hydrogel nanocomposites.

I. Chapter 1 is based on the background of water purification, research problem statement, rationale and lastly the aim and objectives of the study.

II. Chapter 2 presents a literature review on water pollution, dyes, biopolymer hydrogels and their nanocomposites for use as dye adsorbents from aqueous solution. This chapter briefly discusses the content which is of paramount importance in this research project.

III. Chapter 3 gives a brief discussion of the analytical techniques used to characterise all the synthesised materials in this research.

IV. Chapter 4 focuses on the synthesis of carboxymethyl cellulose crosslinked with polyacrylic acid (CMC-cl-pAA) hydrogel modified with magnetic C30B nanocomposite and its adsorption efficiency towards MB.

V. Chapter 5 focuses on the synthesis of sodium alginate hydrogel crosslinked with acrylic acid (SA-cl-pAA) and its modification with zinc oxide (ZnO) for the removal of methylene blue from aqueous solution.

VI. Chapter 6 gives the overall conclusions drawn from the study and the recommendations for future research.

1.6 REFERENCES

1. Muller, M. (2017). Understanding Cape Town's Water Crisis. Civil Engineering, 25, 11-16.
2. http://www.randwater.co.za/CorporateResponsibility/WWE/Pages/WaterPollution.asp.
3. Li, X., Liu, Y., Zhang, C., Wen, T., Zhuang, L., Wang, X., & Wang, X. (2018). Porous Fe_2O_3 microcubes derived from metal-organic frameworks for efficient elimination of organic pollutants and heavy metal ions. Chemical Engineering Journal, 336, 241–252.
4. Dawood, S., & Sen, T. K. (2014). Review on dye removal from its aqueous solution into alternative cost-effective and non-conventional adsorbents. Journal of Chemical and Process Engineering, 1(1), 1–11.
5. Zhang, G., Yi, L., Deng, H., & Sun, P. (2014). Dyes adsorption using a synthetic carboxymethyl cellulose-acrylic acid adsorbent. Journal of Environmental Sciences, 26(5), 1203–1211.
6. Arami, M., Limaee, N. Y., Mahmoodi, N. M., & Tabrizi, N. S. (2006). Equilibrium and kinetics studies for the adsorption of direct and acid dyes from aqueous solution by soy meal hull. Journal of Hazardous Materials, 135(1–3), 171–179.
7. Reza, G., & Adeleh, M. (2013). Synthesis of kappa-carrageenan-g-poly(acrylamide)/ sepiolite nanocomposite hydrogels and adsorption of cationic dye. Polymer Bulletin, 70, 2451–2470.
8. Benhalima, T., Ferfera-Harrar, H., & Lerari, D. (2017). Optimization of carboxymethyl cellulose hydrogels beads generated by an anionic surfactant micelle templating for cationic dye uptake: Swelling, sorption, and reusability studies. International Journal of Biological Macromolecules, 105, 1025–1042.
9. Zhou, Y., Zhang, L., & Cheng, Z. (2015). Removal of organic pollutants from aqueous solution using agricultural wastes: A review. Journal of Molecular Liquids, 212, 739–762.

10. Yang, R., Li, D., Li, A., & Yang, H. (2018). Adsorption properties and mechanisms of palygorskite for removal of various ionic dyes from water. Applied Clay Science, 151, 20–28.
11. Robinson, T., McMullan, G., Marchant, R., & Nigam, P. (2001). Remediation of dyes in textile effluent: a critical review on current. Bioresource Technology, 77, 247-255.
12. Zhao, L., & Yang, S. (2017). Preparation and application of carboxylated graphene oxide sponge in dye removal. International Journal of Environmental Research and Public Health Article, 14, 1301.
13. Zhao, X., Li, L., Pan, B., Zhang, W., Zhang, S., & Zhang, Q. (2011). Polymer-supported nanocomposites for environmental application: A review. Journal of Chemical Engineering, 170, 381–394.
14. Yagub, M.T., Sen, T.K., Afroze, S., & HAng, H.M. (2014). Dye and Its Removal from Aqueous Solution by Adsorption: A Review. Advances in Colloid and Interface Science, 209, 172–84.
15. Shi, C., Tao, F., & Cui, Y. (2018). Evaluation of nitriloacetic acid modified cellulose film on adsorption of methylene blue. International Journal of Biological Macromolecules, 114, 400–407.
16. Pereira, L., & Alves, M. (n.d.). Dyes-Environmental Impact and Remediation. Environmental Protection Strategies for Sustainable, 111-162.
17. Gupta, V. K., & Suhas. (2009). Application of low-cost adsorbents for dye removal – A review. Journal of Environmental Management, 90(8), 2313–2342.
18. Guilherme, M.R., Aouada, F.A., Fajardo, A.R., Martins, A.F., Paulino, A.T., Davi, M.F.T., Rubira, A.F., & Muniz, E.C. (2015). Superabsorbent Hydrogels Based on Polysaccharides for Application in Agriculture as Soil Conditioner and Nutrient Carrier: A Review. European Polymer Journal, 72, 365–85.
19. Zheng, Y., Monty, J., & Linhardt, R.J. (2015). Polysaccharide-based nanocomposites and their applications. Carbohydrate Research, 405, 23-32.

20. Petri, D. F. S. (2019). Carboxymethyl cellulose / poly (acrylic acid) interpenetrating polymer network hydrogels as multifunctional adsorbents. Cellulose, 26(1), 597–615.
21. Peng, N., Hu, D., Zeng, J., Li, Y., Liang, L., & Chang, C. (2016). Superabsorbent cellulose−clay nanocomposite hydrogels for highly efficient removal of dye in water. ACS Sustainable Chemistry and Engineering, 4, 7217−7224.
22. Dai, H., Huang, Y., & Huang, H. (2018). Eco-friendly polyvinyl alcohol/carboxymethyl cellulose hydrogels reinforced with graphene oxide and bentonite for enhanced adsorption of methylene blue. Carbohydrate Polymers, 185, 1–11.
23. Begum, H. A., Khalid, M., & Mahbub, B. (2013). Effectiveness of Carboxymethyl Cellulose for the Removal of Methylene Blue from Aqueous Solution, 61(2), 193–198.
24. Karthiga, G., Kumar, D.P.S., & Kumar, K. (2016) Green synthesis of novel silver nanocomposite hydrogel based on sodium alginate as an efficient bio-sorbent for the dye wastewater treatment: prediction of isotherm and kinetic parameters, Desalination and Water Treatment, 57 (57), 27686-27699
25. Fosso-kankeu, E., Mittal, H., Mishra, S. B., & Mishra, A. K. (2015). Journal of Industrial and Engineering Chemistry Gum ghatti and acrylic acid based biodegradable hydrogels for the effective adsorption of cationic dyes. Journal of Industrial and Engineering Chemistry, 22, 171–178.
26. Bao, Y., Ma, J., & Li, N. (2011). Synthesis and swelling behaviours of sodium carboxymethyl cellulose-g-poly (AA-co-AM-co-AMPS)/MMT superabsorbent hydrogel. Carbohydrate Polymers, 84(1), 76–82.
27. Tally, M., & Atassi, Y. (2015). Optimized synthesis and swelling properties of a pH-sensitive semi-IPN superabsorbent polymer based on sodium alginate-g-poly (acrylic acid-co-acrylamide) and polyvinylpyrrolidone and obtained via microwave irradiation. Journal of Polymer Research, 22 (9), 181.
28. Jiang, Y., Liu, B., Xu, J., Pan, K., Hou, H., Hu, J., & Yang, J. (2018). Cross-linked chitosan/β-cyclodextrin composite for selective removal of methyl orange. Carbohydrate Polymers, 182, 106–114.

29. Chawla, P., Ranjan, S.A., Pandey, P., & Chawla, V. (2014). Hydrogels: A journey from diapers to gene delivery. Mini Reviews in Medicinal Chemistry, 14(2), 154-167(14).
30. Reddy, D. H. K., & Lee, S. (2013). Application of magnetic chitosan composites for the removal of toxic metal and dyes from aqueous solutions. Advances in Colloid and Interface Science, 201–202, 68–93.
31. Zhang, M., Chang, L., Zhao, Y., & Yu, Z. (2019). Fabrication of Zinc Oxide / Polypyrrole Nanocomposites for Brilliant Green Removal from Aqueous Phase. Arabian Journal for Science and Engineering, 44(1), 111–121.
32. Liu, C., Omer, A. M., & Ouyang, X. (2018). Adsorptive removal of cationic methylene blue dye using carboxymethyl cellulose/k-carrageenan/activated montmorillonite composite beads: Isotherm and kinetic studies. International Journal of Biological Macromolecules, 106, 823–833.
33. Gong, J. L., Wang, B., Zeng, G. M., Yang, C. P., Niu, C. G., Niu, Q. Y., & Liang, Y. (2009). Removal of cationic dyes from aqueous solution using magnetic multi-wall carbon nanotube nanocomposite as adsorbent. Journal of Hazardous Materials, 164(2–3), 1517–1522.
34. Mahdavinia, G., Afzali, A., Etemadi, H., & Hosseinzadeh, H. (2017). Magnetic / pH-sensitive nanocomposite hydrogel based carboxymethyl cellulose-g-polyacrylamide / montmorillonite for colon targeted drug delivery. Nanomedicine Research Journal, 2(2), 111–122.

CHAPTER TWO

REMOVAL OF METHYLENE BLUE FROM WASTEWATER USING HYDROGEL NANOCOMPOSITES: A REVIEW.

This chapter was submitted for possible publication in the International Journal of Water

CHAPTER SUMMARY

Water pollution by organic dyes continues to pose serious health and environmental threat to the ecosystem. Although adsorption using biopolymer-based hydrogels has proven to be an ideal technique for the treatment of these dye contaminants from aqueous solutions, these hydrogels suffer from lack of mechanical stability and recoverability as compared to synthetic polymers. Herein, we review the low-cost synthesis of hydrogel nanocomposites incorporated with metal oxides to improve the mechanical stability and separation of the hydrogel in removing methylene blue (MB) dye from aqueous solution. The literature reports hydrogels and their nanocomposites as noble adsorbents well-known for addressing water pollution issues. In adsorption technology, hydrogel nanocomposites act as absorbents, prominent to improve performance of removal efficiency. This review emphasises the preparation and use of hydrogels as efficient adsorbents. In-depth discussions on adsorption and diverse synthetic routes of hydrogels have been devoted to applications of these nanocomposites and are compared in this contribution to the removal efficiency of MB dye from wastewater.

2.1. INTRODUCTION

Water is very important for the survival of living things on earth [1]. Despite the need for this resource, water pollution continues to be a problem in most countries including South Africa, where the mainstream water supplies are underground and surface water [2]. Water pollution may be defined as any water that is unsafe for drinking by humans and animals [2]. There are two classes of water contaminants namely; point sources and non-point sources in which they are defined as a source of pollution at a fixed location (mines, industries, power stations, water treatment station, etc.) and pollution from moving sources (cars, buses, and trains), respectively [3, 4]. In point source, water pollutants may be classified as either inorganic (fertilisers and toxic metals), organic (dyes), or microbial (viruses and bacteria) [5]. For example, dyes are organic complexes mostly used by textile industries to give colour to fabrics and contribute largely to pollution [6]. Other applications may include use in medical, pharmaceutical, paper, rubber, plastics, leather, food, and cosmetics industries [7]. Dyes contain aromatic rings in their structure and can be made up of either chromophores or auxochromes [7, 8]. Chromophores are responsible for the production of colour (OH, NH_2, NHR, NR_2, Cl, COOH) and auxochromes (NO_2, NO, and N=N) improve chromophores, make molecules soluble in water and improve their affinity to bind materials [8]. The discharging of dye effluents into either surface and/or groundwater sources leads to contamination which ultimately results in various health and environmental problems [8, 9]. Consumption of contaminated water by humans can lead to vomiting, mutation, cancer, breathing problems, diarrhoea, eyes burn, nausea shock, cyanosis, jaundice and tissue necrosis [7, 8-10]. The environmental issues include the death of aquatic organisms, leading to the development of foul smell [11, 12]. Hence, the need to eliminate dyes from waste effluents before discharging into rivers and other water streams.

Due to the above-mentioned health and ecological problems, various techniques have been employed for eliminating dyes from wastewater [13]. However, because of the chemical stability and non-biodegradable nature of the dyes, most of these methods are not effective [7]. Additionally, each method has its major disadvantage as shown in Table 2.1 below. The adsorption technique is most favoured owing to its cheap

synthesis and operation costs, easy design and fast removal of dye [15-17]. This review summarises the recent advances and developments of adsorbents for wastewater treatment. This is realised by doing a detailed review of the reactions and mechanisms of adsorption including an overview of the adsorption of methylene blue (MB) dye. Then, we introduce hydrogel nanocomposite as an adsorbent for MB removal with great emphasis on the structure and synthetic routes.

Table 2.1: Methods of removing dyes from water.

Adsorbent method	Disadvantage	References
membrane filtration	membrane fouling and production of concentrated sludge	[17]
Ion-exchange	ineffective for all dye types	[6,18]
Photochemical method	production of by-products	[17]
electrochemical destruction	moderately high flow rates that decrease the amount of dye removed	[17]
Anaerobic bioremediation systems	lead to the production of methane and hydrogen sulphide which are harmful	[18,19]
Adsorbent using activated carbon	The adsorbent is expensive	[19]

2.2. ADSORPTION

2.2.1. BACKGROUND

The attachment or adherence of molecules on the surface of solid material is known as adsorption [20]. The adsorbent material contains active adsorptive sites on its surface to which molecules (gas or liquid) from the bulk solution (adsorbate solution) bind to [21,

22]. Adsorption of molecules may occur either physically or chemically [23]. The mass transfer process may occur in the form of migration, diffusion, or convection, in which liquid or gaseous molecules are transferred to a solid phase [24, 25]. Interactions such as Lewis acid-base, van der Waals, and Columbic are characteristic of physisorption [26, 27]. Whereas chemisorption is distinguished through the development of new adsorbate-adsorbent bonds [28]. The adsorptive sites can have the same or different energy, depending on the nature of the material [29]. Owing to its principle, adsorption has gained interest for application in hydrogen storage, sensing, drug delivery, gas capture, and water treatment [30-33].

The recent interest in applying adsorption for the treatment of dyes from wastewater was attracted by its low operation costs, easy design, efficiency and fast removal of dye [34,35]. Before applying an adsorbent material on an industrial scale (column adsorption), it is first optimized in batch mode experiments, then if it possesses a high removal efficiency, it can be employed for column adsorption studies [36,37]. Factors that affect the adsorption process in wastewater treatment include [31,32,36]

- the adsorbent and adsorbate charges,
- the solution pH,
- temperature,
- dye concentration,
- adsorbent dose, and
- the surface area of the solid material.

When an adsorption process reaches equilibrium, it means the active sites of the adsorbent are saturated with adsorbate molecules and no further adsorption can take place [37].

2.2.2 ADSORPTION PARAMETERS

2.2.2.1 Adsorption isotherms

The isotherms of adsorption are significant for describing the adsorbate-adsorbent interactions [38]. Additionally, they provide information about the mechanisms of adsorption, adsorption capacity, and surface properties. This study employs the

Langmuir, Freundlich, and Temkin, isotherm models. Below are their brief descriptions including their linear and non-linear equations.

2.2.2.1.1 Langmuir isotherm model

The Langmuir isotherm was established in 1916 by Irving Langmuir [39]. The model theory assumes that the active sites on the solid surface have the same energy, leading to homogeneous adsorption of adsorbate molecules (monolayer coverage) [40]. Graphically, adsorption equilibrium is observed by a plateau, which is a point where all active sites are fully occupied and no further adsorption can occur [41, 42]. The model is expressed as follows, non-linear (Equation 2.1) and linear (Equation 2.2) forms;

$$q_e = \frac{q_m b C_e}{1 + b C_e} \tag{2.1}$$

$$\frac{c_e}{q_e} = \frac{1}{K_L q_m} + \frac{c_e}{q_m} \tag{2.2}$$

Where *Ce* is the equilibrium concentration (mg/L) and *qe* the amount adsorbed at equilibrium (mg/g). The Langmuir constants q_m (mg/g) represent the monolayer adsorption capacity and *b* relates to the heat of adsorption.

The R_L is a dimensionless constant denoted as the separation factor. R_L is calculated using the following Equation 2.3.

$$R_L = \frac{1}{1 + b C_o} \tag{2.3}$$

If $R_L > 1$, adsorption is not favoured. If $R_L = 1$, adsorption is linear. If $R_L < 1$, adsorption is favoured, and if $R_L = 0$, the reaction is irreversible [42].

2.2.2.1.2 Freundlich isotherm

The model assumes multilayer coverage of the adsorbent. The model is expressed by the following equations in a non-linear (Equation 2.4) and linear (Equation 2.5) form;

$$q_e = K_F C_e^{1/nF} \quad (2.4)$$

$$\ln q_e = \ln K_F + \frac{1}{n} \ln c_e \quad (2.5)$$

Where q_e (mg/g) and C_e (mg/L) are the amounts adsorbed and the solution concentration, respectively at equilibrium. K_F is the sorption enthalpy and varies with temperature. K_F and n are the sorption capacity and sorption intensity [43]. The n determines the non-linear relation between adsorption and the concentration of the solution [43].

2.2.2.1.3 Temkin isotherm

The Temkin isotherm theory ignores the concentration values and assumes that the decrease in heat of adsorption concerning the temperature is linear instead of decreasing logarithmically as suggested in the Freundlich equation. The non-linear (Equation 2.6) and linear (Equation 2.7) forms of Temkin model are expressed as follows below;

$$q_e = \frac{RT}{b_T} \ln(K_T C_e) \quad (2.6)$$

$$q_e = \frac{RT}{b_T} \ln_{aT} + \frac{RT}{b_T} \ln C_e \quad (2.7)$$

where aT is the equilibrium binding constant corresponding to the maximum binding energy (L/g), b_T is the Temkin constant related to the heat of adsorption (kJ/mol), R is the universal gas constant (8.314 J/mol/K) and T is the absolute temperature (K) [44].

2.2.2.2 Kinetic isotherms

Adsorption is a process that involves the transfer of mass of a solute from the liquid phase to the surface of the adsorbent [45]. The mechanism of adsorption can be researched using either the Lagergren's pseudo-first-order equation or pseudo-second-order equation. The amount of contaminant adsorbed with time can be analysed provided an appropriate model is used [46]. To identify which model is appropriate, the

correlation coefficient (R^2) is measured and must be close or equal to 1. The model with a higher R^2 is the most suitable model for adsorption kinetics of a contaminant.

The non-linear (Equation 2.8) and linear (Equation 2.9) equations for the pseudo-first-order kinetic model are;

$$q_e = q_e[1 - \exp(K_1 t) \quad (2.8)$$

$$\ln(q_e - q_t) = \ln(q_e) - K_1 t \quad (2.9)$$

Where q_e and q_t refer to the amount of dye adsorbed (mg/g) at equilibrium and at any time, t (min). K_1 is the equilibrium rate constant of pseudo-first-order sorption (1/min). K_1 will be determined using the slope and intercept of the plot of ln ($q_e - q_t$) versus t [47].

The non-linear and linear equations for the pseudo-second-order kinetic model are;

$$q_e = \frac{K_2 q_e^2 t}{1 + K_2 q_e t} \quad (10)$$

$$\frac{t}{q_e} = \frac{1}{K_2 q_e^2} + \frac{t}{q_e} \quad (11)$$

Where K_2 is the equilibrium rate constant of pseudo-second-order adsorption (g/mmol min). K_2 will be determined using the slope and intercept of the plot of t/qt versus t.

2.2.2.3 Thermodynamics

During the adsorption process, thermodynamic parameters such as enthalpy ($\Delta H°$), entropy ($\Delta S°$) and Gibbs free energy ($\Delta G°$) are required to determine spontaneity and heat change [48]. Thermodynamics parameters may be calculated according to the formulas below;

$$K_D = \frac{q_e}{C_e} \quad (12)$$

$$\Delta G^{\circ} = -RT\ln K_D \quad (13)$$

$$\ln K_D = \frac{\Delta S}{R} - \frac{\Delta H}{RT} \quad (14)$$

Where K_D represents the distribution coefficient of the adsorbate, $q_e$and C_e represent the equilibrium concentration (mg/g) and in the solution (mg/L). *R* represents the universal gas constant (8.314J/mol K) and *T* is the temperature (K). ***ΔH°*** and ***ΔS°*** may be calculated from the slope and intercept of the plot $\ln K_D$ vs 1/*T*. Negative ΔG values at different temperatures are an indication of a spontaneous adsorption process [47, 49]. If ΔG decreases when the temperature is increased, it means there is a more efficient interface during adsorption. A positive ΔH value indicates an endothermic adsorption process [50].

2.2.3 ADSORBENT MATERIALS FOR METHYLENE BLUE

Although the adsorption technique is effective for dye removal. Its efficiency is limited by the type of adsorbent used [51]. Various materials have been used for methylene blue dye removal. For example, activated carbon is reported to be the most frequently used nano-adsorbent for removing a variety of inorganic and organic contaminants owing to its high surface area, porous structure, thermal stability and amphoteric nature [52, 53]. However, activated carbon has some drawbacks such as intraparticle resistance in industrial application, high production costs and regeneration costs [53-55]. Recent researches have attempted to find ways to improve the regeneration of activated carbon and produce it at a lower cost [53]. On the other hand, alternative adsorbents such as fly ash, graphene, clay, carbon nanotubes, and polysaccharides were reported for removal of MB [56-63]. Among these adsorbents. Mittal *et al*. [56] reported using polysaccharides as promising adsorbents for methylene blue dye removal from aqueous solutions owing to their enhanced adsorption capacity amongst other attractive properties.

2.2.3.1 Polysaccharides

Polysaccharides can be defined as highly hydrophilic and non-toxic natural polymers made up of multiple small units of saccharides that are connected through glycosidic

bonds [59-61]. These biopolymers are found and used in plants or animals for structural support and energy storage [62]. Examples of polysaccharides include; carboxymethyl cellulose, alginate, carrageenan, chitosan, guar gum, starch and locust bean gum [61-63]. These natural polymers offer the advantages of high absorption capacity, biodegradability, and cheap synthesis [64]. However, due to low solubility and other physical drawbacks, synthetic polymers are incorporated into the biopolymeric backbone to improve their properties [65]. Polysaccharides-based materials have recently attracted use for adsorption of dyes and toxic metals because of their non-toxic nature, biodegradability, easy availability and low-cost synthesis [66]. Amongst other polysaccharides, carboxymethyl cellulose and alginate offer more attractive properties for application as dye adsorbents.

2.2.3.1.1 Carboxymethyl cellulose (CMC)

Cellulose is the main component of most plants [67]. Carboxymethyl cellulose (CMC) is a highly reactive, hydrophilic, water-dissolving derivative of cellulose with many carboxyl groups on its surface [68]. Commercially it can be obtained as sodium carboxymethyl cellulose with different degrees of saturation (DS), which may range from 0.6-.95 depending on how it was prepared, and the solvent used [69, 70]. CMC is mostly used in paper, packaging, textile, food, cosmetics, and pharmaceuticals [61,68]. Due to its sensitivity to pH, non-toxic nature, hydrophilicity, low cost and ability to form gels, CMC has been applied on its own or in a composite form as an adsorbent for removing inorganic and organic contaminants [71, 72].

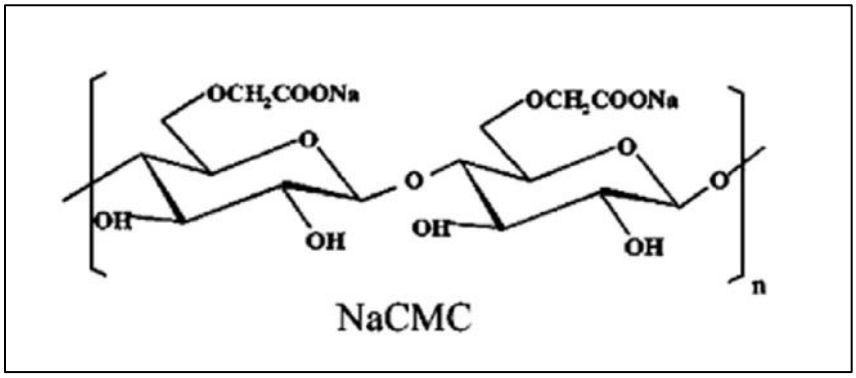

Figure 2. 1: Structure of sodium carboxymethyl cellulose [74].

CMC (Figure 2.1) is a cellulose derivative with carboxymethyl groups at carbon 2, 3 and 6 [74]. In a study conducted by Kono [75], the resonances of CMC were determined using ^{13}C NMR as shown in Figure 2.2 spectra of CMC. In the spectrum of CMC, the carbonyl carbon (C1, C4), overlap of C2, C3, C5, the carboxymethyl groups, and C6 were assigned to broad ^{13}C resonances at 178, 104, 83, 75, and 63 ppm [75]. The existence of carboxylic groups (COO^-) on the polymer chains of CMC allows for interactions with multivalent metal cations (Al^{3+} and Fe^{3+}) which results in the formation of stabilised ionotropic hydrogels. Interactions with metal ions through the hydroxyl groups of the CMC may improve the water insolubility and stability of the polymer aggregates [74, 75].

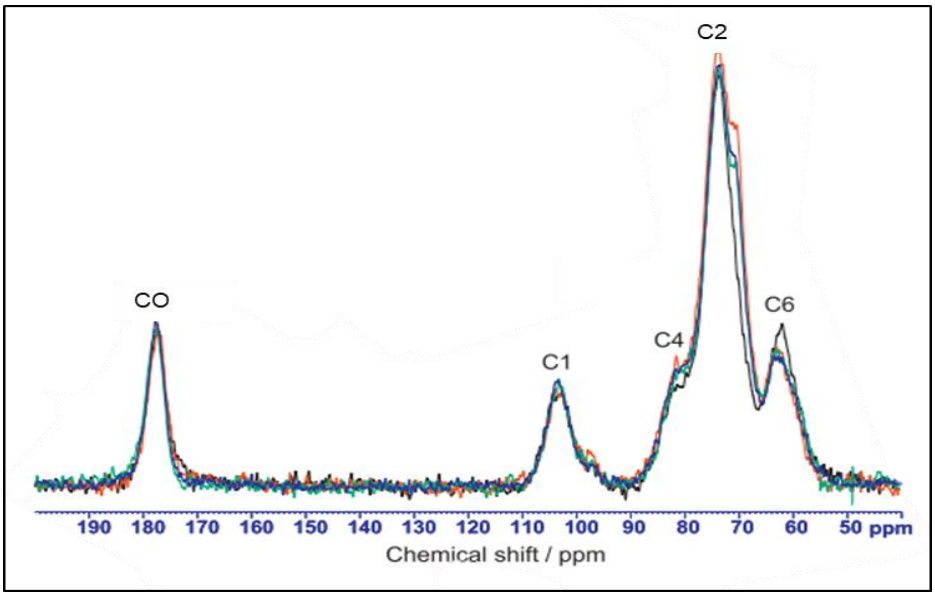

Figure 2. 2: 13C NMR of CMC [75].

The reaction of cellulose with mono chloroacetic acid (MCA) or its sodium salt in the presence of an organic solvent under basic conditions produces NaCMC [76]. There are various materials of which CMC can be derived from, for example, Petri [77] prepared CMC from pineapple peels and in another study, Begum *et al*. [78], prepared CMC from sugarcane bagasse. The synthesis of CMC occurs in three steps; (1) alkalisation, (2) carboxymethylation, and (3) neutralisation as outlined in the steps below.

Step 1: Cell-OH + NaOH → Cell-OH.NaOH

Step 2: $Cell\text{-}OH.NaOH + ClCH_2COONa \rightarrow Cell\text{-}O\text{-}CH_2COO^- Na^+ + NaCl + H_2O$

Step 3: $NaOH^+ Cl^-CH_2COONa \rightarrow HO\text{-}CH_2COONa + NaCl$

During the synthesis process, carboxymethyl groups replace hydroxyl groups at positions 2, 3, and 6 of cellulose. In the synthesis of CMC, it is important to consider the degree of substitution which will govern the porosity and adsorption capacity of CMC [78]. Degree of Substitution (DS) refers to the number of hydroxyl groups replaced by carboxymethyl groups. Each β-glucopyranose unit of cellulose has three hydroxyl groups therefore, hypothetically DS value will range between 0 and 3.0 [79]. Various factors may affect the DS of CMC such as the solvent, temperature, and the NaOH concentration [80]. For example, most researches report that the use of isopropanol as the solvent yields CMC with very high DS [80]. Huang *et al.* [81] synthesised CMC from the pulp of six different plants, the conditions that yielded the best CMC were 20% NaOH concentration, the temperature of 60 ^oC, and 3-5 g of MCA. The group reported that CMC yield increased with increasing MCA content. The degree of saturation influences the application of CMC [81]. The hydrophilicity of CMC increases with an increase in DS. When DS > 0.4 (higher), CMC becomes soluble in water, has better viscosity, enhanced cationic exchangeability and improved covalent cross-linking through radiation. Whereas when DS < 0.4 (lower), CMC is insoluble, and it swells in solution [81]. For example, a study reported the degradation of a polymer with irradiation of 10% CMC (0.7 DS), whereas irradiation of CMC of 1.32 DS resulted in outstanding crosslinking and high gel-fraction [82]. For adsorption, the properties of CMC can be modified by crosslinking to form a gel, which will improve the solubility and hydrophilicity of CMC.

2.2.3.1.2 Alginate

Alginate is a sentimental term used in the dietetic, cosmetic, pharmaceutical, and biotechnological industries [83]. The alginate can be found in salts of magnesium (Mg), potassium (K), calcium (Ca), and sodium (Na) [83]. Alginates were discovered in 1929 by E.C.C Stanford who was a pharmacist [84]. SA is found in brown algae, marine algae and produced by some bacteria, hence abundant in nature [85, 86]. Applications of sodium alginate include drug delivery, thicker, gel-forming agent, binder during the

production of tablets, use as a stabiliser, and matrixing agent [84-87]. The recent use of polysaccharides as adsorbents for dyes and other pollutants is mostly due to the attractive properties that polysaccharides possess, such as high hydrophilic structures, their non-toxic nature, biodegradability and cheap synthesis [88-90].

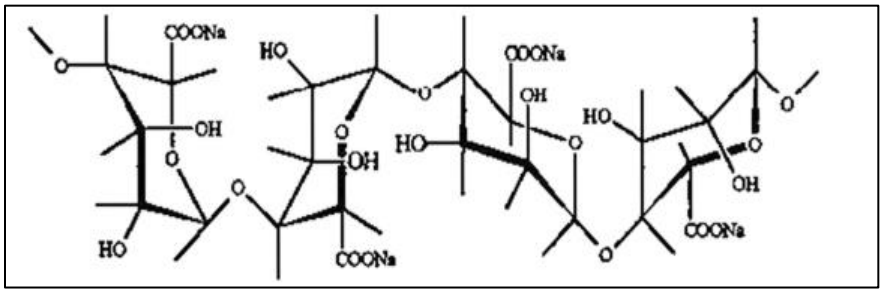

Figure 2.3: Structure of sodium alginate [62]

Sodium alginate (SA, Figure 2.3) is made up of poly-β-1, 4-D- mannuronic acid and α-1, 4-L-guluronic acid [91]. The structure consists of carboxylic groups and hydroxyl groups which can react with metal ions or crosslinking agents to form hydrogels [92]. Alginate can be extracted from its salt forms by ion-exchange methods [93]. As a result of the presence of divalent ions, monovalent, water-soluble salts of alginates can transform into water-insoluble salts. The COO^- and -OH functional groups on the alginate backbone will allow adsorption of cationic dye pollutants [94]. However, sodium alginate just like other polysaccharides suffers from lack of stability [90]. To enhance the stability of SA and its adsorption capacity, the biopolymer may be crosslinked with synthetic polymers into forming a hydrogel [95, 96]. This will allow their use as adsorbents without them dissolving in the adsorbate solution. The major disadvantage of polysaccharides as adsorbents is that they dissolve in water and have low mechanical stability [95,96]. To resolve this problem, polysaccharides are crosslinked to form hydrogels, which do not dissolve in water.

2.3 HYDROGELS

2.3.1. BACKGROUND

Hydrogels are hydrophilic polymer chains that are crosslinked to form gel structures that swell in aqueous solution and trap fluids for long period without dissolving [59, 60]. Hydrogels may contain carboxylic, amine, imide, hydroxyl and sulfonyl groups in their 3D structure which are responsible for the hydrophilicity and swelling capacity [97]. Depending on the nature of the hydrogel, it can be classified based on various properties. Classification of hydrogels (Table 2.2) can be based on whether they are synthetic (involves the use of synthetic monomers), natural (involves using biopolymers) or combination of synthetic and natural monomer resulting in a hybrid hydrogel [98]. The polymeric composite classification can be based on the method used to synthesise the hydrogel [98];

(a) Homopolymeric hydrogels: they are hydrogels consisting of the same type of monomer.

(b) Copolymeric hydrogels: these hydrogels comprise of two or more different kinds of monomers such that the network would have at least one hydrophilic component on the polymer network chain.

(c) Multipolymer Interpenetrating polymeric hydrogel (IPN): the hydrogel network consists of two components (natural and/or a synthetic polymer) that are independently crosslinked.

It was also demonstrated that hydrogels can be categorised based on whether they are [99];

a. Crystalline,

b. Amorphous or,

c. Semicrystalline: showing properties of both crystalline and amorphous phases.

The other classification is based on whether the crosslinking of hydrogels occurs via chemical or physical means. Briefly;

a. Physical crosslinking in hydrogels may be through, (1) formation of a hydrogen bond, (2) hydrophobic interactions between chains, in which the dissipation energy of the bond prevents breakage and improves the hydrogel strength, (3) crystallisation where gels are subjected to freeze and thaw process in PVA/PVP solution 10 hours at 15℃, then placed at room temperature for 2 hours. Lastly, (4) between oppositely charged groups [60].

b. Chemical crosslinking can be achieved by (1) using aldehydes such as acetaldehyde, glutaraldehyde and formaldehyde, (2) radiation using an electron beam, gamma rays or ultraviolet rays at room temperature in which a free radical is formed, monomers are added to the chain for growth and the gel forms at the critical gelling point. Lastly, (3) free radical polymerisation using a crosslinker, for example, MBA. In this method an initiator such as potassium persulfate generates free radicals, the radicals react with other monomers and then MBA is added to the polymer chain to form the hydrogel [60,100].

In addition, the hydrogels may be classified based on the charge on their crosslinked polymer network [101,102]. The charge may be;

a. Ionic (cationic/ anionic)

b. Non-ionic (neutral).

c. Amphoteric (comprising of both basic and acidic groups).

d. Zwitterionic (contains anionic and cationic components on each repeating structural unit). The net charge of the gel is zero.

Lastly, hydrogels can also be categorised according to what stimulates their response. These hydrogels are sometimes called smart hydrogels [98,100]. There are two categories of stimulus namely; physical stimuli and chemical stimuli as stipulated in the table below. The swelling or de-swelling of hydrogels caused by changes in the

environment can be too much to a point that the hydrogel changes phase (volume collapse).

Table 2.2: Physical and chemical stimuli classifications.

Physical stimuli	Chemical stimuli
Light	Composition of solvent
Magnetic field	pH
Temperature	Molecular species
Sound	Ionic strength
Electric field	
Pressure	

2.3.2. APPLICATION OF HYDROGELS

Hydrogels have gained much attention for use in various applications owing to their outstanding qualities, these include use in the making of disposable diapers, absorbent pads, use in hydrogen storage, sensing, CO_2 capture, biomedical field (drug & cell delivery systems), immobilisation of enzymes, wastewater treatment, and agriculture for trapping water [11,24,25]. The ideal properties of a hydrogel depend on its specific application. For application in water treatment, the hydrogel must have the following properties below [98];

- High absorption capacity
- Low residue monomer and soluble content

- Cost-effective
- Recoverable
- High biodegradability and not produce harmful by-products.
- Must retain neutral pH after swelling in water.
- Easy recoverability

The swelling capacity of hydrogels is indicative of its absorptive capacity. Which may be affected by factors such as; the intermolecular spaces in the 3D network, the existence of hydrophilic groups on the hydrogel polymer backbone, and the pore size of the hydrogel surface [10]. Hence parameters such as the amount of initiator, crosslinker, polymer, monomer, and solvent volume are optimised during the preparation of the hydrogel to obtain optimum conditions for preparing an ideal hydrogel [101].

2.3.3 PREPARATION METHODS

As stated previously that biopolymers suffer poor mechanical, thermal stability and they dissolve in water [65]. Most researches have reported that crosslinking, grafting and modification with inorganic constituents such as metal oxides and clay improves solubility and stability problems associated with biopolymers [3,100]. The type of method used to prepare the hydrogel, therefore, affects its structural make-up or physical properties. Amongst several physical and chemical techniques used for hydrogel synthesis, the most widely used methods are discussed below.

2.3.3.1 Grafting

Grafting is the modification of the polymer backbone using synthetic polymers such as acrylamide, acrylic acid, methacrylamide, and vinyl alcohol as support materials [102]. During grafting, a free radical site is created by an initiator, then a monomer unit is added on the generated free radical site [103]. Grafting can occur either via a chemical or radiation. Chemical grafting involves using chemical reagents such as ammonium persulfate (APS), potassium persulfate (KPS) or other chemical initiators [104].

Radiation grafting involves initiating free radicals using UV visible or microwave radiation [105].

It was shown in the literature that using a microwave radiation method for synthesising hydrogels produces sterilised hydrogels [105]. Naturally, polysaccharides suffer from poor chemical and physical stability [65]. Grafting has been reported to solve these issues including enhancing the performance of hydrogels through the introduction of new functionalities from grafted monomers [106]. For example, in a study conducted by Tally and Atassi [62], it could be observed from the TGA curves of (a) SA and (b) SA-g-P(AA-co-AM)/ PVP semi-IPN SAP (Figure 4) that grafting with synthetic polymers enhanced the thermal stability of hydrogels by more than 20% weight loss at above 200 ^{o}C.

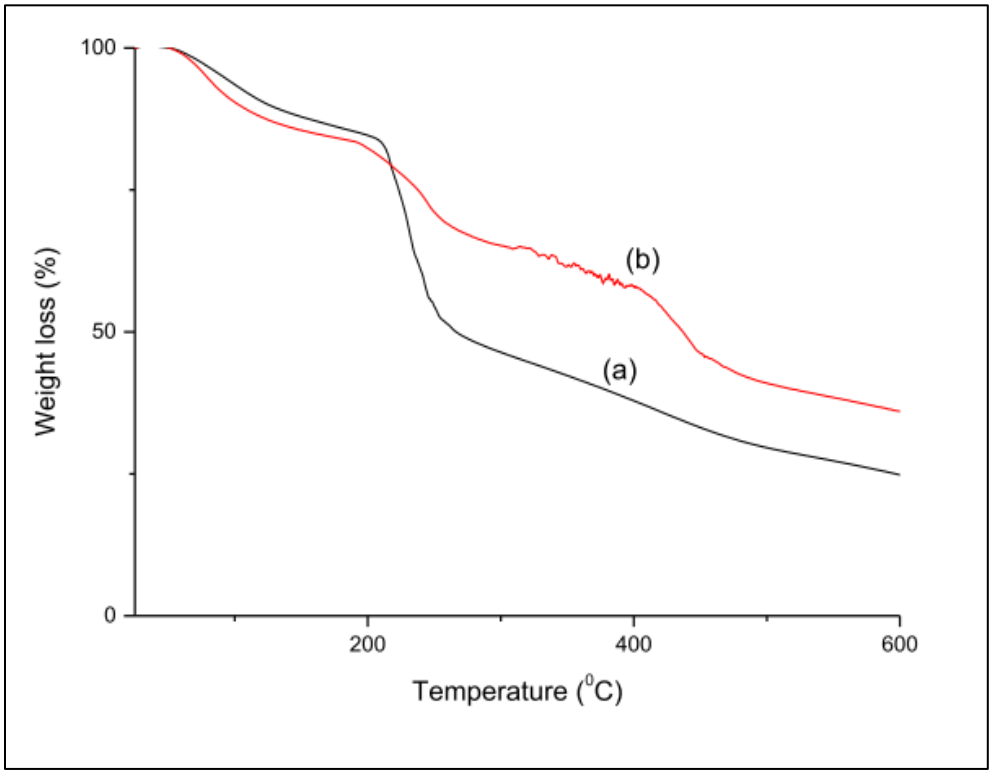

Figure 2.4: Thermogravimetric analysis of (a) SA and (b) SA-g-P(AA-co-AM)/PVP semi-IPN SAP [62].

A study of the modification of CMC by grafting with poly (3-sulfopropyl methacrylate), P(SPMA), in the presence of KPS initiator for methylene blue (MB) removal was carried out [68]. The main vibrational peaks at C=O (1718 cm^{-1}), S=O (1085 cm^{-1}), and S-O (626 cm^{-1}) were observed in Figure 2.5(A) of the Fourier transform infrared (FTIR) of the CMC-g-P(SPMA) hydrogel [68]. The scanning electron microscopy (SEM) image showed the well-defined pores and 3D interconnections of CMC-g-P(SPMA) hydrogel, for which the hydrogel could allow easy penetration of dye molecules in solution through its pores as observed in Figure 2.5(B) [68]. The adsorption of MB by the hydrogel was characterised by an absorption peak at 664 nm corresponding to the characteristic absorption band of MB (Figure 2.5(C)). From the XRD (Figure 5(D)), the partially crystalline structure of CMC was characterised by sharp peaks at 2θ = 9.4 and 20.1° resulting from the inter- and intramolecular hydrogen bonding between carboxylic groups and hydroxyl groups of the biopolymer. Upon grafting on the CMC-g-P(SPMA) it could be observed that the peaks were broader, indicating the hydrogen bonds were destructed, allowing grafting to take place [68].

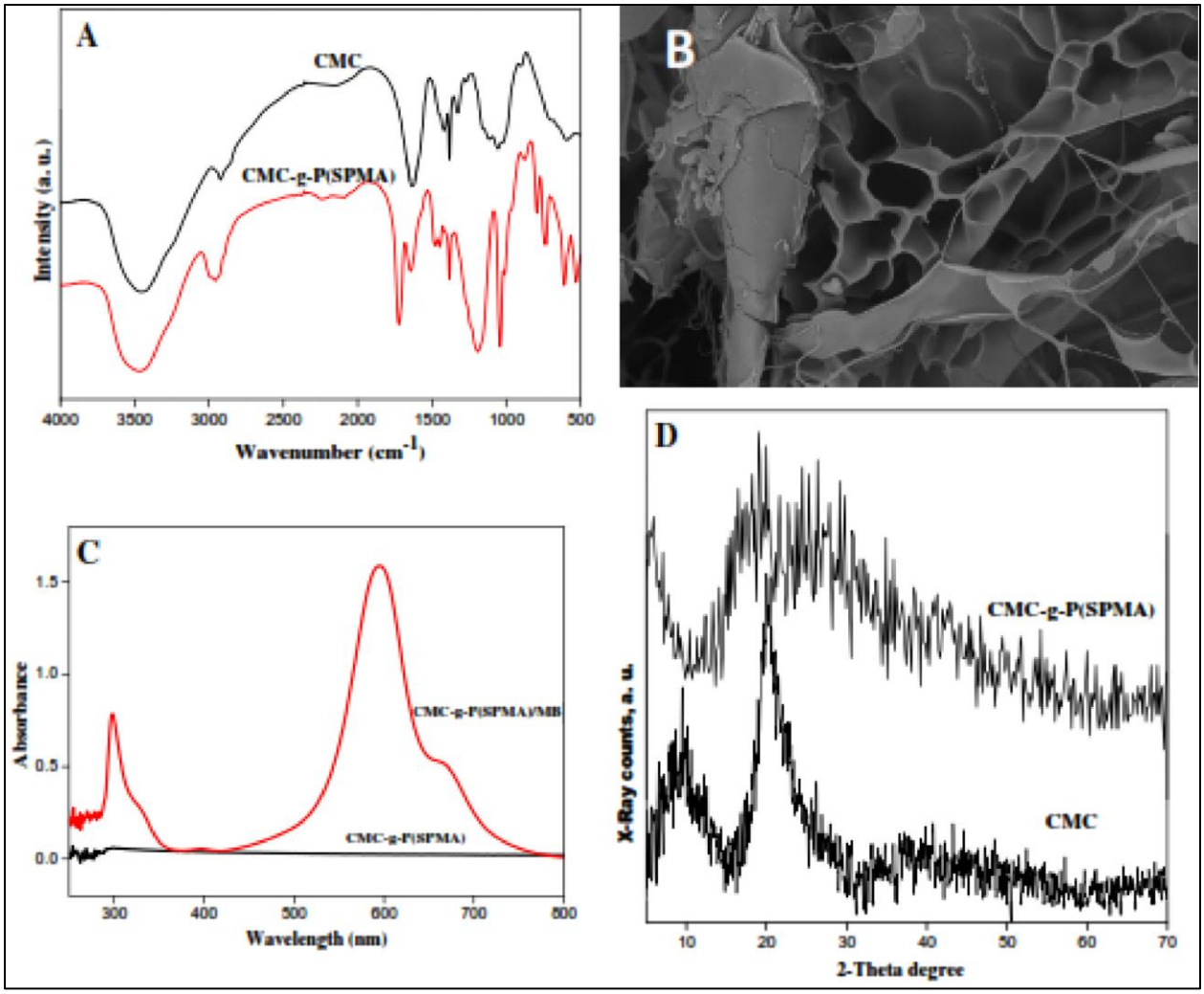

Figure 2.5: FTIR spectra (a), SEM images (b), UV-vis (c), and XRD spectra (d) of CMC-g-P(SPMA) [68].

2.3.3.2 Crosslinking

The process of crosslinking can occur through physical or chemical interactions. Physical interactions are irreversible and include electrostatic interactions, hydrogen bonding, and the van der Waals forces [107]. Chemical crosslinking involves forming irreversible covalent bonds in the hydrogel polymer chain usually through the reaction of complementary groups [108]. Chemically crosslinked hydrogels are mostly used in medical applications. For example, Liu *et al*.[109] synthesised chitosan based-hydrogels from PEG for application in drug delivery. In another study by Kumar *et al.,* crosslinked

hydrogels were produced from glutaraldehyde (GA) as a covalent crosslinker (Scheme 2.1) [110].

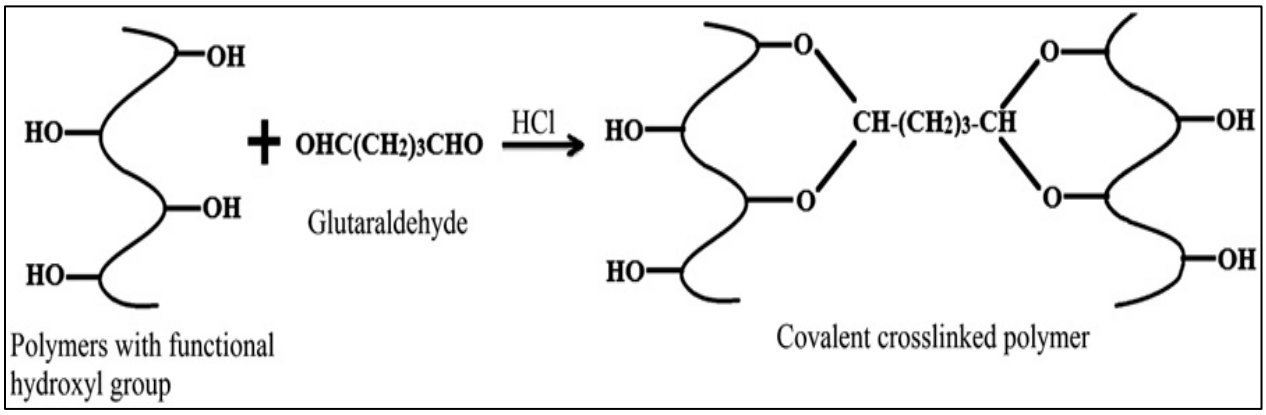

Scheme 2.1: Crosslinking using glutaraldehyde (GA) to produce hydrogel [110].

The most commonly used chemical crosslinkers include ethyleneglycol dimethyl-acrylate, N, N-methylene-bis-acrylamide (MBA), tetra-ethyleneglycol dimethyl-acrylate (EGDMA) or tri-propyleneglycol diacrylate (TPGDA) [111]. However, these crosslinkers are usually toxic and result in non-biodegradable hydrogels [112]. Additionally, as a result of the lack of internal structural homogeneity and an effective mechanism for energy dissipation, chemically crosslinked hydrogels are very brittle [113]. This prompted many researchers to consider introducing nanocomposites, ionic interactions, hydrogen bonding, and hybrid hydrogel systems to improve the hydrogel properties [114-116]. A hybrid system consists of physical interactions that will aid in energy dissipation and chemical interaction, which will mainly improve structural properties [117]. Figure 2.6 illustrates the preparation of hydrogel beads through ionic interactions by Rahmani *et al.* [118] briefly a mixture containing gum tragacanth (GT), graphene oxide (GO) and calcium carbonate ($CaCO_3$) was added dropwise into a concentrated solution of Ca^{2+} which interacted with -OH and COO^- groups on the GT and GO to form hydrogel beads. Ionic crosslinking offers the advantage of less toxicity [112].

Figure 2.6: Showing the preparation of GT-based hydrogel beads [118].

In a study by Eftekhari-sis *et al*. [119], hybrid hydrogels constructed from poly (N-isopropyl acrylamide-co-itaconic acid) and non-toxic octa-vinyl polyhedral oligomeric silsesquioxane (OV-POSS) crosslinker were prepared. Their obtained SEM (Figure 2.7), XRD and TGA (Figure 2.8) results are discussed. The rough non-homogeneous surface was observed on the SEM image (a) of poly (NIPAM-co-IA). Upon hybridisation with 8% POSS (b), 12% POSS (c) and 12% POSS (d), the morphology changed to a honey-comb like structure with homogeneous pores of varying pore sizes as POSS content was increased. The study reported that at 12% POSS the honey-comb pattern was disrupted, indicating that the degree of uniformity in the hydrogel hybrid can be controlled by changing the crosslinking content [119].

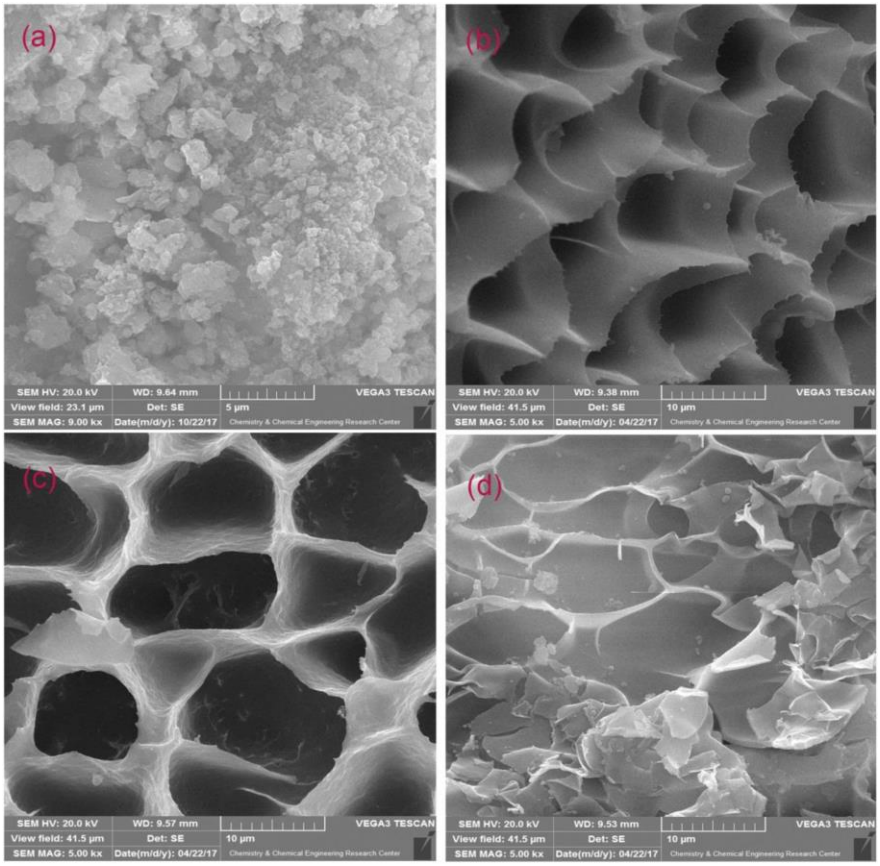

Figure 2.7: SEM images of poly (NIPAM-co-IA) hydrogel (a) and hybrid poly (NIPAM-co-IA)/OV-POSS (8%, 10% and 12% POSS) (b-d) [119].

For example, the XRD patterns in Figure 2.8(a) showed a successful hybridisation and a uniform dispersion of the crosslinker as confirmed by the disappearance of characteristic crystalline diffraction peaks of OV-POSS at 2θ=9.8, 23.1 and 23.9° [119]. The TGA thermogram (Figure 2.8(b)) of showed that the crosslinking with POSS in the hybrid hydrogels, increased the thermal stability, wherein the weight loss at temperatures 340 to 500 °C, was less than weight loss obtained for poly (NIPAM-co-IA) at the same temperature [119]. From the obtained literature it could be observed that chemical and physical properties of the hydrogels were improved, including creating porous structures that enable penetration of adsorbate molecules.

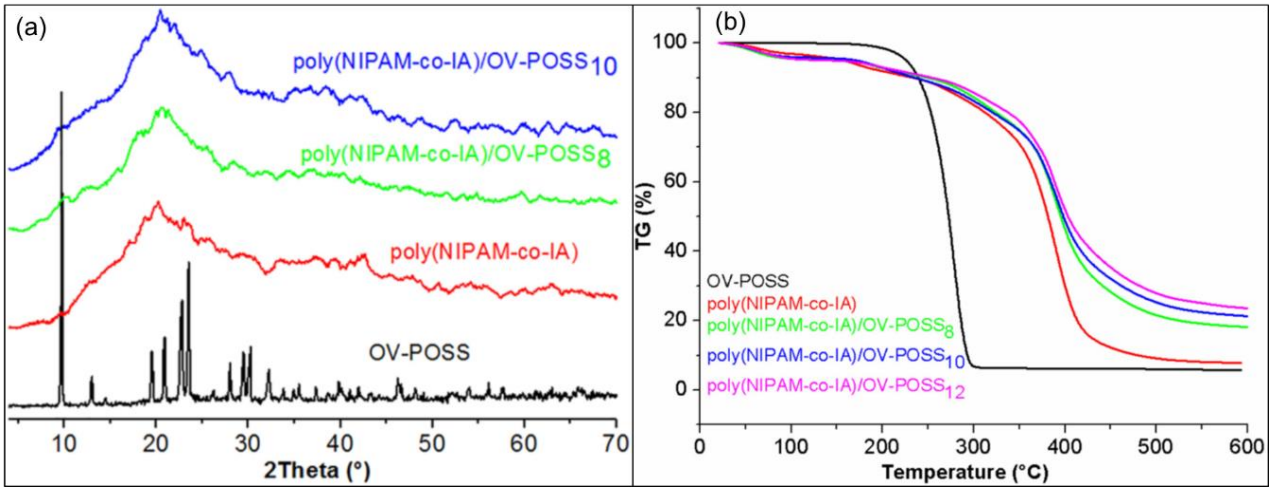

Figure 2.7: XRD and TGA analysis [119].

2.3.3.3 Free radical-polymerisation

Free radical polymerisation is a technique in which polymerisation is achieved by generating free radicals to which chain growth occurs in succession [120]. This method involves a combination of grafting and crosslinking. The decomposition of the initiator may occur using temperature, light or photon which then forms a free radical [121]. Decomposition by photon offers advantages such as low costs, it allows better spatial and time-based control of the reaction process and does not use chemical solvent [122]. Scheme 2.2 below shows a schematic representation of an overview of free radical polymerisation for synthesising hydrogels. Firstly, the generation of free radicals by an initiator (initiation). Secondly, the free radicals react with the monomer to generate vacant active sites (propagation) and lastly, the formation of a polymer network through crosslinking (termination) [123].

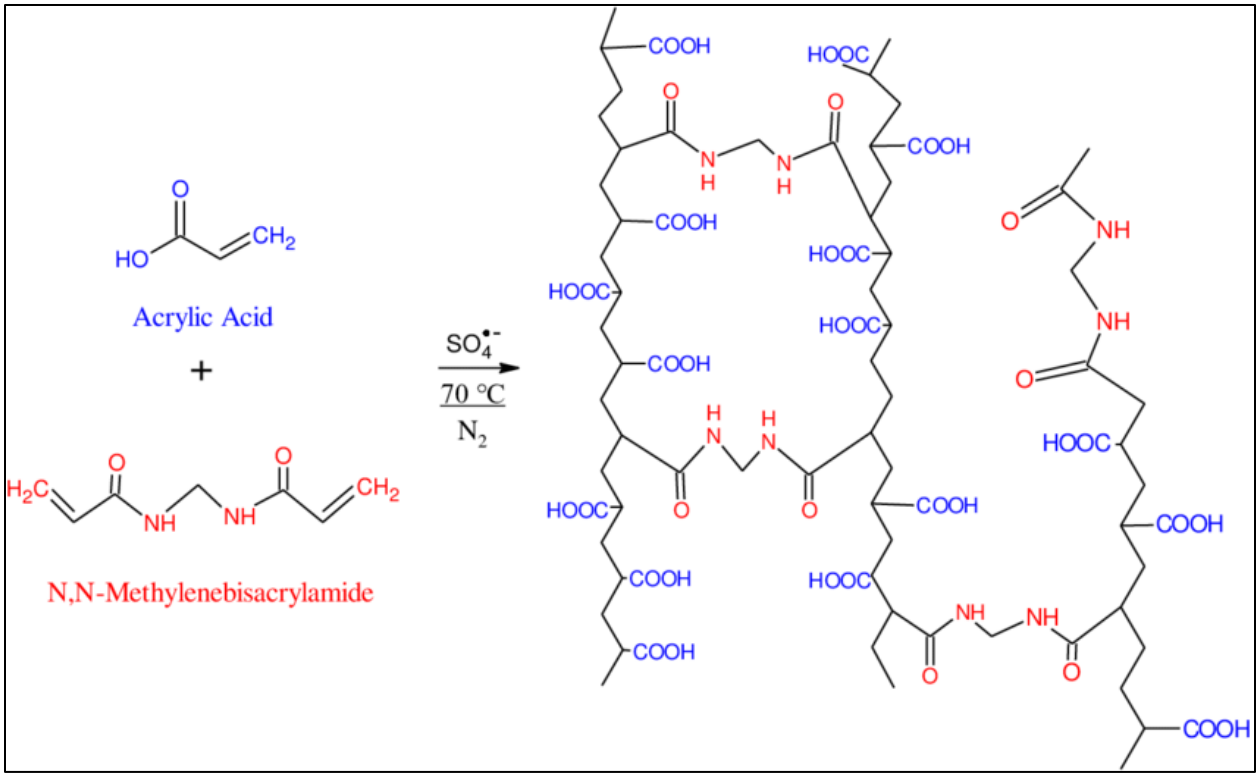

Scheme 2.2: An overview of thermal free radical polymerisation and cross-linking [123].

Free radical polymerisation is the most frequently used procedure in the polymer industry [1]. The advantages of using free radical polymerisation are that it is easy to carry-out, convenient, it is not easily affected by impurities, and it is suitable for designing and preparing polymers that can be used for a variety of applications. Free radical polymerisation allows well-characterised reaction kinetics and achievement of in situ properties [124].

2.3.3.4 Modification with inorganic materials

Depending on the intended application of the hydrogels, their physical properties can be further enhanced through incorporation inorganic materials. For example, for use in removing contaminants from aqueous solutions, the hydrogel must be mechanically and thermally stable for application especially for removing effluents from industries that utilise water for cooling reactions [125,126]. Wherein the contaminants may be introduced at that point. Additionally, the hydrogels must be easy to recover. Many

recent studies have incorporated nanofillers such as clay-based materials, carbon-based materials, and metal oxides into the hydrogel matrix during the polymerisation process to improve stability and recoverability. The blended product is then called a hydrogel nanocomposite.

2.3.3.4.1 Carbon-based hydrogels

Carbon-based hydrogel nanocomposites are hydrogels synthesised by incorporating materials such as graphene oxide (GO), biochar, activated carbon and carbon nanotubes [127,128]. GO is a carbon material prepared by oxidising graphene through chemical or thermal reduction processes. It contains highly hydrophilic groups such as hydroxyl, carboxylic and epoxy groups that are essential for adsorbing dyes and toxic metals [129]. GO may interact with contaminants through pi-to-pi interactions, electrostatic interactions or hydrogen bonding [130]. Owing to its outstanding mechanical, electrical and thermal properties, GO has attracted its use in the biomedical, energy and environmental field [131].

Carbon nanotubes are simply graphene sheets rolled up in cylinders of 1nm in diameter [132]. As a result of their porous structure, large surface area, high tensile strength (0.15 TPa) and elastic modulus (0.91 TPa), CNTs have attracted interests in use for adsorption of pollutants such as dyes, dichlorobenzene, ethylbenzene, and some heavy metals [133,134]. CNTs can be categorised into two forms, namely; single-walled carbon nanotubes (SWCNTs), which are made up of single layers of graphene sheets and multiwalled carbon nanotubes (MWCNTs), which are made up of multiple layers of concentric cylinders [132,135]. For example, the incorporation of CNTs in gels improves the mechanical properties however the rate of degradation decreases. This is because carbon-based materials have high hydrothermal stability, which makes them resistant to harsh environments [133]. Scheme 2.3 shows various interactions or applications that carbon-based materials can take part in such as surface complexation, physical adsorption through its surfaces and electrostatic interactions [136].

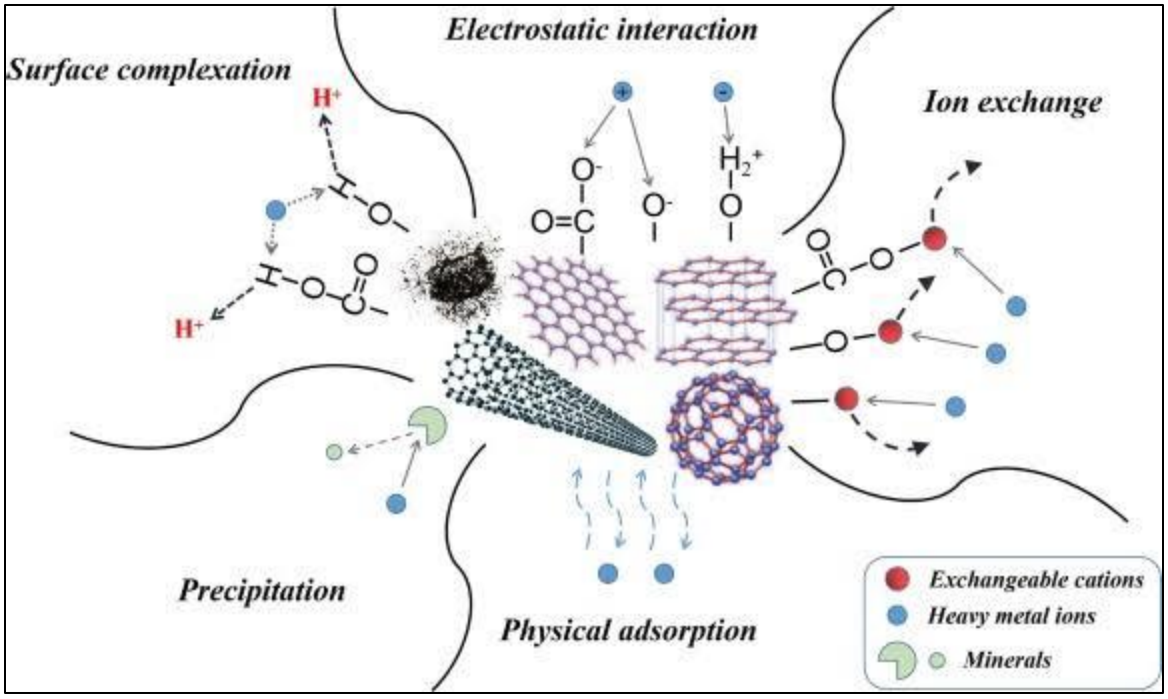

Scheme 2.3: Possible interactions of carbon-based materials [136].

Amongst recent studies that have used carbon-based materials to modify properties of the hydrogel, the incorporation of MWCNT's onto XG/PAA hydrogel improved the surface hydrophilicity and specific area of xanthan gum [10]. Makhado *et al.*, [98] conducted studies on xanthan gum polymer crosslinked with polyacrylic acid and incorporated with reduced graphene oxide (rGO), the successful synthesis was confirmed by FTIR. Various carbon-based nanocomposite hydrogels and their adsorption properties for removing contaminants from aqueous solutions are listed in Table 2.3.

Table 2.3: Carbon-based adsorbent hydrogels and their adsorption properties in removing contaminants from aqueous solution.

Adsorbent	Crosslinker	Dye	Adsorption parameter					Ref
			q_e (mg/g)	pH	Dosage (mg)	Isotherm models	Kinetics models	
CMC-AAm-GO	MBA	AB-133	185.45	6	100	-	-	[9]
XG-cl-pAA/o-MWCNTs	MBA	MB	521	6	30	Langmuir	Pseudo-first-order	[10]
XG-cl-pAA/rGO	MBA	MV MB	1052.63 793.65	5	10	Langmuir	Pseudo-second-order	[98]
CS/CNTs beads	Alkaline mixture	CR	450.4	5	20	Langmuir	Pseudo-first-order	[137]
p(AAm)-CB p(AAm)-WB	MBA	Phenol	1112,	10	50	Langmuir	Pseudo-first-order	[138]
k-C-g-pAA/CNT	MBA	CV	118	5-8	200	Langmuir	-	[139]

Acid black-133 = AB-133

2.3.3.4.2 Clay-based hydrogels

Natural clays and their improved forms have recently been used for removing pollutants from water [140]. The most commonly used clays, especially for treating toxic metals and dyes, are modified kaolinite and montmorillonite [141]. However, these clays are difficult to regenerate and reuse because of their colloidal dimensions [142]. This prompted the functionalisation of these clays. For example, the modification of

montmorillonite to form Cloisite 30B clay. In a study where C30B clay was incorporated onto polypropylene grafted with maleic anhydride (PP-g-MA) and thermoplastic starch (TPS), it was reported that the biodegradability of the materials was improved [143]. Modification of adsorbents by introducing functionalised clay components may improve both the physical and chemical properties of adsorbents [142,143]. Other modifications with clay results improve the number of adsorbing active sites, enhanced porosity, and low levels of mineral impurities [143]. In a recent study, C30B was mixed with a culture obtained from an anaerobic sludge to remove hexavalent chromium, where the removal capacity of nearly 100% was obtained [144]. Peng *et al*. [145] prepared cellulose-MMT hydrogels for removing MB. The hydrogels had a maximum removal capacity of 1065 mg/g (Table 2.4). Their viscoelasticity studies from the sweep measurements (Figure 2.9(a)) showed that when G'<G" the cellulose-MMT systems were in a viscous liquid form, however with increasing time when G'>G", the materials were in a gel form. Figure 2.9(b) in this case revealed that increasing clay content decreased the gel formation. Figure 2.9(c) revealed that the storage moduli (G') of hydrogels containing clay was higher than that of unmodified hydrogel and was proportional to the clay content from 10 to 15 wt.%. The incorporation of clay, however, increased the gel strength from 0.3 KPa to 4.7 KPa as shown in Figure 2.9 (d) and (e), which was approximate 16 times higher. Furthermore, the study reported that an increase in clay content from 10-15 wt.% reduced the swelling capacity of the hydrogel (Figure 2.9 (f)), reportedly due to a high degree of crosslinking. Increasing the crosslinking density of the hydrogel enhanced mechanical properties [145].

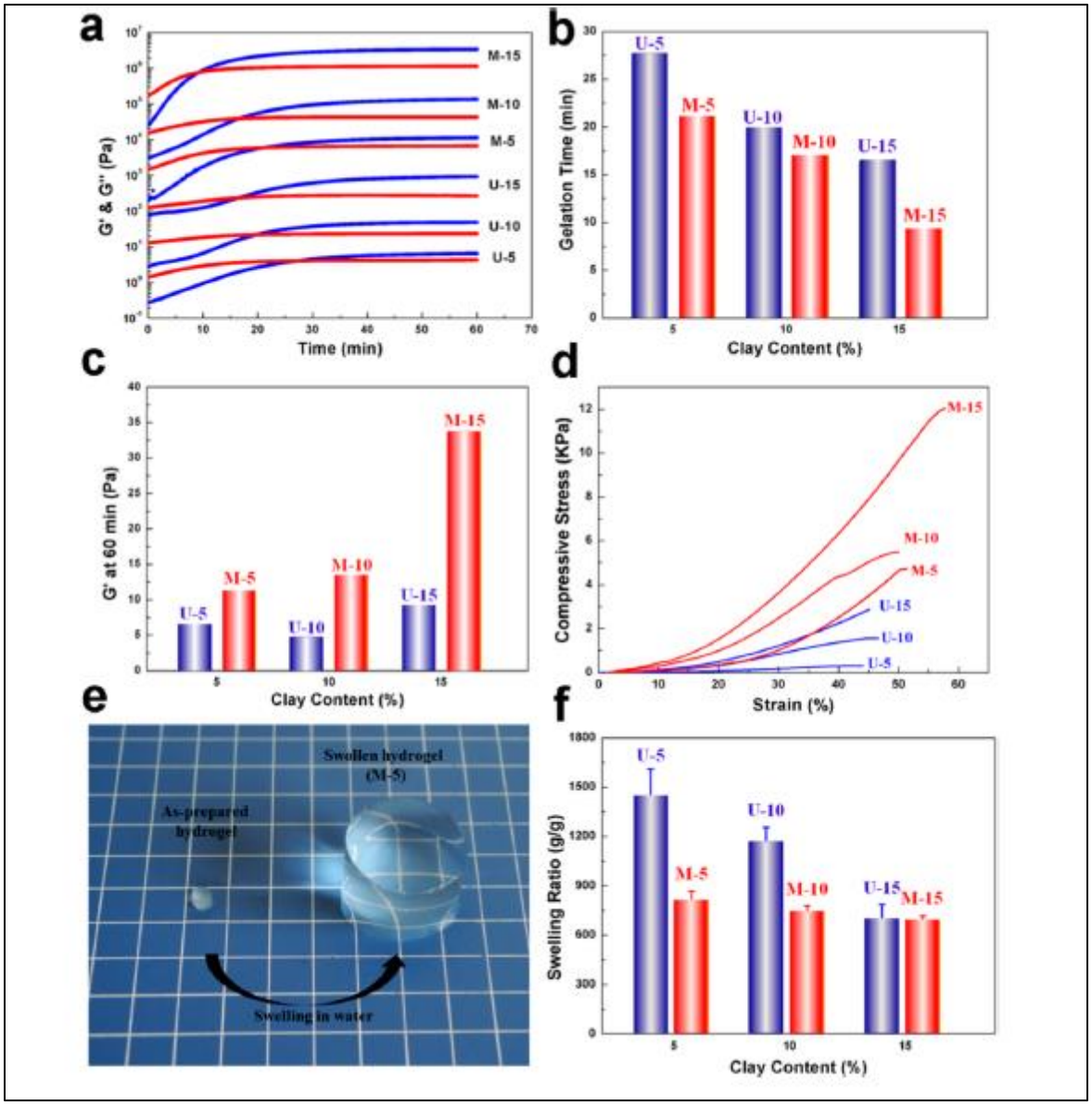

Figure 2.8: (a) Time dependence of storage modulus (G′) and loss modulus (G″), (b) Gelation time (c) Storage modulus at 1 h (d) Compressive-strain curves (e) Photographs of M-5 (f) The swelling ratio in distilled water [145].

Table 2.4: Clay-based adsorbent hydrogels and their adsorption properties in removing contaminants from aqueous solution.

Adsorbent	Cross-linker	Dye	Adsorption parameter					Refs.
			q_e (mg/g)	pH	Dosage (mg)	Isotherm models	Kinetics models	
K-Carra-AAm-MMT	APS	MB	49.52	7	50	Langmuir	Pseudo-second-order	[146]
CMC-MMT	ECH	MB	1065	1-10	500	Langmuir	Pseudo-second-order	[145]
P(AA-co-AMPS)/MMT	MBA	MB	192	10	-	Redlich–Peterson	Pseudo-second-order	[147]
CS-g-IA/BT	MBA	MB	500	6	30	Langmuir	Pseudo-second-order	[148]

2.3.3.4.3 Metal oxide-based hydrogels

Metal oxide-based nanoparticles have been reported to have a high density and restricted size, which are responsible for their very interesting and unique chemical and physical properties [149,150]. Examples of metal oxides include titanium dioxide (TiO_2), iron oxide (Fe_3O_4), magnesium oxide (MgO), aluminium oxide (Al_2O_3). Owing to their non-toxic nature, high surface area, high chemical stability, and economical friendliness, Fe_3O_4 nanoparticles are widely used for the removal of toxic metals and organic pollutants from water [149-153]. Ion-oxide and zinc oxide nanoparticles are one of the most frequently used metal oxides in treating dyes from aqueous solutions [154].

2.3.3.4.3.1 Magnetic (Fe_3O_4) nanocomposite hydrogels

Magnetite (Fe_3O_4) also known as black iron oxide amongst other transition metals has the strongest magnetism and is stable at ambient temperatures [155]. Magnetite is

prepared from the coprecipitation of iron oxide salts that result in an inverse spinel crystal structure consisting of half of the Fe^{3+} in tetrahedral coordination and the other half Fe^{2+} ions in octahedral coordination (Figure 2.10) [156,157]. The co-precipitation method is the most useful and suitable technique in preparing magnetite at both lab-scale and industrial scale [158].

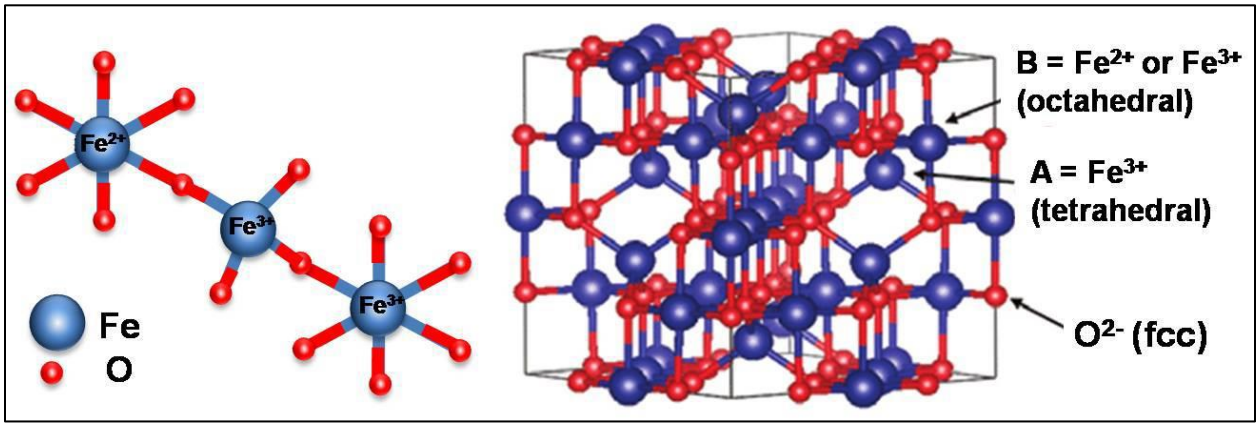

Figure 2.9: The inverse spinel structure of magnetite Fe_3O_4 [156]

Due to their cheap synthesis costs, susceptibility, stability high porosity, magnetic properties, biocompatibility, and easy chemical modification, MNP's have attracted much use in the wastewater treatment field [153-157]. The introduction of MNPs into polymer structures to produce nanocomposite hydrogels leads to a hybrid hydrogel with advantages of both components, thus improved chemical and physical properties. An example of such hybridized hydrogel is Fe_3O_4-g-pAA hydrogel synthesised via radical polymerisation in the presence of MBA crosslinker, which resulted in a highly adsorptive hydrogel of 507.7 mg/g removal capacity for MB [159] as shown in Table 2.5. However, according to Flory's theory, the swelling degree of a hydrogel depends on the density of crosslinking, the ionic osmotic pressure, and the attraction of the gel for the liquid [160]. When the crosslinking density is high, the space between the polymer chains decreases making the gel to be stiff due to small nonexpendable pores [160]. Additionally, an increase in the amount of MNPs increases the thermal properties but consequently reduces the swelling capacity as the Fe^{3+} from the incorporated MNPs may act as a physical crosslinking agent [161]. The greatest advantage of incorporation MNPs into

the hydrogel matrix is the improved stability and easy recovery of the material after application [162].

2.3.3.4.3.2 Zinc oxide-based hydrogels

Zinc-oxide (ZnO) can be found in nature as zincite mineral, however, the majority of it is prepared synthetically. Its crystal structure can be found in a hexagonal wurtzite form or cubic zincblende form (Figure 2.11). The form that is most stable and commonly found at ambient temperature is the wurtzite structure [163]. ZnO is commonly used for treating skin related problems such as nappy rash, dandruff, and incorporation in ointments used in wound dressing [163]. Other applications of ZnO include the use in catalysis, batteries, sensors, and adsorption of contaminants [164-167]. Their application as adsorbent material was reported in a study by Khan *et al*. [168], where a guar gum adsorbent hydrogel incorporated with ZnO nanoparticles was used for removing chromium (VI) from water. The group reported that incorporating ZnO nanoparticles improved the recovery of the adsorbent from the aqueous solution after the removal of Cr (VI). In another study, CMC hydrogel was modified with ZnO for antimicrobial activity, which was influenced by their inexpensiveness and lack of colour [169]. Therefore, looking at these properties, the ZnO would be ideal for preparing hydrogels for adsorbing dyes.

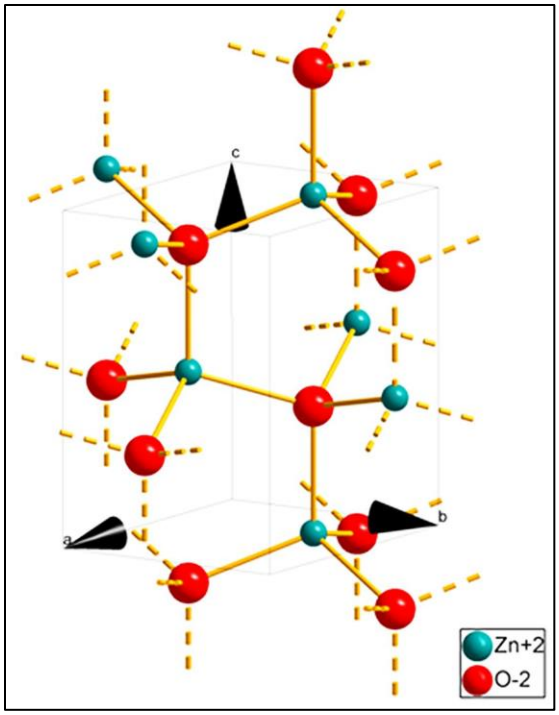

Figure 2.10: Crystal structure of zinc oxide [163]

.

Table 2.5: Metal oxide-based adsorbents for organic dyes removal.

Adsorbent	Cross-linker	Dye	Adsorption parameter					Refs.
			q_e (mg/g)	pH	Dosage (mg)	Isotherm models	Kinetics models	
Fe_3O_4/p (Am-co-Na Ac)	MBA	MB	641	7	50	Langmuir	Pseudo-second-order	[170]
PAA-grafted MNPs	MBA	MB	507.7	4	20	Langmuir	Pseudo-second-order	[159]
CMC coated Fe_3O_4@SiO_2 nanocomposite	-	MB	22.7	11	30	Langmuir	Pseudo-second-order	[171]
Fe_3O_4/CA gel beads	$CaCl_2$	MV	713	-	20-40	modified Langmuir – Freundlich	Pseudo-second-order	[172]
ZnO–clay–alginate hydrogel beads	Clay	CR	546.89	5-7	200	Temkin	Pseudo-first-order	[173]
ZnO-PPy nanocomposite	-	BG	140.8	-	50-200	Langmuir	Pseudo-second-order	[174]
Fe_3O_4-CS-Clay	Clay	MB	82	9-12	500	-	-	[162]
chitosan/silica/ZnO NC	-	MB	293.3	-	-	Langmuir	Pseudo-second-order	[175]

2.4 CONCLUSIONS

In conclusion, this review discusses recent studies applied for removing MB from aqueous solution using a biopolymer-based HNCs. Owing to various advantages such as low cost and easy design, the adsorption method is recognised as the most promising treatment technique for the removal of MB dye. This work discussed the principle behind the adsorption method, common adsorbent materials used and its advantages. We also briefly explained the hydrogels and methods to improve their properties. Three isothermal models: Langmuir, Freundlich, and Temkin models have been thoroughly explained with their respective principles. From this review, it was observed that the preparation of hydrogels can be affected by various factors and its removal capacity is affected by pH, temperature and dye concentration. This contribution emphasised the importance of incorporating metal oxide nanoparticles in hydrogels for the removal of dyes, and also their advantages and disadvantages towards the gel structure and properties. With regards to the research up to date, it has been observed that the realisation of hydrogels for practical purposes needs more research, especially the preparation of hydrogel nanocomposites with ability to remove organic contaminants such as dyes. It was seen that both magnetic nanoparticles and ZnO nanoparticles have contributed greatly to improving stability and enabling easy separation of adsorbent materials after application. The actual wastewater solutions are complex to be treated because they comprise of various ions and pollutants. More consideration needs to be paid on adsorption experimentations involving actual industrial water samples. Because the adsorbent performance may be noticeably different from the one carried in batch mode in the laboratory.

2.5 REFERENCES

1. Gupta, V. K., Ali, I., Saleh, T. A., & Agarwal, S. (2012). Chemical treatment technologies for waste-water recycling. Journal of Royal Society of Chemistry Advances, 6380–6388.
2. Muller, M. (2018). Understanding the origins of Cape Town' s water crisis, (June 2017).
3. Park, Y., Ayoko, G. A., & Frost, R. L. (2011). Application of organoclays for the adsorption of recalcitrant organic molecules from aqueous media. Journal of Colloid and Interface Science, 354(1), 292–305.
4. Shmeis, R. A. (2018). Water Chemistry and Microbiology. Comprehensive Analytical Chemistry, 81, 1-56.
5. Bodzek, M. (2015). Membrane technologies for the removal of micropollutants in water treatment. Advances in Membrane Technologies for Water Treatment: Materials, Processes and Applications, 465-517.
6. Yagub, M. T., Sen, T. K., Afroze, S., & Ang, H. M. (2014). Dye and its removal from aqueous solution by adsorption: A review. Advances in Colloid and Interface Science, 209, 172–184.
7. Liu, C., Omer, A. M., & Ouyang, X. (2018). Adsorptive removal of cationic methylene blue dye using carboxymethyl cellulose/k-carrageenan/activated montmorillonite composite beads: Isotherm and kinetic studies. International Journal of Biological Macromolecules, 106, 823–833.
8. Dawood, S., & Sen, T. K. (2014). review on dye removal from its aqueous solution into alternative cost effective and non-conventional adsorbents. Journal of Chemical and Process Engineering, 1(1), 1–11.
9. Varaprasad, K., Jayaramudu, T., & Rotimi, E. (2017). Removal of dye by carboxymethyl cellulose, acrylamide and graphene oxide via a free radical polymerization process Removal of dye by carboxymethyl cellulose, acrylamide and graphene oxide via a free radical polymerization process. Carbohydrate Polymers, 186–194.

10. Makhado, E., Pandey, S., Nomngongo, P. N., & Ramontja, J. (2018). Journal of Colloid and Interface Science Preparation and characterization of xanthan gum-cl-poly (acrylic acid)/ o-MWCNTs hydrogel nanocomposite as highly effective re-usable adsorbent for removal of methylene blue from aqueous solutions. Journal of Colloid and Interface Science, 513, 700–714.
11. Arami, M., Limaee, N. Y., Mahmoodi, N. M., & Tabrizi, N. S. (2006). Equilibrium and kinetics studies for the adsorption of direct and acid dyes from aqueous solution by soy meal hull. Journal of Hazardous Materials, 135(1–3), 171–179.
12. Okechukwu, O., & Nonso, O. (2017). Equilibrium, Kinetic and Thermodynamics Adsorption Study of Cationic Dye from Aqueous Solution onto Modified Awka Clay, 4(1), 1–16.
13. Science, A. (2016). Adsorption of cationic dyes on activated carbon obtained from waste Elaeagnus stone. Adsorption Science and Technology, 34,9–10), 512–525
14. De Gisi, S., Lofrano, G., Grassi, M., & Notarnicola, M. (2016). Characteristics and adsorption capacities of low-cost sorbents for wastewater treatment: A review. Sustainable Materials and Technologies, 9, 10–40.
15. Salleh, M. A. M., Mahmoud, D. K., Karim, W. A. W. A., & Idris, A. (2011). Cationic and anionic dye adsorption by agricultural solid wastes: A comprehensive review. Desalination, 280(1–3), 1–13.
16. Katheresan, V., Kansedo, J., & Lau, S. Y. (2018). Journal of Environmental Chemical Engineering Efficiency of various recent wastewater dye removal methods: A review, 6(May), 4676–4697.
17. Salleh, M. A. M., Mahmoud, D. K., Karim, W. A., & Idris, A. (2011). Cationic and anionic dye adsorption by agricultural solid wastes: A comprehensive review. Desalination, 280(1–3), 1–13.
18. Adegoke, K. A., & Bello, O. S. (2015). Dye sequestration using agricultural wastes as adsorbents. Water Resources and Industry, 12, 8–24.
19. Mohammadzadeh Pakdel, P., & Peighambardoust, S. J. (2018). A review on acrylic based hydrogels and their applications in wastewater treatment. Journal of Environmental Management, 217, 123–143.

20. Hameed, B. H., Ahmad, A. A., & Aziz, N. (2007). Isotherms, kinetics and thermodynamics of acid dye adsorption on activated palm ash, 133, 195–203.
21. Crini, G., Lichtfouse, E., Wilson, L., & Morin-Crini, N. (2019). Adsorption-oriented processes using conventional and non-conventional adsorbents for wastewater treatment. Environmental Chemistry for a Sustainable World 18, 23-71.
22. Crini, G., & Morcellet, M. (2002). Synthesis and applications of adsorbents containing cyclodextrins. Journal of Separation Science, 25, 789–813.
23. Lavrenko, V. A., Podchernyaeva, I. A., & Shchur, D. V. (2018). Nanostructured materials features of physical and chemical adsorption during interaction of polycrystalline and nanocrystalline materials with gases, 56(517), 504–511.
24. Yan, F., Chub, Y., Zhang, K., Zhang, F., Bhandari, N., Ruana, G., Dai, Z., Liu, Y., Zhang, Z., Kana, A.T., & Tomson, M.B. (2015). Determination of adsorption isotherm parameters with correlated errors by measurement error models. Chemical Engineering Journal, 281, 921–930.
25. Foo, K.Y., & Hameed, B.H. (2010). Insights into the modelling of adsorption isotherm systems," Chem. Eng. J., vol. 156, pp. 2–10, 2010.
26. Milonjić, S.K. (2007). Short communication a consideration of the correct calculation of thermodynamic parameters of adsorption. Journal of the Serbian Chemical Society, 72, 1363–1367.
27. Hintermeyer, B.H., Lacour, N.A., Padilla, A.P., & Tavani, E.L. (2008). Separation of the chromium (iii) present in a tanning wastewater by means of precipitation, reverse osmosis and adsorption. Latin American Applied Research, 71, 63–71.
28. Hibbitts, D. D., & Iglesia, E. (2019). Hydrogen Chemisorption Isotherms on Platinum Particles at Catalytic Temperatures: Langmuir and Two-Dimensional Gas Models Revisited. The Journal of Physical Chemistry, 123, 8447−8462.
29. Balis, N., Zaky, A. A., Perganti, D., Kaltzoglou, A., Sygellou, L., Katsaros, F., & Falaras, P. (2018). Dye Sensitization of Titania Compact Layer for Efficient and Stable Perovskite Solar Cells. ACS Applied Energy Materials, 1, 6161–6171
30. Worch, E. (2012). Adsorption Technology in Water Treatment Fundamentals, Processes, and Modeling," © 2012 Walter de Gruyter GmbH & Co. KG, Berlin/Boston, ISBN 978-3-11-024022-1.

31. Monama, G.R., Mdluli, S.B., Mashao, G., Makhafola, M.D., Ramohlola, K.E., Molapo, K.M., Hato, M.J., Makgopa, K., Iwuoha, E.I., & Modibane, K.D. (2018). Palladium deposition on copper (II) phthalocyanine/metal-organic framework composite and electrocatalytic activity of the modified electrode towards the hydrogen evolution reaction. Renewable energy, 119, 62–72.
32. Xia, L., Wei, Z., & Wan, M. (2010). Conducting polymer nanostructures and their application in biosensors. Journal of Colloid and Interface Science, 341, 1–11.
33. Padash, R., Nasab, A. S., Nasrabadi, M. R., Ehrlich, M. M. H., & Peyravi, A. S. R. M. (2018). Is it possible to use X 12 Y 12 (X = Al, B, and Y = N, P) nanocages for drug-delivery systems? A DFT study on the adsorption property of 4-aminopyridine drug. Applied Physics A, 124(9), 1–11.
34. Ji, H., Song, X., Shi, Z., Tang, C., Xiong, L., Zhao, W., & Zhao, C. (2018). Reinforced-Concrete Structured Hydrogel Microspheres with Ultrahigh Mechanical Strength, Restricted Water Uptake, and Superior Adsorption Capacity. ACS Sustainable Chemistry & Engineering, 6, 5950–5958.
35. Cheng, S. Y., Show, P., Lau, F., Chang, J., & Ling, T. C. (2019). Review New Prospects for Modified Algae in Heavy Metal Adsorption. Trends in Biotechnology, 37(11), 1255–1268.
36. Sham, A. Y. W., & Notley, S. M. (2018). Journal of Environmental Chemical Engineering Adsorption of organic dyes from aqueous solutions using surfactant exfoliated graphene. Journal of Environmental Chemical Engineering, 6(1), 495–504.
37. Jawad, A. H., Solehah, S., Norrahma, A., Hameed, B. H., & Ismail, K. (2019). International Journal of Biological Macromolecules Chitosan-glyoxal film as a superior adsorbent for two structurally different reactive and acid dyes: Adsorption and mechanism study. International Journal of Biological Macromolecules, 135, 569–581.
38. Sun, C., Sun, L., & Sun, X. (2013). Graphical Evaluation of the Favourability of Adsorption Processes by Using Conditional Langmuir Constant. Industrial & Engineering Chemistry Research, 52, 14251−14260.

39. Boutahala, M., Sahnoun, S., & Gomri, F. (2014). Adsorption characteristics, isotherm, kinetics, and diffusion of modified natural bentonite for removing the 2,4,5-trichloropheno. Applied Clay Science, 90, 81–87.
40. Li, D., Wang, J., Guo, Z., Li, J., & Shuai, J. (2017). Pectin gels cross-linked by Ca^{2+}: An efficient material for methylene blue removal. Journal of Molecular Liquids, 238, 36–42.
41. State, K., State, E., & State, K. (2012). Langmuir, Freundlich, Temkin and Dubinin – Radushkevich Isotherms Studies of Equilibrium Sorption of Zn^{2+} Unto phosphoric acid modified rice husk. Journal of Applied Chemistry, 3(1), 38–45.
42. Seidel-morgenstern, A. (2004). Experimental determination of single solute and competitive adsorption isotherms. Journal of Chromatography A, 1037, 255–272.
43. Erdogan, F. O. (2019). Freundlich, Langmuir, Temkin and Harkins-Jura isotherms studies of H_2 adsorption on porous adsorbents, Chemistry & Chemical Technology, 13(2), 129–135.
44. Ng, C., Losso, J. N., Marshall, W. E., & Rao, R. M. (2002). Freundlich adsorption isotherms of agricultural by-product-based powdered activated carbons in a geosmin – water system. Bioresource Technology, 85,131–135
45. Azizian, S. (2004). Kinetic models of sorption: a theoretical analysis. Journal of Colloid and Interface Science, 276, 47–52.
46. Ho, Y.S., & Mckay, G. (1999). Pseudo-second order model for sorption processes. Process Biochemistry, 34, 451–465.
47. Salvestrini, S. (2018). Analysis of the Langmuir rate equation in its differential and integrated form for adsorption and pseudo-second-order models. Reaction Kinetics, Mechanisms and Catalysis, 123(2), 455–472.
48. Yusuff, S. M., Khim, O. K., Zin, W., Yunus, W., Ahmad, M., Ibrahim, N. A., & Tech, P. (2019). Isotherms and Thermodynamics of CO_2 Adsorption on Thermally Treated Alum Sludge. Nature Environment and Pollution Technology, 18 (1), 247-250.
49. Wu, P., Cai, Z., Jin, H., & Tang, Y. (2019). Science of the Total Environment Adsorption mechanisms of five bisphenol analogues on PVC microplastics. Science of the Total Environment, 650, 671–678.

50. Process, G., Zhao, Z., Bai, P., Li, L., Li, J., Wu, L., & Tan, L. (2019). The Reaction Thermodynamics during Plating Al on Graphene Process. Materials,12 (2), 330.
51. Gómez, V., Larrechi, M.S., & Callao, M.P. (2007). Kinetic and adsorption study of acid dye removal using activated carbon. Chemosphere, 69, 1151–1158.
52. Malik, R., Ramteke, D.S., & Wate, S.R. (2007). Adsorption of malachite green on groundnut shell waste-based powdered activated carbon. Waste Management, 27, 1129–1138.
53. Ismadji, S., Sudaryanto, Y., Hartono, S.B., Setiawan, L.E.K., & Ayucitra, A. (2005). Activated carbon from char obtained from vacuum pyrolysis of teak sawdust: pore structure development and characterization. Bioresource Technology, 96, 1364–1369.
54. Lillo-Rodensas, M.A., Carzrola-Ameros, D., & Linares-Solano, A. (2003). Chemical reactions between carbons and NaOH and KOH – an insight into chemical activation mechanisms. Carbon, 41, 265–267.
55. Kyzas, G. Z., Bomis, G., Kosheleva, R. I., & Efthimiadou, E. K. (2019). Nanobubbles effect on heavy metal ions adsorption by activated carbon. Chemical Engineering Journal, 356, 91–97.
56. Mittal, H., Ray, S. S. & Okamoto, M. (2016). recent progress on the design and applications of polysaccharide-based graft copolymer hydrogels as adsorbents for wastewater purification. Macromolecular Material Engineering, 301,496-522
57. Moreno-lópez, A. Y., González-lópez, M. E., Manríquez-gonzález, R., & Robledo-ortíz, J. R. (2019). Evaluation of the Cr (VI) adsorption performance of xanthate polysaccharides supported onto agave fiber-LDPE foamed composites. Water, Air, and Soil Pollution, 230, 133.
58. Largitte, L., & Pasquier, R. (2016). A review of the kinetics adsorption models and their application to the adsorption of lead by an activated carbon. Chemical Engineering Research and Design, 109, 495–504.
59. Gupta, V. K., & Suhas. (2009). Application of low-cost adsorbents for dye removal – A review. Journal of Environmental Management, 90(8), 2313–2342.
60. Guilherme, M.R., Aouada, F.A., Fajardo, A.R., Martins, A.F., Paulino, A.T., Davi, M.F.T., Rubira, A.F., & Muniz, E.C. (2015). Superabsorbent Hydrogels Based on

Polysaccharides for Application in Agriculture as Soil Conditioner and Nutrient Carrier: A Review. European Polymer Journal, 72, 365–85.

61. Zheng, Y., Monty, J., & Linhardt, R.J. (2015). Polysaccharide-based nanocomposites and their applications. Carbohydrate Research, 405, 23-32.

62. Tally, M., & Atassi, Y. (2015). Optimized synthesis and swelling properties of a pH-sensitive semi-IPN superabsorbent polymer-based on sodium alginate-g-poly (acrylic acid-co-acrylamide) and polyvinylpyrrolidone and obtained via microwave irradiation. Journal of Polymer Research, 22,181.

63. Pakdel, P.M, & Peighambardoust, S.J. (2018). A Review on Acrylic Based Hydrogels and Their Applications in Wastewater Treatment. Journal of Environmental Management, 217, 123–43.

64. Essawy, H.A., Ghazy, MBM., El-Hai, F.A., & Mohamed, M.F. (2016). Superabsorbent hydrogels via graft polymerization of acrylic acid from chitosan-cellulose hybrid and their potential in controlled release of soil nutrients. International Journal of Biological Macromolecules 89 (2016) 144–151.

65. Chen, P., Liu, X., Jin, R., Nie, W., & Zhou, Y. (2017). Dye adsorption and photo-induced recycling of hydroxypropyl cellulose/molybdenum disulfide composite hydrogels. Carbohydrate Polymers, 167, 36–43.

66. Benhalima, T., Ferfera-Harrar, H., & Lerari, D. (2017). Optimization of carboxymethyl cellulose hydrogels beads generated by an anionic surfactant micelle templating for cationic dye uptake: Swelling, sorption, and reusability studies. International Journal of Biological Macromolecules, 105, 1025–1042.

67. Yagub, M.T., Sen, T.K., Afroze, S., & HAng, H.M. (2014). Dye and Its Removal from Aqueous Solution by Adsorption: A Review. Advances in Colloid and Interface Science, 209, 172–84.

68. Salama, A. (2018). Preparation of CMC-g-P(SPMA) super adsorbent hydrogels: Exploring their capacity for MB removal from wastewater. International Journal of Biological Macromolecules, 106, 940–946.

69. Yu, W., Song, D., Li, A., & Yang, H. (2019). Control of gypsum-dominated scaling in reverse osmosis system using carboxymethyl cellulose. Journal of Membrane Science, 577, 20–30.
70. Shi, C., Tao, F., & Cui, Y. (2018). Evaluation of nitriloacetic acid modified cellulose film on adsorption of methylene blue. International Journal of Biological Macromolecules, 114, 400–407.
71. Zhu, X., Bao, L., Wei, Y., Ma, J., & Kong, Y. (2016). International Journal of Biological Macromolecules Removal of toxic indigo blue with integrated biomaterials of sodium carboxymethyl cellulose and chitosan. International Journal of Biological Macromolecules, 91, 409–415.
72. Colombo, P., Bettini, R., Sabti, P., & Peppas, N. A. (2000). Swellable matrices for controlled drug delivery: gel-layer behaviour, mechanisms and optimal performance. Pharmaceutical Science and Technology Today, 3, 198–204
73. Pakdel, P. M., & Peighambardoust, S. J. (2018). A review on acrylic based hydrogels and their applications in wastewater treatment. Journal of Environmental Management, 217, 123–143.
74.. Son, Y., Yop, K., & Park, S. (2015). Influence of reduced graphene oxide on mechanical behaviors of sodium carboxymethyl cellulose. Composites Part B, 83, 36–42.
75. Kono, H. (2014). Characterization and properties of carboxymethyl cellulose hydrogels crosslinked by polyethylene glycol. Carbohydrate Polymers, 106, 84–93.
76. Zhu, X., Bao, L., Wei, Y., Ma, J., & Kong, Y. (2016). International Journal of Biological Macromolecules Removal of toxic indigo blue with integrated biomaterials of sodium carboxymethyl cellulose and chitosan. International Journal of Biological Macromolecules, 91, 409–415.
77. Petri, D. F. S. (2019). Carboxymethyl cellulose/poly (acrylic acid) interpenetrating polymer network hydrogels as multifunctional adsorbents. Cellulose, 26(1), 597–615.

78. Begum, H. A., Khalid, M., & Mahbub, B. (2013). Effectiveness of Carboxymethyl Cellulose for the Removal of Methylene Blue from Aqueous Solution, 61(2), 193–198.
79. Lee, J., Park, S., Roh, H., Oh, S., Kim, S., Kim, M., & Park, J. (2018). Preparation and Characterization of Superabsorbent Polymers Based on Starch Aldehydes and Carboxymethyl Cellulose. Polymers, 10(605), 1–16.
80. Saputra, A. H., Qadhayna, L., & Pitaloka, A. B. (2014). Synthesis and Characterization of Carboxymethyl Cellulose (CMC) from Water Hyacinth Using Ethanol-Isobutyl Alcohol Mixture as the Solvents. International Journal of Chemical Engineering and Applications, 5(1), 36-40.
81. Huang, C. M. Y., Chia, P. X., Lim, C. S. S., Nai, J.Q., Ding, D. Y., Seow, P.B., Wong, C.W., & Chan, E. W. C. (2017). cellulose chemistry and technology synthesis and characterisation of carboxymethyl cellulose from various agricultural wastes. Cellulose chemistry and Technology, 51, 665–672.
82. El-din, H. M. N., Abd, S. G., & El-naggar, A. W. M. (2010). Swelling and drug release properties of acrylamide/carboxymethyl cellulose networks formed by gamma irradiation. Radiation Physics and Chemistry, 79(6), 725–730.
83. Tønnesen, H. H., Karlsen, J., Tønnesen, H. H., & Karlsen, J. (2002). Alginate in Drug Delivery Systems. Drug Development and Industrial Pharmacy, 28 (6), 621-630.
84. Ertesvag. H., & Valla S. (1998). Biosynthesis and applications of alginates. Polymer Degradation and Stability, 59 (1–3), 85–91.
85. Mc Neely, W. H. and Pettitt, D. J., Algin. (1973). Industrial Gums; Polysaccharides and their Derivatives, Whistler, R.L. and Be Miller, J.N.,Eds, New York: Academic, 2nd ed, 1-50.
86. Gupta, S., & Abu-ghannam, N. (2011). Bioactive potential and possible health effects of edible brown seaweeds Shilpi Gupta and. Trends in Food Science & Technology, 22(6), 315–326.
87. Liu, S., Li, Y., & Li, L. (2017). Enhanced stability and mechanical strength of sodium alginate composite films. Carbohydrate Polymers, 160, 62–70.

88. Liu, Y., Hu, X., Wang, H., Chen, A., Liu, S., Guo, Y., et al. (2013). Photoreduction of Cr (VI) from acidic aqueous solution using TiO_2-impregnated glutaraldehyde-crosslinked alginate beads and the effects of Fe (III) ions. Chemical Engineering Journal, 226, 131–138.
89. Li, J., Ma, J., Chen, S., Huang, Y., & He, J. (2018). Adsorption of lysozyme by alginate/graphene oxide composite beads with enhanced stability and mechanical property. Materials Science & Engineering C, 89, 25–32.
90. Li, C., Wang, X., Meng, D., & Zhou, L. (2018). International Journal of Biological Macromolecules Facile synthesis of low-cost magnetic biosorbent from peach gum polysaccharide for selective and efficient removal of cationic dyes. International Journal of Biological Macromolecules, 107, 1871–1878.
91. Wang W, Wang A (2010) Synthesis and swelling properties of pH-sensitive semi-IPN superabsorbent hydrogels based on sodium alginate-g-poly (sodium acrylate) and polyvinylpyrrolidone. Carbohydrate Polymer, 80,1028–1036.
92. Rashidzadeh, A., Olad, A., & Salari, D. (2015). The Effective Removal of Methylene Blue Dye from Aqueous Solutions by NaAlg-g-Poly (Acrylic Acid-Co-Acryl Amide)/Clinoptilolite Hydrogel Nanocomposite. Fibers and Polymers, 16, 354–62.
93. Sterner, M., Ribeiro, M. S., Gröndahl, F., & Edlund, U. (2017). Cyclic fractionation process for Saccharina latissima using aqueous chelator and ion exchange resin, 3175–3189.
94. Hefnawy, M. El. (2018). Preparation and Properties of a Novel Eco-friendly Carboxymethylcellulose / K- Carrageenan / Graphene oxide Gel Beads for the Removal of Heavy Metals from Water, 58, 6–16.
95. Ren, H., Gao, Z., Wu, D., Jiang, J., Sun, Y., & Luo, C. (2016). Efficient Pb (II) removal using sodium alginate–carboxymethyl cellulose gel beads: Preparation, characterization, and adsorption mechanism. Carbohydrate Polymers, 137, 402–409.
96. Lan, W., He, L., & Liu, Y. (2018). Preparation and Properties of Sodium Carboxymethyl Cellulose/Sodium Alginate/Chitosan Composite Film. Coatings, 8(8), 291.

97. Shirsath, S. R., Patil, A. P., Patil, R., Naik, J. B., Gogate, P. R., & Sonawane, S. H. (2014). Removal of Brilliant Green from wastewater using conventional and ultrasonically prepared poly (acrylic acid hydrogel loaded with kaolin clay: A comparative study. Sachin Ultrasonics - Sonochemistry, 20(3), 914–923.
98. Makhado, E., Pandey, S., & Ramontja, J. (2018). Microwave-assisted synthesis of xanthan gum-cl-poly (acrylic acid) based-reduced graphene oxide hydrogel composite for adsorption of methylene blue and methyl violet from aqueous solution. International Journal of Biological Macromolecules,119, 255-269.
99. Garg, S., & Garg, A. (2016). Hydrogel: Classification, Properties, Preparation and Technical Features. Asian Journal of Biomaterial Research, 2(6), 163-170.
100. Çankaya, N. (2016). Synthesis of Graft Copolymers onto Starch and Its Semiconducting Properties. Results in Physics, 6, 538–42.
101. Ahmed, E. M. (2015). Hydrogel: Preparation, characterization, and applications: A review. Journal of Advanced Research, 6(2), 105–121.
102. Liang, Y., Zhao, X., Ma, P. X., Guo, B., Du, Y., & Han, X. (2019). Journal of Colloid and Interface Science pH-responsive injectable hydrogels with mucosal adhesiveness based on chitosan-grafted-dihydrocaffeic acid and oxidized pullulan for localized drug delivery. Journal of Colloid and Interface Science, 536, 224–234.
103. Singh, V., Kumar, P., & Sanghi, R. (2012). Progress in Polymer Science Use of microwave irradiation in the grafting modification of the polysaccharides – A review. Progress in Polymer Science, 37(2), 340–364.
104. Mishra, S., Rani, G.U., & Sen, G. (2012). Microwave initiated synthesis and application of polyacrylic acid grafted carboxymethyl cellulose. Carbohydrate Polymers, 87, 2255– 2262.
105. Cook, J.P., Goodall, G.W., Khutoryanskaya, O.V., & Khutoryanskiy, V.V. (2012). Microwave-Assisted Hydrogel Synthesis: A New Method for Crosslinking Polymers in Aqueous Solutions. Macromolecular Rapid Communications, 33 (4), 332-336.

106. Anah, L., & Astrini, N. (2017). Influence of pH on Cr (VI) ions removal from aqueous solutions using carboxymethyl cellulose-based hydrogel as adsorbent. IOP Conference Series: Earth and Environmental Science, 60, 012010.

107. Ismail, H., Irani, M., & Ahmad, Z. (2013). Starch-based hydrogels: Present status and applications. International Journal of Polymeric Materials and Polymeric Biomaterials, 62(7), 411–420.

108. Shen, C., Shen, Y., Wen, Y., Wang, H., & Liu, W. (2011). Fast and highly efficient removal of dyes under alkaline conditions using magnetic chitosan-Fe(III) hydrogel. Water Research, 45(16), 5200–5210.

109. Liu, L., Gao, Q., Lu, X., & Zhou, H. (2016). In situ forming hydrogels based on chitosan for. Asian Journal of Pharmaceutical Sciences, 11(6), 673–683.

110. Kumar, T., Thakur, A., Alexander, A., Badwaik, H., & Tripathi, D. K. (2012). Modified chitosan hydrogels as drug delivery and tissue engineering systems: present status and applications. Acta Pharmaceutica Sinica B, 2(5), 439–449.

111. Song, L., Zhu, M., Chen, Y., & Haraguchi, K. (2008). Temperature-and pH-sensitive nanocomposite gels with semi-interpenetrating organic/inorganic networks. Macromolecular Chemistry and Physics, 209 (15), 1564–1575.

112. Zhu, M., Xiong, L., Wang, T., Liu, X., Wang, C., & Tong, Z. (2010). High tensibility and pH-responsive swelling of nanocomposite hydrogels containing the positively chargeable 2-(dimethylamino) ethyl methacrylate monomer. Reactive and Functional Polymers 70 (5),267–271.

113. Xu, J., Liu, X., Ren, X., & Gao, G. (2018). The role of chemical and physical crosslinking in different deformation stages of hybrid hydrogels. European Polymer Journal, 100, 86–95.

114. Ye, X., Li, X., Shen, YT., Chang, G., Yang, J., & Gu, Z. (2017). Self-healing pH-sensitive cytosine- and guanosine-modified hyaluronic acid hydrogels via hydrogen bonding. Polymer, 108, 348–360.

115. Huang, T., Xu, H.G., Jiao, K.X., Zhu, L.P., Brown, H.R., & Wang, H.L. (2007). A novel hydrogel with high mechanical strength: a macromolecular microsphere composite hydrogel. Advanced Materials, 19, 1622–1626.

116. Sun, J.Y., Zhao, X., Illeperuma, W.R.K., Chaudhuri, O., Oh, K.H., Mooney, D.J., Vlassak, J.J., & Suo, Z. (2012). Highly stretchable and tough hydrogels, Nature, 489, 133–136.

117. Hu, M., Gu, X., Hu, Y., Wang, T., Huang, J., & Wang, C. (2016). Low chemically cross-linked PAM/C-Dot hydrogel with robustness and super stretchability in both as-prepared and swelling equilibrium states. Macromolecules, 49, 3174–3183.

118. Rahmani, Z., Sahraei, R., & Ghaemy, M. (2018). Preparation of spherical porous hydrogel beads based on ion-crosslinked gum tragacanth and graphene oxide: Study of drug delivery behavior. Carbohydrate Polymers, 194(April), 34–42.

119. Eftekhari-sis, B., Rahimkhoei, V., Akbari, A., & Araghi, H. Y. (2018). Cubic polyhedral oligomeric silsesquioxane nano-cross-linked hybrid hydrogels: Synthesis, characterization, swelling and dye adsorption properties. Reactive and Functional Polymers, 128(May), 47–57.

120. Braun, D. (2009). Origins and Development of Initiation of Free Radical Polymerization Processes. Journal of Polymer Science A, 1-10

121. Chen, M., Zhong, M., & Johnson, J.A. (2016). Light-controlled radical polymerization: mechanisms, methods, and applications. Chemical Reviews, 116, 10167-1021.

122. Kamoun, E. A., Omer, A. M., Khattab, S. N., Ahmed, H. M., & Elbardan, A. A. (2018). In-situ UV-photopolymerized PVA-g-GMA hydrogels for biomedical applications: I. Synthesis, Characterizations and Grafting Optimization. Journal of Applied Pharmaceutical Science,8 (01), 034-042.

123. (2017). Tunable nanocomposite membranes for water remediation and tunable nanocomposite membranes for water remediation and separations. Chemical and Materials Engineering,

124. Ranganathan N., Joseph Bensingh R., Abdul Kader M., Nayak S.K. (2018) Synthesis and Properties of Hydrogels Prepared by Various Polymerization Reaction Systems. In: Mondal M. (eds) Cellulose-Based Superabsorbent Hydrogels. Polymers and Polymeric Composites,

125. Dannert, C., Stokke, B.T., & Dias, R.S. (2019). Nanoparticle-Hydrogel Composites: From Molecular Interactions to Macroscopic Behavior. Polymers, 11(2), 275.

126. Guanghui, J., Wang, L., Yu., Wael, A., & Zhang, L. (2013). Recent progress on study of hybrid hydrogels for water treatment. Colloids and Surfaces A: Physicochemical and Engineering Aspects. 416. 86–94.

127. Smith, S. C., & Rodrigues, D. F. (2015). Carbon-based nanomaterials for removal of chemical and biological contaminants from water: A review of mechanisms and applications. CARBON, 91, 122–143.

128. Biswas, S., Sen, T.K., Yeneneh, A.M., & Meikap, B.C. (2019). Synthesis and characterization of a novel Ca-alginate-biochar composite as efficient zinc (Zn^{2+}) adsorbent: Thermodynamics, process design, mass transfer and isotherm modelling. Separation Science and Technology, 54(7), 1106-1124

129. Bai, H., Li, C., & Shi, G. (2010). A pH-sensitive graphene oxide composite hydrogel. Chemical Communications, 46, 2376–2378.

130. Wang, X., Liu, X., Yuan, H., Liu, H., Liu, C., Li, T., & Guo, Z. (2018). Non-covalently functionalized graphene strengthened poly (vinyl alcohol). Materials and Design, 139, 372–379.

131. Fazil, S., Bangesh, M., Rehman, W., Liaqat, K., Saeed, S., Sajid, M., & Bibi, I. (2019). Mechanical, thermal, and dielectric properties of functionalized graphene oxide/polyimide nanocomposite films. Nanomaterials and Nanotechnology, 9, 1–8.

132. Elhissi, A. M. A., Ahmed, W., Hassan, I. U., Dhanak, V. R., & Emanuele, A. D. (2012). Carbon Nanotubes in Cancer Therapy and Drug Delivery Carbon Nanotubes in Cancer Therapy and Drug Delivery. Journal of Drug Delivery, 2012

133. Zhou, Y., Tang, L., Zeng, G., Chen, J., Cai, Y., Zhang, Y., Yang, G., Liu, Y., Zhang, C., & Tang, W. (2014). Mesoporous carbon nitride-based biosensor for highly sensitive and selective analysis of phenol and catechol in compost bioremediation. Biosensors and Bioelectronics, 61, 519–525.

134. Demczyk, B.G., Wang, Y.M., Cumings, J., Hetman, M., Han, W., Zettl, A., & Ritchie, R.O. (2002). Direct mechanical measurement of the tensile strength

and elastic modulus of multiwalled carbon nanotubes. Materials Science and Engineering, 334,173– 178.

135. Aqel, A., El-nour, K. M. M. A., Ammar, R. A. A., & Al-warthan, A. (2012). Carbon nanotubes, science and technology part (I) structure, synthesis and characterisation. Arabian Journal of Chemistry, 5(1), 1–23.

136. Yang, X., Wan, Y., Zheng, Y., He, F., Yu, Z., & Huang, J. (2019). Surface functional groups of carbon-based adsorbents and their roles in the removal of heavy metals from aqueous solutions: A critical review. Chemical Engineering Journal, 366, 608–621.

137. Chatterjee, S., Lee, M. W., & Woo, S. H. (2010). Adsorption of Congo red by chitosan hydrogel beads impregnated with carbon nanotubes. Bioresource Technology, 101(6), 1800–1806.

138. Karakoyun, N., Kubilay, S., Aktas, N., Turhan, O., & Kasimoglu, M. (2011). Hydrogel–Biochar composites for effective organic contaminant removal from aqueous media. Desalination 280 (2011) 319–325.

139. Cadena, F., Rizvi, R., & Peters, R.W. (1990). Feasibility studies for the removal of heavy metal from solution using tailored bentonite, hazardous and industrial wastes. Proceedings of the 22ndMid-Atlantic Industrial Waste Conference, pp. 77–94.

140. Gopal, K., & Sen, S. (2008). Adsorption of a few heavy metals on natural and modified kaolinite and montmorillonite: A review. Advances in Colloid and Interface Science, 140,114–131.

141. Yuan, G., Theng, B. K. G., North, P., Zealand, N., Churchman, J., & Gates, W. P. (2013). Clays and Clay Minerals for Pollution Control. Developments in Clay Science, 1, 624-675.

142. Abreu, A. S., Oliveira, M., & Machado, A. V. (2015). Applied Clay Science Effect of clay mineral addition on properties of bio-based polymer blends. Applied Clay Science, 104, 277–285.

143. Lytras, G., Lytras, C., Argyropoulou, D., Dimopoulos, N., & Malavetas, G. (2017). A novel two-phase bioreactor for microbial hexavalent chromium removal from wastewater. Journal of Hazardous Materials, 336, 41–51.

144. Peng, N., Hu, D., Zeng, J., Li, Y., Liang, L., & Chang, C. (2016). Superabsorbent Cellulose − clay nanocomposite hydrogels for highly efficient removal of dye in water. ACS Sustainable Chemistry and Engineering, 4, 7217−7224.

145. Mahdavinia, G. R., Baghban, A., Zorofi, S., & Massoudi, A. (2014). Kappa-Carrageenan Biopolymer-Based Nanocomposite Hydrogel and Adsorption of Methylene Blue Cationic Dye from Water, 5(2), 330–337.

146. Hossein Hosseinzadeh & Neda Khoshnood (2016) Removal of cationic dyes by poly (AA-co-AMPS)/montmorillonite nanocomposite hydrogel, Desalination and Water Treatment, 57:14, 6372-6383

147. Shakib, F., Koohi, A.D., & Pirzaman, A.K. (2017). Adsorption of methylene blue by using novel chitosan-g-itaconic acid/bentonite nanocomposite – equilibrium and kinetic study. Water Science & Technology, 75.8, 1932–1943.

148. Atta, A., Akl, M.A., Youssef, A.M., & Ibraheim, M. A. (2013). Superparamagnetic Core-Shell Polymeric Nanocomposites for Efficient Removal of Methylene Blue from Aqueous Solutions. Adsorption Science and Technology, 31(5), 397–419.

149. Pasqui, D., Atrei, A., Giani, G., Cagna, M. De, & Barbucci, R. (2011). Metal oxide nanoparticles as cross-linkers in polymeric hybrid hydrogels. Materials Letters, 65(2), 392–395.

150. Zia, M., Phull, A.R., & Ali, J.S. (2016). challenges of iron oxide nanoparticles. Nanotechnology, Science and Applications, 2016(9), 49–67.

151. Stankic, S., Suman, S., Haque, F., & Vidic, J. (2016). Pure and multi-metal oxide nanoparticles: synthesis, antibacterial and cytotoxic properties. Journal of Nanobiotechnology, 1–20.

152. Rao, K. G., Ashok, C. H., Rao, K. V., & Chakra, C. H. S. (2014). Structural properties of MgO Nanoparticles: Synthesized by Co-Precipitation Technique. International Journal of Science and Research, 8–9.

153. Markides, H., Rotherham, M., & Haj, A. J. El. (2012). Biocompatibility and Toxicity of Magnetic Nanoparticles in Regenerative Medicine, 2012, 13–15.

154. Majewski, P., & Thierry, B. (2007). Functionalized magnetite nanoparticles—Synthesis, properties, and bio-applications. Critical Reviews in Solid State and Materials Sciences, 32(3-4), 203-215.

155. Rivani, D. A., Retnosari, I., & Saraswati, T. E. (2019). Influence of TiO_2 addition on the magnetic properties of carbon-based iron oxide nanocomposites synthesized using submerged arc-discharge Influence of TiO_2 addition on the magnetic properties of carbon-based iron oxide nanocomposites synthesized using submerged arc-discharge. IOP Conference Series: Materials Science and Engineering, 509, 012034.

156. Frimpong, R. A., & Hilt, J. Z. (2008). hydrogel coatings on magnetite nanoparticles via atom transfer radical polymerization. Nanotechnology, 19 175101.

157. Leslie-pelecky, D. L., & Rieke, R. D. (1996). Magnetic Properties of Nanostructured Materials. Chemistry of Materials, (8), 1770–1783.

158. Pooresmaeil, M., Mansoori, Y., Mirzaeinejad, M., & Khodayari, A. L. I. (2015). Efficient Removal of Methylene Blue by Novel Magnetic Hydrogel Nanocomposites of Poly (acrylic acid), 21665, 1–13.

159. Koetting, M. C., Peters, J. T., Steichen, S. D., & Peppas, N.A. (2016). Stimulus-responsive hydrogels: Theory, modern advances, and applications. Materials Science & Engineering R: Reports, 93,1–49.

160. Pooresmaeil, M., Mansoori, Y., Mirzaeinejad, M., & Khodayari, A. L. I. (2015). Efficient Removal of Methylene Blue by Novel Magnetic Hydrogel Nanocomposites of Poly (acrylic acid), 21665, 1–13.

161. Bée, A., Obeid, L., Mbolantenaina, R., Welschbillig, M., & Talbot, D. (2017). Magnetic chitosan/clay beads: A magsorbent for the removal of cationic dye from water. Journal of Magnetism and Magnetic Materials, 421, 59–64.

162. Stefaniuk, I., Cieniek, B., Rogalska, I., Virt, I.S., & Kosciak, A. (2017). Magnetic properties of ZnO: Co layers obtained by pulsed laser deposition method. Materials Science-Poland, 2017-0114.

163. Ahmad, M., Shi, Y., Nisar, A., Sun, H., Shen, W., Wei, M., & Zhu, J. (2011). Synthesis of hierarchical flower-like ZnO nanostructures and their

functionalization by Au nanoparticles for improved photocatalytic and high-performance Li-ion battery anodes. Journal of Materials Chemistry, 21, 7723–7729.

164. Nassar, M.Y., Ali, A.A., & Amin, A.S. (2017). A facile Pechini sol–el synthesis of $TiO_2/Zn_2TiO_2/ZnO/C$ nanocomposite: an efficient catalyst for the photocatalytic degradation of orange G textile dye. RSC Advances, 7, 30411–30421.

165. Young, S.J., & Tang, W.L. (2019). Wireless Zinc Oxide Based pH Sensor System. Journal of The Electrochemical Society,

166. Farrokhi, M., Hosseini, S.C., Yang, J.K., & Shirzad-Siboni, M. (2014). Application of ZnO–Fe3O4 nanocomposite on the removal of azo dye from aqueous solutions: kinetics and equilibrium studies. Water, Air, & Soil Pollution, 225, 1–12.

167. Khan, T.A., Nazir, M., Ali, I., & Kumar, A. (2017). Removal of Chromium (VI) from aqueous solution using guar gum–nano zinc oxide biocomposite adsorbent. Arabian Journal of Chemistry,10 (2), S2388-S2398.

168. Li, J., Fang, L., Tait, W. R., & Sun, L. (2017). Preparation of conductive composite hydrogels from carboxymethyl cellulose and polyaniline with a nontoxic crosslinking agent. RSC Advances, 7, 54823–54828.

169. Atta, A., Akl, M. A., Youssef, A. M., & Ibraheim, M. A. (2013). Superparamagnetic Core-Shell Polymeric Nanocomposites for Efficient Removal of Methylene Blue from Aqueous Solutions. Adsorption Science and Technology, 31 (5), 397–419.

170. Zirak, M., Abdollahiyan, A., Eftekhari-sis, B., & Saraei, M. (2017). Carboxymethyl cellulose coated Fe3O4 @ SiO2 core-shell magnetic thermodynamic studies Carboxymethyl cellulose coated $Fe_3O_4@SiO_2$ core-shell magnetic nanoparticles for methylene blue removal: equilibrium, kinetic, and thermodynamic studies. Cellulose, 25(1), 503–515.

171. Asadi, S., Eris, S., & Azizian, S. (2018). Alginate-based hydrogel beads as a biocompatible and efficient adsorbent for dye removal from aqueous solution. American Chemistry Society, 3 (11), 15140-15148.

172. Vahidhabanu, S., Karuppasamy, D., & Adeogun, I. (2017). Impregnation of zinc oxide modified clay over alginate beads: a novel material for the effective removal of Congo red from wastewater. RSC Advances, 7, 5669–5678.

173. Zhang, M., Chang, L., Zhao, Y., & Yu, Z. (2019). Fabrication of Zinc Oxide / Polypyrrole Nanocomposites for Brilliant Green Removal from Aqueous Phase. Arabian Journal for Science and Engineering, 44(1), 111–121.

174. Hosseini, H., & Mashaykhi, M. (2019). New chitosan/silica/zinc oxide nanocomposite as adsorbent for dye removal. International Journal of Biological Macromolecules, 131, 520-526.

CHAPTER THREE

ANALYTICAL TECHNIQUES

3.1 INTRODUCTION

This chapter gives a brief discussion of various analytical instruments, their principles, advantages, and disadvantages as well as their recent applications. Analytical techniques are instruments used for the identification of samples, quantification and isolating components in a sample. Some of these instruments help us study the structural composition of materials, determine the nature or phase of composite materials, study their physical properties such as mechanical and thermal stability, whilst others help us quantify samples. Characterisation techniques can be categorised into physical, spectroscopy, and microscopy. Examples of physical techniques used in this study include the x-ray diffraction (XRD), thermogravimetric analysis (TGA), and dynamic mechanical analysis (DMA). Spectroscopical methods include the Fourier transform infrared (FTIR) spectroscopy and ultraviolet-visible (UV-vis) spectroscopy, which are used to reveal information about the composition of materials. Then lastly the microscopy techniques include scanning electron microscopy (SEM) and transmission electron microscopy (TEM). In this study, the above-mentioned techniques were used to characterise CMC-cl-pAA and SA/AA hydrogels, Fe_3O_4-C30B and ZnO nanoparticles, and the hydrogel nanocomposites

3.2 PHYSICAL METHODS

These techniques are focused on analysing the structural properties of materials such as the surface area, mechanical stability, crystallinity, and thermal stability. examples of such techniques include XRD, TGA, and DMA in this study.

3.2.1 XRD

XRD is an analytical instrument employed for identifying the phase of a material. The principle of XRD focuses on the constructive interference between the X-rays of a single light and the crystalline material [1] as shown in Figure 3.1.

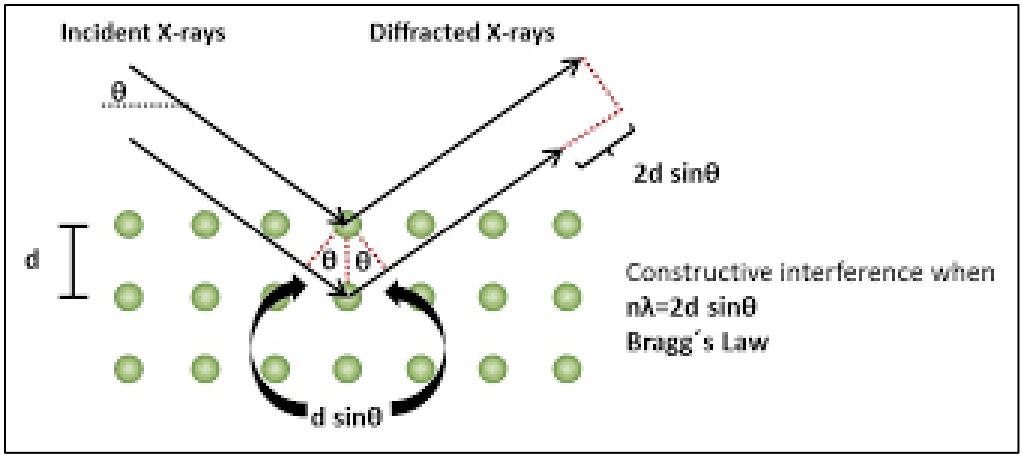

Figure 3.1: Representation of the XRD principle [2].

During the analysis of samples, Braggs law must be satisfied, as expressed in Equation 3.1.

$$n\lambda = 2d\sin\theta \quad (3.1)$$

where λ represents the wavelength of the radiation beam, d is the interplanar spacing between two diffracting lines, θ denotes the diffraction angle, and n represents an integer usually equal to 1 [3]. The XRD technique has the advantage that unknown materials can be analysed fast (<20 min). Its major drawbacks include peak overlay and the detection limit of solid materials is approximately 2% [4]. Vahidhabanu *et al.* [5] prepared clay-alginate hydrogel beads modified with ZnO NP's (Figure 3.2). The ZnO NP's were observed to be crystalline with their characteristic peaks appearing at 20.46°, 34.3 °, 39.9 °, 57.9 °, 61.3 °, and 67.8 ° (Figure 3.2(a)). Incorporation of the ZnO NP's into the clay-alginate matrix resulted in a shift of the peaks which demonstrated further intercalation of the clay and the appearance of a new broad peak was due to the amorphous alginate (Figure 3.2 (b-c)), confirming successful modification of clay-alginate beads with ZnO NP's [5]. As shown in (Figure 3.2(d),) the peak at 20.46° disappeared after adsorption of dye. In this study, XRD was employed for phase identification of the synthesised materials (CMC-pAA, Fe_3O_4-C30B NPs, CMC-pAA/Fe_3O_4-C30B HNC, SA/AA, ZnO NPs, and SA/AA/ZnO) by comparing them to known reference spectra.

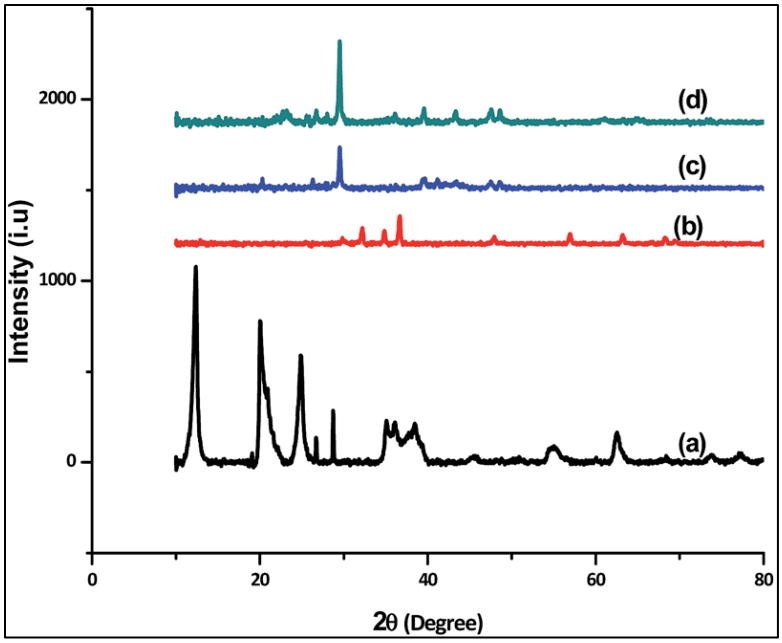

Figure 3. 2 XRD patterns of (a) ZnO NP (b) clay–alginate NC (c and d) ZnO–clay alginate beads before and after adsorption [5].

3.2.2 Thermogravimetric analysis

During TGA analysis, a sample is placed inside a furnace and heated steadily with increasing time [4]. During the heating process, the sample weight loss percentage (wt. %) is measured relative to temperature to determine its thermal stability [6]. The uses of TGA include understanding thermal processes such as vaporisation, adsorption, desorption, sublimation, decomposition, reduction, and oxidation [4]. Furthermore, gaseous or volatile products that get lost during chemical reactions can be assessed using TGA. These involve nanomaterials, polymers, polymer nanocomposites, etc [7,8].

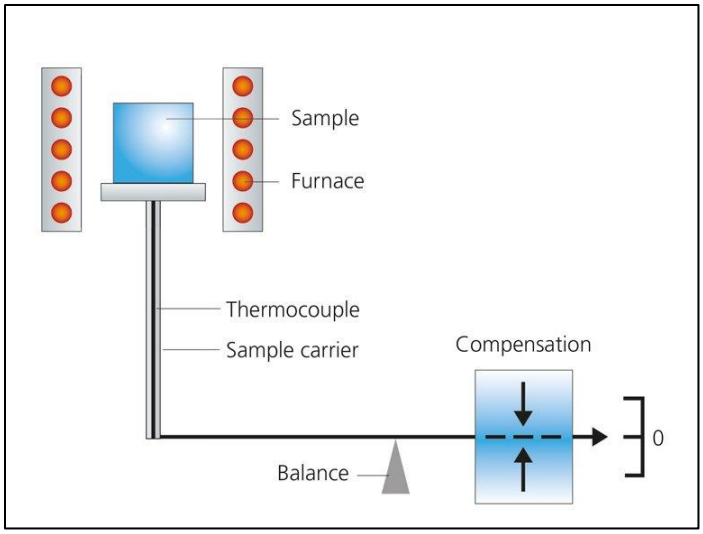

Figure 3. 3: General representation of TGA [9].

Figure 3.3 shows a general setup of TGA. Generally, if the material is thermally stable, no change in mass will be observed [9]. For example in a study by Salama [9], it was observed that modification of carboxymethyl cellulose graft polyacrylic acid (CMC-g-pAA) with calcium phosphate (CaP) improved the weight loss percentage from 83% to 59.4% (Figure 3.4). This confirmed mineralisation and improved thermal stability of the hydrogel by CaP [10] Reported modification of CMC hydrogel by Fe_3O_4@SiO_2 in another study, improved the thermal stability by more than 10% as temperature increased. This confirmed the successful coating by the metal oxides NP's [11]. In this study, the thermal stabilities of the prepared materials (CMC-pAA, Fe_3O_4-C30B NPs, CMC-pAA/Fe_3O_4-C30B HNC, SA/AA, ZnO NPs, and SA/AA/ZnO) were determined.

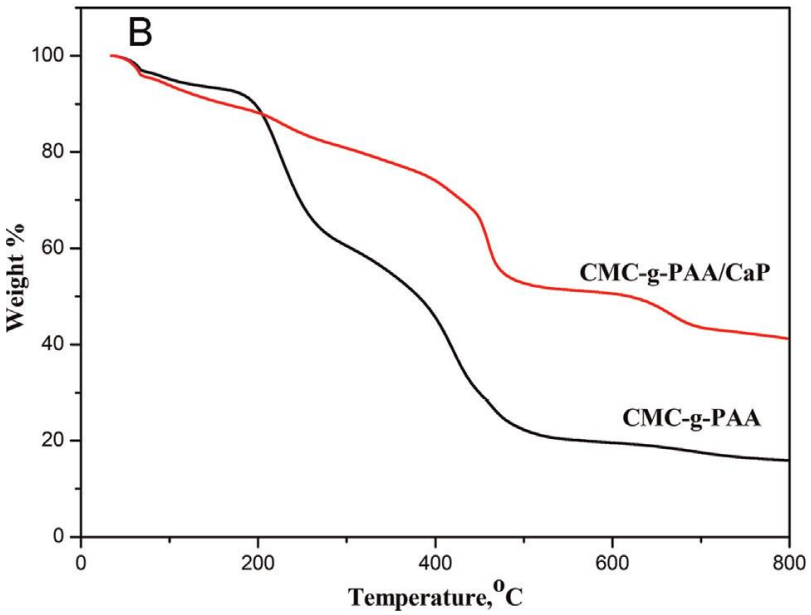

Figure 3. 4: TGA of C MC-g-PAA and CMC-g-PAA/CaP [11].

3.2.3 Dynamic mechanical analysis

During a dynamic mechanical analysis of materials, the stress or strain response of materials is measured relative to the applied oscillatory force or deformation with time [12]. From the analysis, information about the storage modulus (G'), loss modulus (G") and tan delta (δ) can be obtained. DMA analysis is based on either forced frequency or free resonance. In which the signal is applied at a specific frequency or the material is agitated and permitted to exhibit free resonance decay [12]. Most frequently when working with polymers, the modulus and viscosity are measured as a function frequency because polymeric or fluids melt with the response to the rate of strain not to the amount of stress applied. Thus, viscosity is the main reason most researchers run frequency scans. For example, in Figure 3.5, at low frequency, the polymer structure behaves as a fluid and at a higher frequency, it behaves like a solid material [13]. In this study, the DMA analysis of CMC-pAA hydrogel, CMC-pAA/Fe_3O_4-C30B HNC, SA/AA hydrogel, and SA/AA/ZnO HNC was investigated.

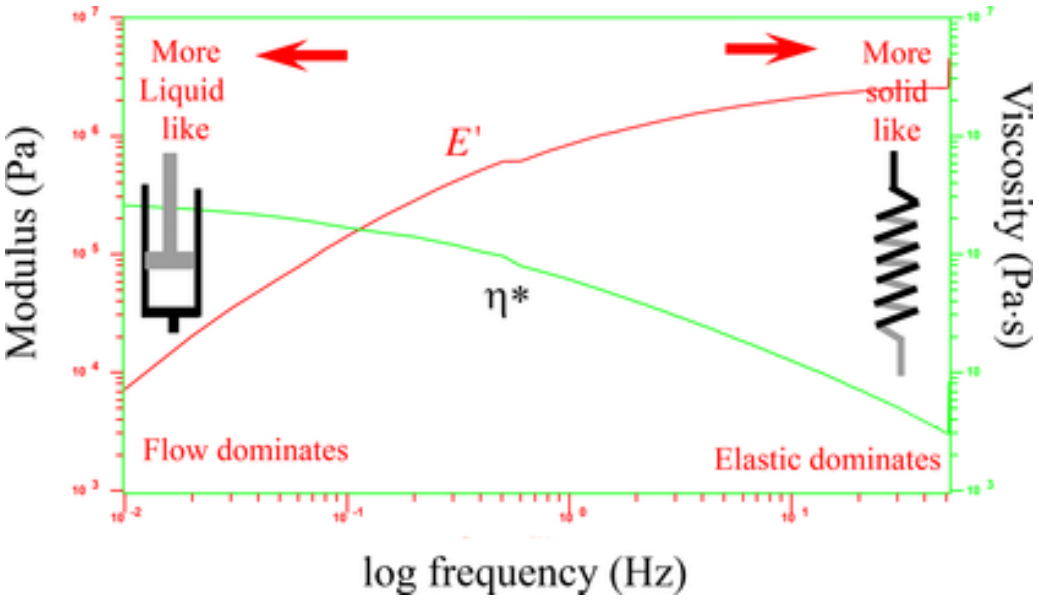

Figure 3. 5: General representation of how the frequency influences the modulus and viscoelastic characteristic of polymer materials [14].

3.3 SPECTROSCOPY

Spectroscopy focuses on how materials interact with the electromagnetic radiation which can be used to help in identifying, for example, the structure and bonds in the material. Moreover, it can be used to give quantitative information about the various atoms and molecules [15].

3.3.1 Fourier transform infrared spectroscopy

This analytical technique is used to obtain the infrared spectrum of absorption or emission response by liquid, solid, or gaseous samples [16]. Figure 3.6 shows the basic components of FTIR [16]. The general working principle of FTIR is that light is shone onto a sample, the sample then absorbs the light within the infrared region of the electromagnetic spectrum, depending on the type of bonds present in the molecule, a specific frequency that is the characteristic frequency of that bond is obtained [17]. Thus, allowing the characterisation of functional groups or bonds that are present in the structure or molecule. The frequencies of the vibrations are obtained in wavenumbers within the range 4000–400 cm^{-1} [17]. The instrument initially records the background emission spectrum, which will be used to correct the spectra reading of analyte, and then secondly the emission spectrum of the IR source of the sample of interest. The

ratio between the sample spectrum and the background spectrum directly correlates with the sample's absorption spectrum [18,19].

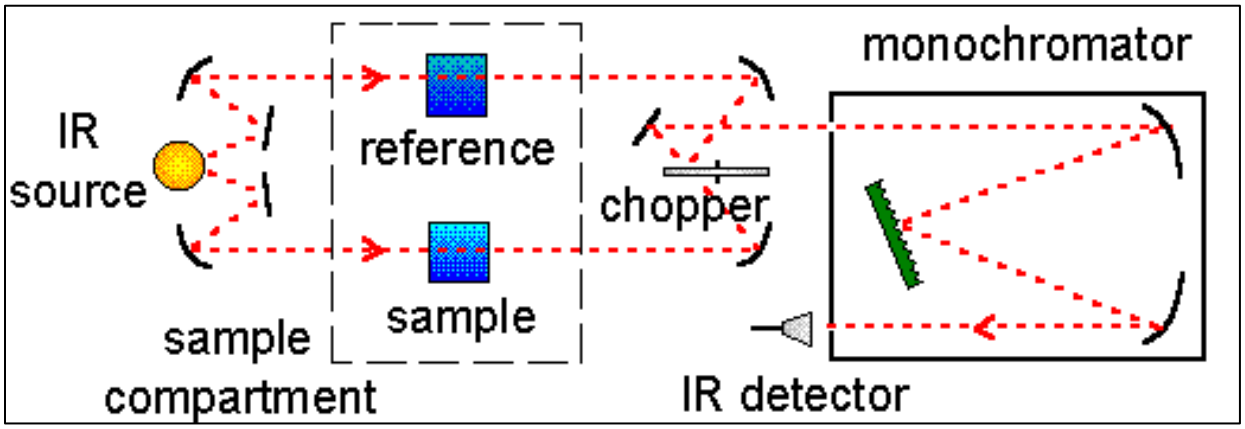

Figure 3. 6: Basic components of FTIR [16].

For example, in Figure 3.7(a) the peaks at 3506.46, 468.6, and 912 cm^{-1} correspond to the -OH, Zn-O and Zn-O-H vibrations [5]. Observation of clay-alginate hydrogel in Figure 3.7(b) displayed the characteristic vibration of Si-O-Si of clay at 1035.7 cm^{-1}. Other peaks between 1383 and 1634 cm^{-1} were reported to belong to the COO^- asymmetric and symmetric stretches. Upon incorporation of ZnO NP's to clay-alginate, two distinctive peaks at 940 and 822 cm^{-1} were observed, which were due to Zn-O and Si-O-H vibrations, respectively [5]. The results confirmed the successful preparation of the materials. In another study, conducted by Atta et al, the characteristic vibration of Fe-O of magnetite was observed at 586 cm^{-1} [20] In this study the FTIR was used to confirm the structures of the prepared materials (CMC-pAA hydrogel, Fe_3O_4-C30B NPs, CMC-pAA/Fe_3O_4-C30B HNC, SA/AA hydrogel, and ZnO NPs.

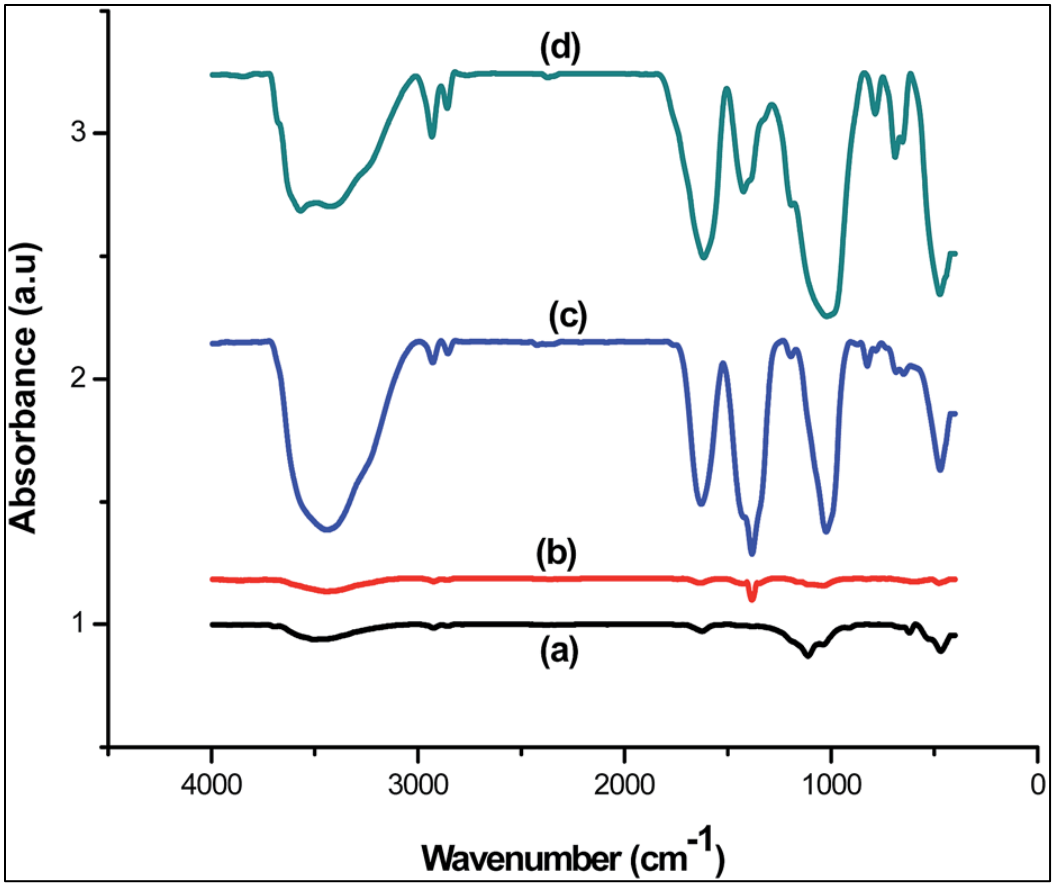

Figure 3. 7: FTIR spectra of (a) ZnO (b) clay–alginate (c and d) ZnO, clay and modified ZnO–clay–alginate beads before and after adsorption.

3.3.2 Ultraviolet-visible spectroscopy

Ultraviolet-visible spectroscopy refers to a study focusing on the absorption or reflection of a monochromatic beam of light by a sample in the ultraviolet-visible region [21]. In this case, light is shone onto a molecule, the light is then absorbed by π–electrons or nonbonding electrons in the sample [22]. The UV technique is governed by the Beer-Lambert law, which states that: when a monochromatic beam of light is passed through a solution containing absorbing molecules, the rate at which the intensity of radiation decreases relative to the depth of the absorbing solution is proportional to the concentration of the solution and the incident light [21]. Mathematically Beer-Lamberts law is expressed as in Equation 3.2.

$$A=abc \tag{3.2}$$

where *A* represents the absorbance of the analyte. *a, b and c* represent the absorptivity constant, the path length of a cell and the concentration of the analyte, respectively [22]. Since the concentration of the analyte is commonly measured in molarity, M (mol/L), Beer's law can be written as follows [3.3]:

$$A=\varepsilon bc \tag{3.3}$$

where ε is the molar absorptivity of the analyte which may be used to deduce the conductivity of the materials [22,23]. In this research, UV-vis was employed for determining the methylene blue (MB) concentration remaining in solution after removal with hydrogel nanocomposites.

3.4 MICROSCOPY

Microscopy is the study of samples or materials using microscopes to view images at a scale that is not limited to the resolution range of an unaided eye. Microscopy can be categorised into electron microscopy, scanning microscopy, and optical microscopy.

3.4.1 Scanning electron microscopy

Scanning electron microscopy is a method that produces high-resolution images of material surfaces by making use of a fixated beam of electrons [24]. The basic principle of SEM (Figure 3.8) is that a ray of electrons is bombarded on the material surface such that the electrons give off signals containing information about the surface and composition of materials through interaction with atoms in the sample [25]. Moreover, the information resulting from the relaxation energy gives the fingerprint of each element present in the sample or material, which is measured by Energy Dispersive Spectroscopy detector (also called EDS) [26]. For example, Vahidhabanu *et al*. [5] used SEM in the preparation of ZnO/clay-alginate nanocomposite (Figure 3.9). From the results, ZnO NPs were spherical and the clay-alginate hydrogel was rough and irregular shaped (Figure 3.9a,b). The group reported that coating of the hydrogel with ZnO NPs resulted in a nanocomposite with rough surface in which the spherical ZnO NPs were observed on the surface of the hydrogel (Figure 3.9(c-d)).

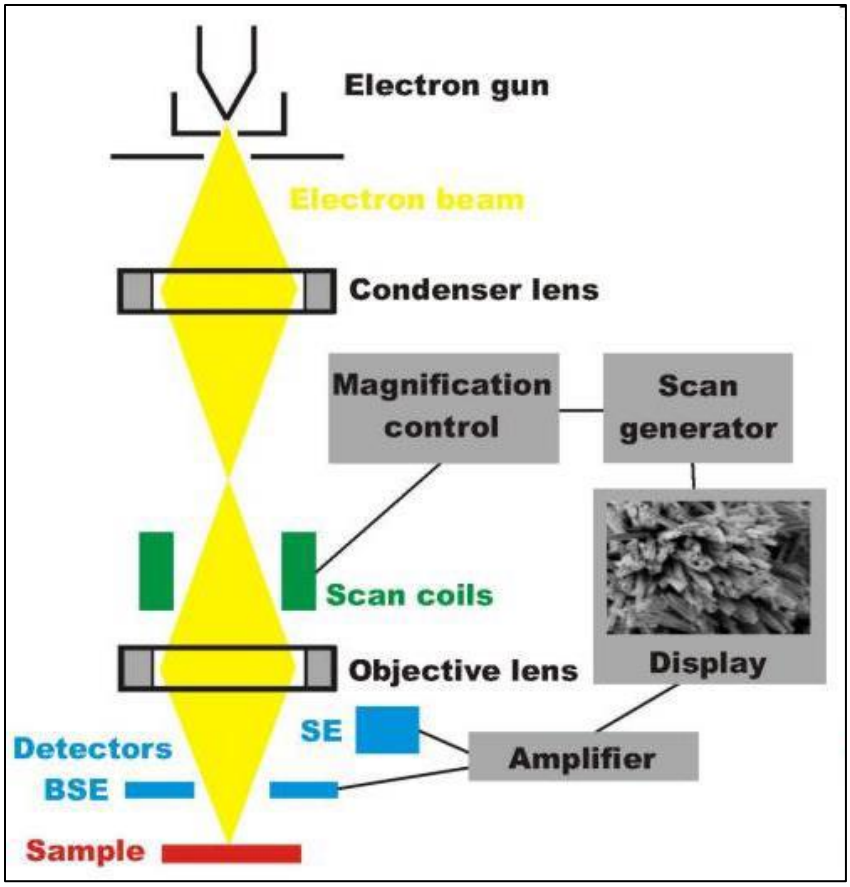

Figure 3. 8: Overview of scanning electron microscopy [26].

Another study reported the morphology of CMC coated with Fe_3O_4@SiO_2 to be spongy-like, with spherical metal oxide nanoparticles on the CMC surface [11]. In a study by Kurdtabar *et al.* [27] CMC incorporated with Fe_3O_4 reported for drug delivery (Figure 9(e)). EDX analysis confirmed the presence of iron oxide nanoparticles in CMC through observation of Fe, O, and C peaks. In this study, the SEM method was employed for studying the morphology of the synthesised SA-based and CMC-based materials, and the metal oxide nanoparticles (Fe_3O_4-C30B and ZnO).

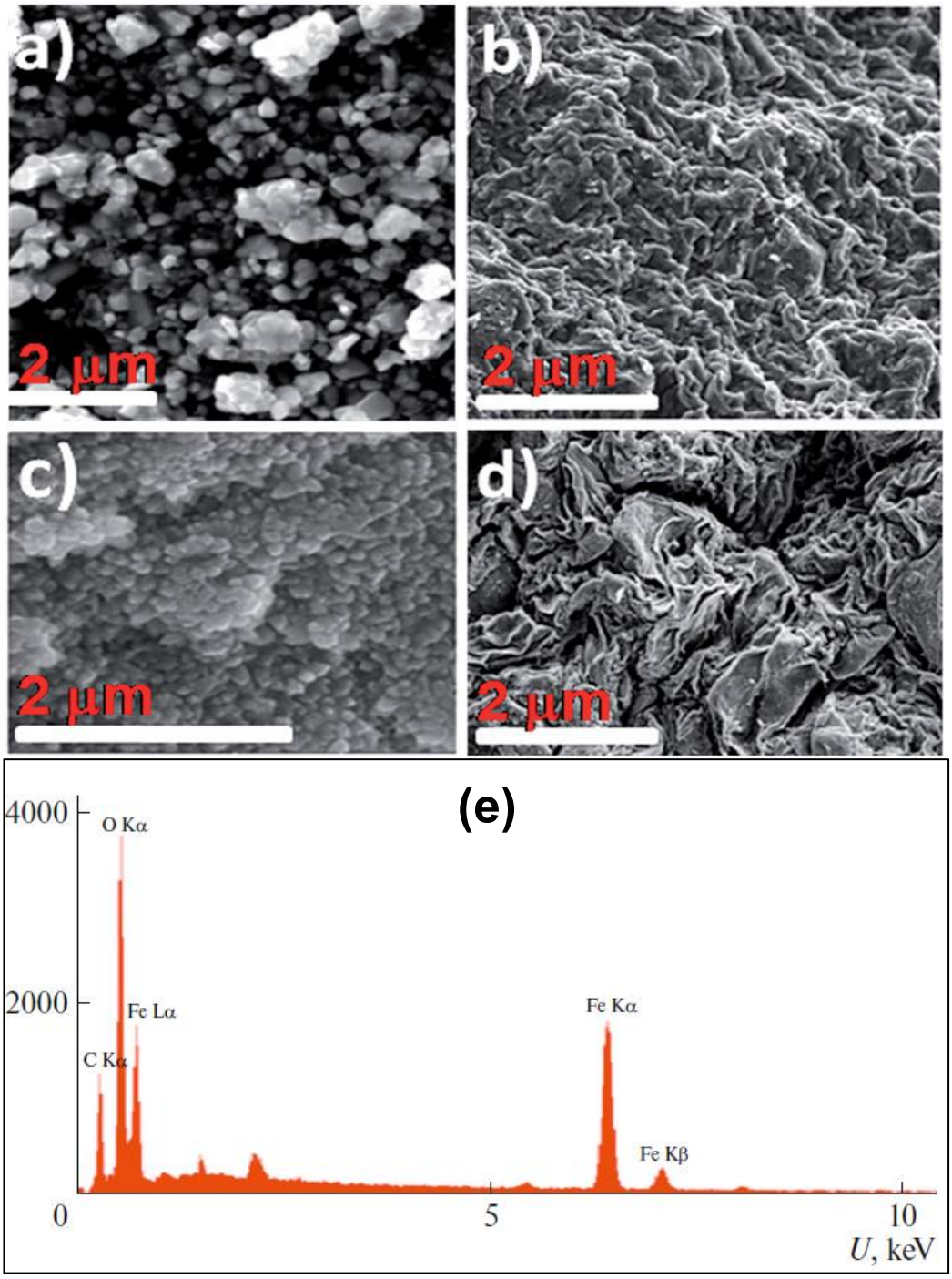

Figure 3. 9: SEM images of (a) ZnO NP's, (b) clay–alginate NC, (c and d) synthesised ZnO–clay–alginate beads, and (e) EDX of MIONs–CMC biopolymer-based hydrogel [5,27]

3.4.2 Transmission electron microscopy

Transmission electron microscopy is an analytical technique that utilises a high energy beam of electrons which are shone through a very thin sample, and the interactions between the electrons and the atoms in the sample give information about the crystal structure, dislocations and grain boundaries on the material [28]. In principle, a beam of electrons is transmitted through an ultra-thin specimen, interacting with the specimen as it passes through an image is formed and magnified as it is focused onto an imaging device to be detected by a sensor [29]. TEM (Figure 3.10) helps determine information about the growth of layers, their composition and defects in semiconductors [30,31]. A high-resolution transmission electron microscope can be used to analyse the quality, shape, size, and density of quantum wells, wires and dots [28].

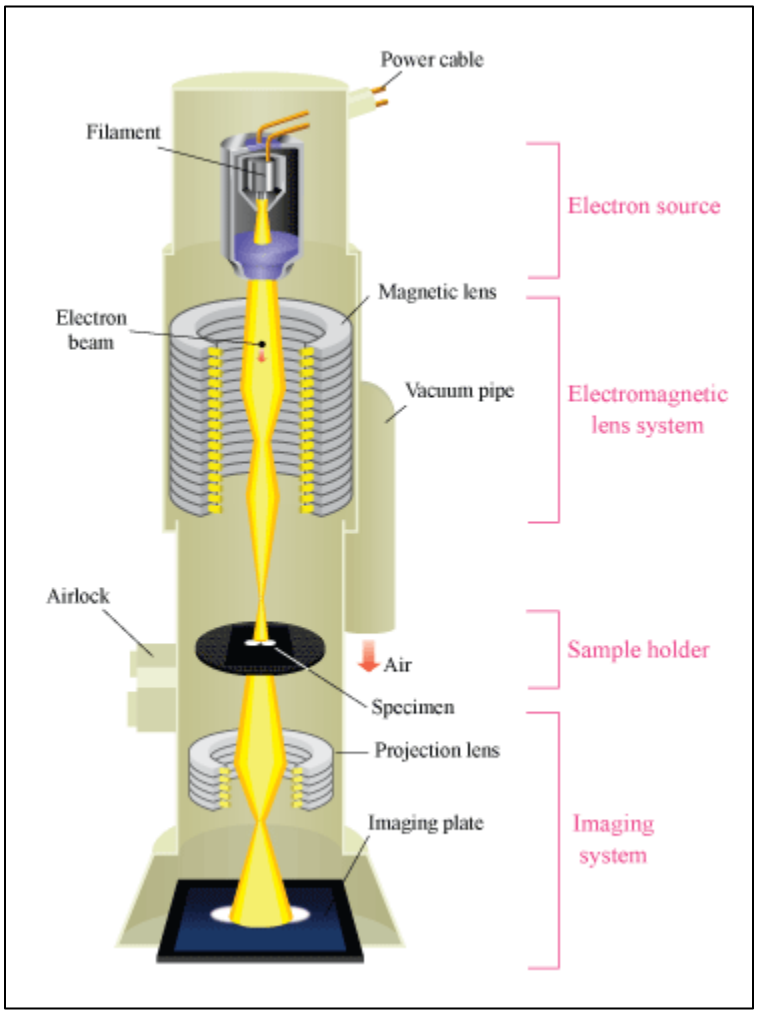

Figure 3. 10: Overview of the transmission electron microscope.

In a study conducted by Hashem *et al.* [32], CMC coated with ZnO was prepared and characterised. TEM analysis (Figure 3.11(a)) of the nanocomposite displayed the irregular shaped CMC structure coated with hexagonal-shaped ZnO nanoparticle crystals [32]. Their diameters ranged from 10 to 20 nm [32]. In another study, Fe_3O_4 nanoparticles were incorporated into polyacrylamide hydrogel (Figure 3.11(b)). The TEM analysis showed spherically shaped magnetite particles dispersed on the smooth surface of PAAm [33].

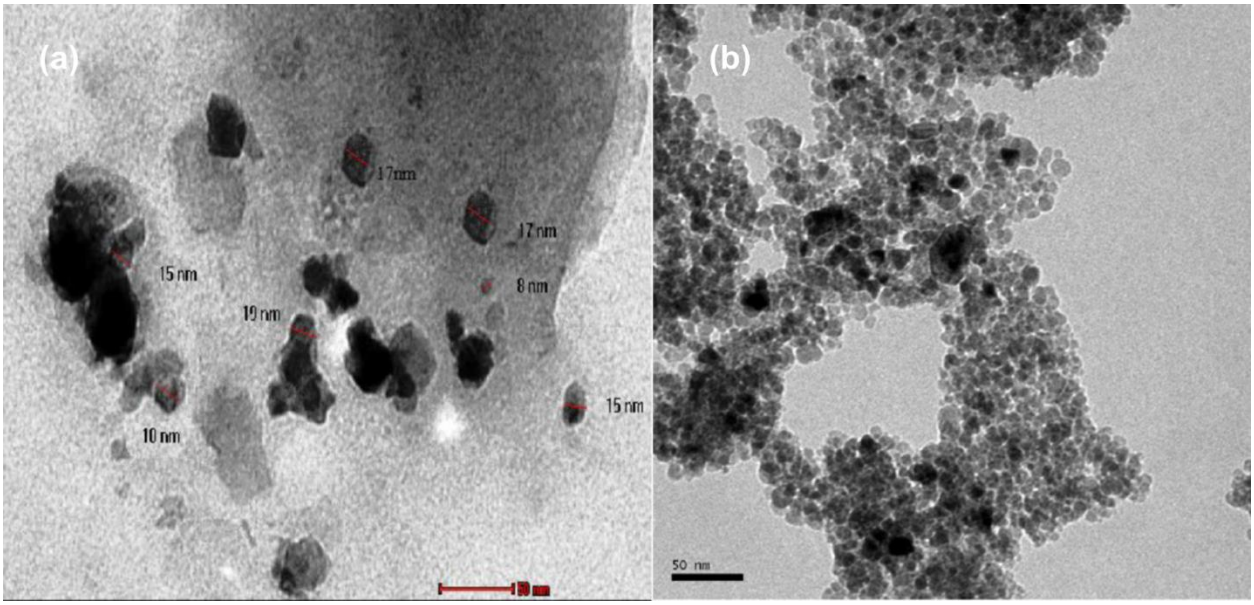

Figure 3. 11: TEM image of (a) CMC/ZnO and (b) PAAm/Fe_3O_4 nanocomposite [32,33].

3.5 CONCLUSIONS

Briefly, this chapter discussed the principles of each analytical technique and recent applications in characterising SA, CMC, Fe_3O_4, ZnO, and nanocomposite materials. The FTIR instrument was used to study the structural properties, hence confirm the successful preparation of the hydrogels and their nanocomposites. XRD was used for phase identification of the prepared materials whether they are crystalline or amorphous. To study the thermal stability of all the prepared materials, TGA was used. SEM/EDS was used for studying the morphology of the SA/PAA and CMC-cl-pAA hydrogels and their respective hydrogel nanocomposites. HR-TEM is used to examine

the internal structures of the synthesised nanocomposites and the prepared nanoparticles for which information about the particle size, the d spacing, and structure of the material can be revealed. Information about the mechanical strength of the hydrogels and their composites is provided by dynamic mechanical analysis (DMA). The UV-vis was used to determine the concentration of MB in solutions.

3.6 REFERENCES

1. Adams, F.C. (2017). X-Ray Absorption and Diffraction: Overview. Encyclopaedia of Analytical Science, 3rd ed, 1-14.
2. https://wiki.anton-paar.com/en/x-ray-diffraction-xrd/
3. Hansford, G.M. (2013). Nuclear instruments and methods in physics research an x-ray diffraction without sample preparation: proof-of-principle experiments. Nuclear Instruments and Methods in Physics Research Section A, 728,102–106.
4. Rennes, D., & Loue, D. (2017). Powder x-ray diffraction, applications. Encyclopaedia of Spectroscopy and Spectrometry, 3rd ed, 723–731.
5. Vahidhabanu, S., Karuppasamy, D., & Adeogun, I. (2017). Impregnation of zinc oxide modified clay over alginate beads: a novel material for the effective removal of congo red from wastewater, 5669–5678.
6. Loganathan, S., Valapa, R.B., Mishra, R.K., Pugazhenthi, G & Thomas, S. (2017). Thermogravimetric analysis for characterization of Nanomaterials. Thermal and Rheological Measurement Techniques for Nanomaterials Characterization, 67-108.
7. Thirunathan, P., Arnz, P., Husny, J., Gianfrancesco, A., & Perdana, J. (2018). Thermogravimetric analysis for rapid assessment of moisture diffusivity in polydisperse powder and thin film matrices. Food Chemistry, 242, 519–526.
8. Karakaya, C., Ricote, S., Albin, D., Sánchez-cortezón, E., Linares-zea, B., & Kee, R.J. (2015). Thermochimica acta thermogravimetric analysis of InCl 3 sublimation at atmospheric pressure. Thermochimica Acta, 622, 55–63.
9. https://www.netzsch-thermal-academy.com/en/advanced-materialsesting/methods/thermogravimetric-analysis/

10. Salama, A. (2015). Carboxymethyl cellulose- g -poly (acrylic acid)/ calcium phosphate composite as a multifunctional hydrogel material. Materials Letters, 157, 243–247.
11. Zirak, M., Abdollahiyan, A., Eftekhari-sis, B., & Saraei, M. (2017). Carboxymethyl cellulose coated Fe_3O_4@SiO_2 core-shell magnetic thermodynamic studies Carboxymethyl cellulose coated Fe_3O_4 @ SiO_2 core-shell magnetic nanoparticles for methylene blue removal: equilibrium, kinetic, and thermodynamic studies. Cellulose, 25(1), 503–515.
12. Dv, F. (nd). Viscoelasticity and dynamic mechanical testing, (1), 1–7.
13. Dunson, B. D. (2017). Characterization of Polymers using Dynamic Mechanical Analysis (DMA).
14. Dmas, M., & Weissenberg, T. (2015). Dynamic mechanical analysis in the analysis. Encyclopedia of Polymer Science and Technology.
15. Mohamed, M.A., Jaafar, J., Ismail, A.F., Othman, M.H.D., & Rahman, M.A. (2017). Fourier transform infrared (FTIR) Spectroscopy. In Membrane Characterization, 3-29.
16. http://chemicalinstrumentation.weebly.com/ir-spectrometry.html.
17. Lee, L.C., Liong, C., & Jemain, A.A. (2017). A contemporary review on Data 103 Pre-processing (DP) practice strategy in ATR-FTIR spectrum. Chemometrics and Intelligent Laboratory Systems, 163, 64–75.
18. Rehbein, M.C., Husmann, S., Lechner, C., Kunick, C., & Scholl, S. (2017). Fast and calibration-free determination of first-order reaction kinetics in API synthesis using in-situ ATR-FTIR. European Journal of Pharmaceutics and Biopharmaceutics, 1–6.
19. Andruch, V., Kocúrová, L., Balogh, I.S., & Jana, Š. (2012). Recent advances in coupling single-drop and dispersive liquid-liquid microextraction with UV – vis spectrophotometry and related detection techniques. Microchemical Journal, 102, 1–10.
20. Atta, A., Akl, M. A., Youssef, A. M., & Ibraheim, M. A. (2013). Superparamagnetic Core-Shell Polymeric Nanocomposites for Efficient Removal of Methylene Blue from Aqueous Solutions, 3(1), 397–419.

21. Mäntele, W., & Deniz, E. (2017). Molecular and biomolecular spectroscopy UV-vis absorption spectroscopy: Lambert-Beer reloaded, SAA, 173, 965–968.
22. Vandergriff, L. J. (1997). Nature and Properties of Light. Fundamentals of Photonics, 1–38.
23. Sancho-Parramon, J., Ferre´-Borrull, J., Bosch, S., Krasilnikova, A., & Bulir, J. (2006). New calibration method for UV-vis photothermal deflection spectroscopy setup. Applied Surface Science, 253,158–162.
24. Yoshida, A., Kaburagi, Y., & Hishiyama, Y. (2016). Scanning electron microscopy. Materials Science and Engineering of Carbon, 71-93.
25. Pereira-da-silva, M.D.A., & Ferri, F.A. (2017). Scanning Electron Microscopy. Nanocharacterization Techniques, 1-35.
26. Kirk, T.L. (2016). A Review of scanning electron microscopy in near field emission mode. Advances in Imaging and Electron Physics, 204.
27. Kurdtabar, M., Nezam, H., & Bardajee, G. R. (2018). Biocompatible Magnetic Hydrogel Nanocomposite Based on Carboxymethylcellulose: Synthesis, Cell Culture Property and Drug Delivery 1, 60(2), 231–242.
28. Wang, Z.L. (2000). Transmission electron microscopy of shape-controlled Nanocrystals and their assemblies. The Journal of Physical Chemistry B,104, 1153–1175.
29. https://www.slideshare.net/NarenYadav2/principle-of-transmission-electron-microscope.
30. Callahan, P.G., Stinville, J.C., Yao, E.R., Echlin, M.P., Titus, M.S., Graef, M., Gianola, D.S., & Pollock, T.M. (2018). Ultramicroscopy Transmission scanning electron microscopy: Defect observations and image simulations. Ultramicroscopy, 186, 49–61.
31. http://www.hk-phy.org/atomic_world/tem/tem02_e.html.
32. Hashem, M., Sharaf, S., El-hady, M. M. A., & Hebeish, A. (2013). Synthesis and characterization of novel carboxymethylcellulose hydrogels and. Carbohydrate Polymers, 95(1), 421–427.

33. Sözeri, H., Baykal, A., Kurtan, U., & Alverog, E. (2013). Fluorescence and magnetic properties of hydrogels containing Fe_3O_4 nanoparticles, 1037, 361–366.

CHAPTER FOUR

SYNTHESIS OF CARBOXYMETHYL CELLULOSE CROSSLINKED WITH POLYACRYLIC ACID (CMC-cl-PAA) HYDROGEL MODIFIED WITH MAGNETIC C30B NANOCOMPOSITE AND ITS ADSORPTION EFFICIENCY TOWARDS METHYLENE BLUE.

CHAPTER SUMMARY

Cellulose-cl-poly(acrylic acid) (CMC-cl-pAA) hydrogel and carboxymethyl cellulose-cl-poly acrylic acid magnetic Cloisite 30B (CMC-cl-pAA/ Fe_3O_4-C30B) hydrogel nanocomposite (HNC) was prepared via in situ free-radical polymerisation for adsorption of methylene blue (MB) dye. The structural, morphological characteristics, as well as thermal and mechanical properties of the prepared materials were studied through XRD, FTIR, SEM/EDS, TEM, STA and DMA. Significant improvements in thermal and mechanical properties were recognised for CMC-cl-pAA/Fe_3O_4-C30B HNC in comparison to CMC-cl-pAA hydrogel. Various factors influencing the adsorption processes such as solution pH, adsorbent dose, contact time, equilibrium concentration and equilibrium temperature were investigated in a batch mode. The adsorption kinetics and isotherm modelling data were best described by pseudo-second-order and Langmuir model. The maximum adsorption capacity for CMC-cl-pAA hydrogel and CMC-cl-pAA/Fe_3O_4-C30B HNC were found to be 1165.0 and 806.5 mg/g, respectively, determined via Langmuir model. The adsorption results conveyed that the CMC-cl-pAA hydrogel had enhanced adsorption capacity than the CMC-cl-pAA/Fe_3O_4-C30B HNC. The improved adsorption and swelling capacity led to decrement in the gel strength in the case of CMC-cl-pAA hydrogel and inverse for the CMC-cl-pAA/Fe_3O_4-C30B hydrogel nanocomposite.

4.1 INTRODUCTION

Methylene blue is a dye mostly applied in the textile and paper industry [1]. It has a planar and complex structure that is responsible for its stubbornness in removing from wastewater [2]. Exposure and indigestion to this dye (even at low concentration) may cause health problems such as vomiting, nausea, eyes burn and breathing difficulties to humans, its accumulation in water may inhibit penetration of sunlight thus hindering photosynthesis from taking place [3,4]. Various water treatment techniques namely oxidation, membrane filtration, coagulation, adsorption, and biological methods have been employed to eliminate MB dye from water [5]. Amongst these techniques, the adsorption method has been reported to be the best candidate for removal of MB owing to their easy operation, low costs, and easy design [6, 7]. Several materials have been applied for MB removal namely; fly ash, activated carbon, graphene oxide, etc [8,9,10]. However, these materials have high costs, and non-biodegradability [11]. Hence, there is dire need to develop adsorbent materials that are effective, inexpensive and easily available to enhance the adsorption efficiency and effectiveness. Hydrogels are crosslinked polymer chains that can trap fluids for a long period and are hydrophilic [7]. For this reason, hydrogels have found their use in agriculture to trap water for plants, use in making contact lenses, drug delivery, diapers, sensing and recently used as an adsorbent material [12]. Biopolymer-based hydrogels offer advantages of biodegradability. Examples of biopolymers used for hydrogel preparation include; cellulose, alginate, chitosan, chitin, and carrageenan [13]. Among these biopolymers, CMC is a negatively charged, polyelectrolyte material that behaves as a polyanion at pH greater than 4.5 and dissolves in water [14]. Due to its biocompatibility and non-toxic nature, CMC attracted much use in environmental, industrial and biomedical fields [15]. Its application in wastewater treatment was attracted by its high degree of hydrophilicity and non-toxicity [14, 16, 17]. However, CMC suffers from a lack of mechanical stability and it dissolves in water [14]. Wang et al. reported that incorporating acrylic acid onto the alumina surface improved stability and sorption of Pd (II) [18]. Hence, in this work, CMC will be crosslinked with acrylic acid using MBA as the crosslinker to form strong 3D structures of hydrophobic networks that are non-dissolvable in aqueous solution

[18]. To enhance the stability of the gel, magnetic nanoparticles and clay are incorporated in this work.

Recent studies reported that the blending of biopolymers with synthetic polymers enhances the solubility and adsorption capacity of the adsorbent [18]. Acrylic acid contains carboxyl (COO^-) functional groups and CMC contains carboxyl (COO^-) and hydroxyl (-OH) functional groups, therefore the resulting hydrogel will have more adsorptive functional groups, thus increasing the swelling and adsorption capacities [17]. Godiya *et al.* [19], successfully synthesised a cost-effective, highly adsorptive CMC/ acrylamide hydrogel composite for removal of $Cd^{2+,}$ Cu^{2+}, and Pd^{2+}. The group reported improved adsorption properties by the hydrogel. Another study reported the improvement in removal capacity of CMC for MB from 83.3 mg/g to 172.1 mg/g by incorporating PVA monomer [20]. Therefore, proof that modification with synthetic polymers improves the capacity of adsorption. Although the adsorption capacity and solubility of CMC are improved, the hydrogel composites are not easy to separate. Therefore, magnetic (Fe_3O_4) nanoparticles modified with cloisite 30B clay will be incorporated to allow easy recovery using an external magnetic force. The incorporation of inorganic materials also enhances the stability of the hydrogel. This work reports the synthesis of CMC-cl-pAA hydrogel and its Fe_3O_4-C30B nanocomposite via in situ polymerisation. The synthesised hydrogel and its hydrogel nanocomposite were characterised using various analytical techniques. The FTIR confirmed the successful incorporation of magnetic nanoparticles onto CMC-cl-pAA hydrogel. The hydrogel nanocomposite was semi-crystalline as observed from XRD. Both thermal and mechanical properties were improved. The magnetic property of CMC-cl-pAA/ Fe_3O_4-C30B HNC allowed for easy recovery of the material after application Hence showing great potential for use in removing MB and possibly other cationic dyes from aqueous solution.

4.2 MATERIALS AND METHODS

4.2.1 Materials

The biopolymer (CMC, acrylic acid (AA, 99%) monomer Initiator potassium persulfate (KPS) (≥98%; 248614), the crosslinker N, N'-methylene bis-acrylamide (MBA)(99%) was supplied by Sigma-Aldrich (South Africa). Acetone, sodium hydroxide (NaOH), ammonia solution (25%) and hydrochloric acid (HCl) were procured from Merck (South Africa). Iron (III) chloride hexahydrate ($FeCl_3.6H_2O$) and iron (II) chloride tetrahydrate ($FeCl_2.4H_2O$) were procured from Sigma Aldrich. C30B clay was supplied by Southern Clay Products (USA). All reagents used were of analytical grade. For all the experiments, deionised (DI) water was utilised. The stock solution of MB (1000 mg/L) was prepared by dissolving an appropriate amount of dye, which was purchased from Merck (South Africa) in 1 L of DI water, and the stock solution was further diluted for batch experiments.

4.2.2 Preparation of CMC-cl-pAA hydrogel

The method for preparing the hydrogel was adopted from Thakur et al., with slight modifications [1]. Briefly, a solution of CMC (0.15 g) in 100 mL deionised water was prepared and mixed with calculated amounts of AA (2.6 mL), KPS (0.108 g), and MBA (0.062 g) to a final volume of 40 mL was maintained. The reaction of crosslinked copolymerisation was initiated by exposing the mixture under a constant temperature of 70 ℃ for three hrs. During this process, the KPS generated free cellulosic radicals, followed by chain elongation through the attachment of AA monomers, crosslinking with MBA and lastly, the polymer chain termination or chain transfer resulting from the high concentration of free radicals. The obtained CMC-cl-pAA hydrogel was allowed to cool at room temperature, diced into small pieces and washed well with acetone to remove unreacted reagents. The hydrogel was further washed with distilled water, filtered and vacuum dried at 70 ℃ for 48 hrs and then ground to a fine powder using mortar and pestle.

4.2.3 Preparation of magnetic-C30B nanocomposite

Briefly, 50 mL solutions of $FeCl_3.6H_2O$ (8.00 g) and $FeCl_2.4H_2O$ (4.00 g) in separate 50 mL DI water were prepared and the two solutions were mixed together. To this mixture, 1 g of C30B clay in 50 ml distilled water was added. Followed by stirring for 30 min at 50-60 ^oC using a magnetic stirrer and addition of ammonium solution until a pH of 10 was obtained. The precipitated magnetic C30B was centrifuged for 10 min at 4000 rpm. The nanocomposite was washed numerous times with distilled water, centrifuged and dried at 70 ^oC for 24 hrs.

4.2.4 Preparation of CMC-cl-pAA/Fe_3O_4-C30B HNC

Briefly, CMC (0.15 g) was dissolved in DI water. To this solution, calculated amounts of KPS (0.108 g), AA (2.6 mL) and MBA (0.062 g) were added, and the total volume was adjusted to 30 mL. To this mixture, 10 mL solution of Fe_3O_4-C30B (0.5 g) dissolved in methanol was added and the procedure followed as discussed in 4.2.2.

4.2.5 Swelling studies

The swelling ratio (S) of the hydrogels was investigated using DI water as follows; 0.1 g of hydrogel was dissolved in 50 mL of distilled water, pH 7.0 at ambient temperature for 24 hrs to reach the maximum swelling capacity. The swollen hydrogel sample was taken out from the water, blotted up with a filter paper and weighed. The swelling ratio of the hydrogels was calculated using Eq. (4.1):

$$S\left(\frac{g}{g}\right) = \frac{W_s - W_d}{W_d} \times 100 \qquad (4.1)$$

Where S (g/g) is the swelling capacity of the hydrogel, W_s represents the mass of swollen hydrogel and W_d represents the mass of the dry hydrogel.

4.2.6 Adsorption studies

For adsorption kinetics studies, solutions with 150, 200, 250, 300, and 350 mg/L initial MB concentrations were prepared and contacted with CMC-cl-pAA hydrogel and CMC-

cl-pAA/Fe_3O_4-C30B HNC to investigate the effect of contact time in removing MB. Typically, CMC-cl-pAA/Fe_3O_4-C30B hydrogel nanocomposite (0.01 g) was mixed with 30 mL of MB solution at a pH of 7.0 in a water bath shaker. The mixture was stirred at 170 rpm and a constant temperature of 25 °C, and aliquots (3 mL) were taken at selected time intervals. The collected samples were filtered using 0.45 µm cellulose acetate syringe filters and analysed. The amount of MB was calculated using the Eq. (4.2):

$$q_e = q_t = \left(\frac{C_O - C_e}{m}\right) V \qquad (4.2)$$

where q_e and q_t represent the equilibrium capacity of MB dye on the adsorbent (mg/g) and amount of MB adsorbed per unit mass of the adsorbent (mg/g) at a certain time (t), respectively. C_e is the equilibrium concentration of MB (mg/L); m is the mass of the adsorbent (g), and V is the volume of the MB dye solution (L).

4.2.7 Regeneration studies

Regeneration experiments were carried out by immersing the MB-loaded adsorbents into 50 mL of ethanol and agitated at 170 rpm for 2 hrs. The collected absorbents were washed with DI water, dried at 50 °C, ground to a fine powder using mortar and pestle, and reused in the next cycle of adsorption. The dye adsorption/desorption runs were repeated at least four times.

4.2.8 Determination of point of zero charge

The point of zero charge (pH_{pzc}) is simply the pH at which the adsorbent surface has a net charge of zero. The pH_{pzc} is obtained from the difference between the initial and the final pH (ΔpH). To determine the pH_{pzc}, measured amounts of the hydrogel and the hydrogel nanocomposite were immersed in aqueous solutions of pH ranging between 2.0-10.0 and agitated in a shaker (170 rpm, ambient temperature) for 48 hrs. The solution pH was recorded and the pH_{pzc} was calculated as shown from the following Eq. (4.3):

$$\Delta pH = pH_{final} - pH_{initial} \quad (4.3)$$

4.2.9 Characterisation techniques

The morphologies of the prepared materials were investigated using the SEM (JSM7500F, JOEL) together with EDS was utilised to observe the morphologies and to acquire elemental mapping of samples. Spectrum II spectrometer (Perkin Elmer) was employed to record FTIR spectra in the wavenumbers between 400 and 4500 cm^{-1}. The thermal analyses were performed by STA instrument (Perkin Elmer), where the prepared materials were heated at a rate of 10 ºC/min from 30 to 600 ºC in nitrogen gas flow rate of 20 mL/min. XRD patterns were acquired with a PAnalytical Xpert Pro spectrometer employing Ni filtered CuK radiation with (λ = 1.5406 Å). The diffraction data were plotted between 5 to 70° in 2Θ utilising continuous scanning at a rate of a step size of 0.01 °/s. To study the internal structures of the synthesised materials the TEM and HR-TEM together with selected area electron diffraction (SAED) were used to study the internal morphology at 200 kV accelerating voltage with camera length of 100 mm (JOEL JEM 2100, Tokyo, Japan).

DMA was conducted on a single-cantilever bending mode using (Perkin Elmer DMA 8000) to study the mechanical stability of the synthesised materials. The frequency dependence of the loss modulus and storage modulus were performed at a fixed temperature (30 °C). The strain amplitude was set at 0.05%, and the ramp rate was 5°C/min in the frequency range 0.01 to 100 Hz. Ultraviolet-visible spectrometer (UV-vis) was utilised to analyse the MB solutions at different concentrations and determine the remaining MB concentrations after adsorption. The pH of the solution was adjusted using (0.1 M) HCl and/or NaOH and the pH readings were obtained with a Henna instrument.

4.3. RESULTS AND DISCUSSION

4.3.1. Optimisation study based on the synthesised hydrogel and hydrogel nanocomposite.

The swelling capacity of hydrogels is controlled by the size of its pores, the presence of hydrophilic groups on its surface and intermolecular spaces in its structure [21]. An increase in the amount of initiator (KPS) between 0.11-0.65 g, resulted in a decline in the swelling capacity of the hydrogel. The decrease in the swelling capacity with increasing content of initiator could be attributed to the presence of many radicals being generated, which encouraged chain termination. Therefore, the optimum KPS content was 0.11 g. These results agree with those obtained by Makhado et al. [21], in removing methylene blue using Xanthan gum-based hydrogel incorporated with o-MWCNTs. Below an initiator amount of 0.11 g, the hydrogel could not form as there was not enough initiator to encourage chain formation. The optimum initiator amount was 0.11 g (Figure 4.1(a)). Optimisation of the cross-linker showed the swelling capacity decreased with an increasing amount of cross-linker (Figure 4.1(b)). This was due to the inability of the hydrophilic polymer chain to dissolve in water as a result of hindrance by the crosslinker (MBA) [22]. During optimisation of the volume of acrylic acid (AA) monomer (Figure 4.1(c)), the swelling capacity of the hydrogel increased at lower volumes, followed by a decrease with increase in AA. The initial increase in swelling capacity could have been due to the abundance in hydrophilic groups. The further decrease may have been due to the inability of the monomer and free radicals to freely move due to increased viscosity or secondly, preferential homo-polymerisation may have been favoured over polymerisation with AA [23].

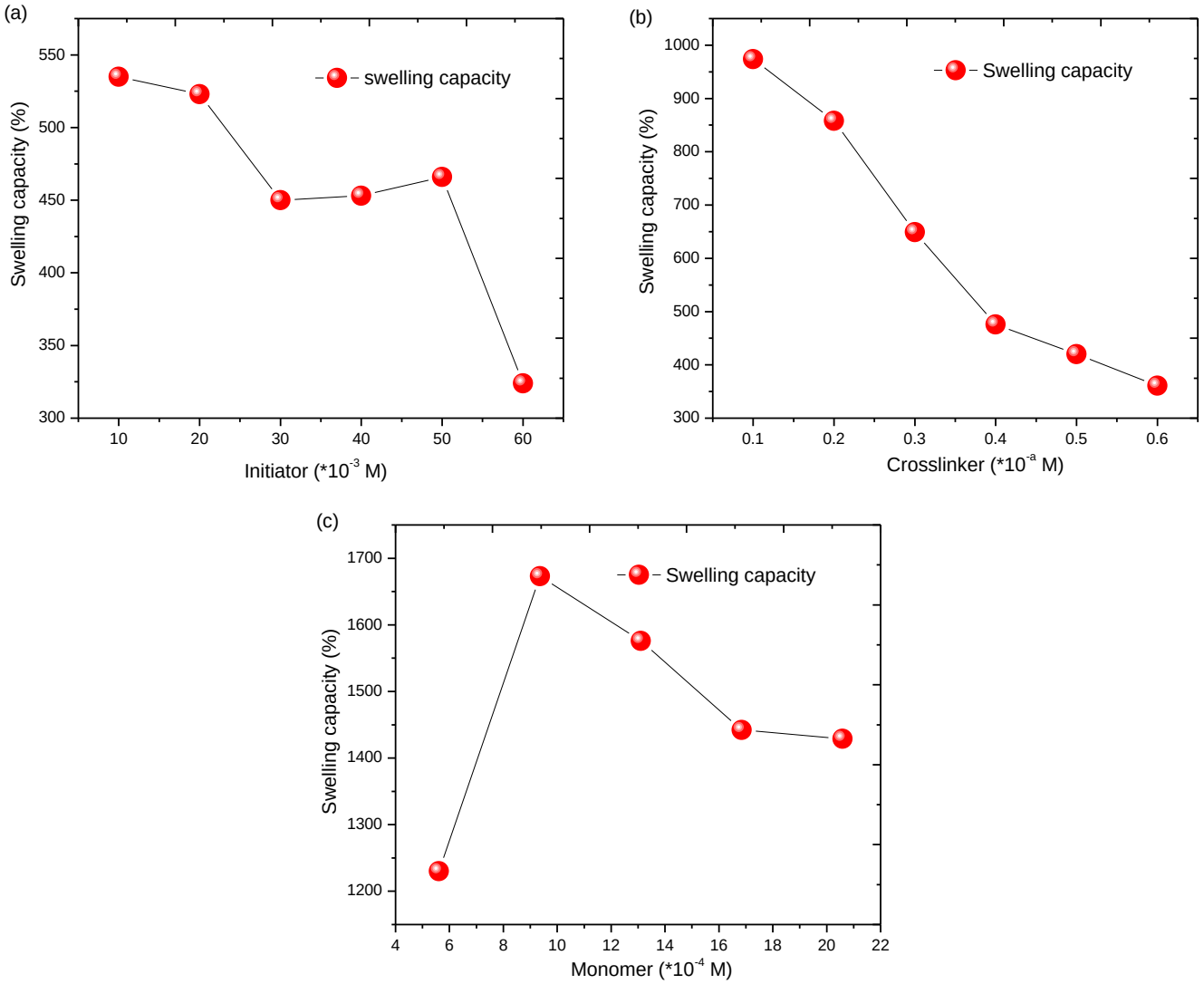

Figure 4.1: Effect of the initiator (a), crosslinker (b), and monomer (c) on the optimisation of the CMC-cl-pAA hydrogel.

4.3.2. Characterisation of materials

4.3.2.1. FTIR analysis

The structural changes on CMC were confirmed by FTIR as revealed in Figure 4.2(a). The spectrum of CMC shows the presence of hydroxyl groups from 3000-3500 cm^{-1}, a CH stretch at 2900 cm^{-1}, asymmetric and symmetric -OH groups of carboxylic acid at 1442 and 1392 cm^{-1} [24,25]. The peaks at 1000 cm^{-1} are assigned to the C-O-C stretches, those at 1650 cm^{-1} match to the carbonyl groups of the carboxylic acid functional groups. These results are in good agreement with the results obtained in the

literature [26]. Upon crosslinking of pAA with CMC, there was a shift in the peaks and an increase in intensities. This could be attributed to the influence of the same groups coming from the acrylic acid moieties. Furthermore, a peak at 1392 cm^{-1} on CMC disappears upon crosslinking with acrylic acid, indicating the symmetric -OH groups took part in reacting with the monomer during polymerisation as also reported by Salama, [27]. Therefore, confirming the successful synthesis of CMC-cl-pAA hydrogel. On the spectrum of Fe_3O_4-C30B, two major peaks at 528 cm^{-1} and 1080 cm^{-1} corresponding to the Fe-O bend of the magnetite and the Si-O-Si stretch of C30B were observed [28, 29]. This suggested the successful incorporation of magnetite particles onto the clay surface. After incorporation of magnetic C30B to the CMC-cl-pAA hydrogel, new peaks were observed on the CMC-cl-pAA/Fe_3O_4-C30B spectrum at approximately 1000 cm^{-1} and 528 cm^{-1}, which correspond to the Si-O-Si stretch of C30B clay and the Fe-O vibration of Fe_3O_4 [30, 31]. The appearance of these peaks confirms the successful preparation of CMC-cl-pAA/Fe_3O_4-C30B hydrogel nanocomposite.

4.3.2.2. XRD analysis

The XRD analysis was carried out for phase identification of all the synthesised materials. In Figure 4.2(b) diffractogram of CMC, two sharp peaks of CMC are observed at 2θ = 9.0° and 2θ = 21.8°, indicating a well organised CMC with a polycrystalline structure [27]. Upon copolymerisation and crosslinking with pAA, the CMC peaks were broader with decreased intensities, indicating the glassy amorphous nature of the hydrogel composite [27]. According to Shen et al., the disruption of the ordered arrangement of CMC indicated that polymerisation had taken place [28]. The CMC-cl-pAA/Fe_3O_4-C30B hydrogel nanocomposite diffractogram shows the CMC/pAA amorphous broad peak at 2θ = 18.5° with the appearance of new peaks at 2θ = 5°, corresponding to the C30B diffraction and 2θ = 30.0° (220), 36.0° (311), 44.1° (400), 57.0° (511) and 62.2° (440) corresponding to the characteristic diffractions of Fe_3O_4 [28,33]. Furthermore, the shape of some peaks changed, some increased in height, others became small and their width broadened in some cases, demonstrating a good distribution of the magnetic clay layers [34]. This suggests cross-linking with Fe_3O_4-C30B was successfully achieved.

4.3.2.3. Thermal analysis

The CMC thermogram in Figure 4.2(c) showed two degradation steps. The 10% weight loss from 100-300 ˚C could be due to the moisture lost and the second 45% weight loss could be the polysaccharide backbone decomposition [32]. On the CMC-cl-pAA hydrogel, three stages are observed, the first degradation from 100-250 ˚C is due to the moisture lost in the structure and residual solvents. From 250-330 ˚C the step is due to degradation of the CMC polymer chains, and the last step from 330-500 ˚C is due to degradation of the pAA moiety. Mishra and Shen reported similar results [32, 35]. From these results, it could be observed that the degradation of CMC-cl-pAA/Fe_3O_4-C30B hydrogel nanocomposite occurs at a slower rate than the hydrogel alone. Degradation of CMC-cl-pAA/Fe_3O_4-C30B hydrogel nanocomposite takes place in two steps. The initial degradation step shows a weight loss of about 11% from 112 to 317 °C, which could be attributed to the loss of moisture and solvents [36]. The second degradation could be attributed to the disruption of the crosslinks in the polymer structure and the decomposition of the CMC-cl-pAA/Fe_3O_4-C30B hydrogel nanocomposite [33, 37, 38]. The slow degradation and decreased weigh loss of the CMC-cl-pAA/Fe_3O_4-C30B HNC indicated that the coating with magnetic C30B enhanced the thermal stability of the hydrogel. At lower temperatures, both the hydrogel composite and the hydrogel nanocomposite are stable, which is important for application in the removal of dyes to ensure that the adsorbent material will be able to remove pollutants without losing its structural integrity.

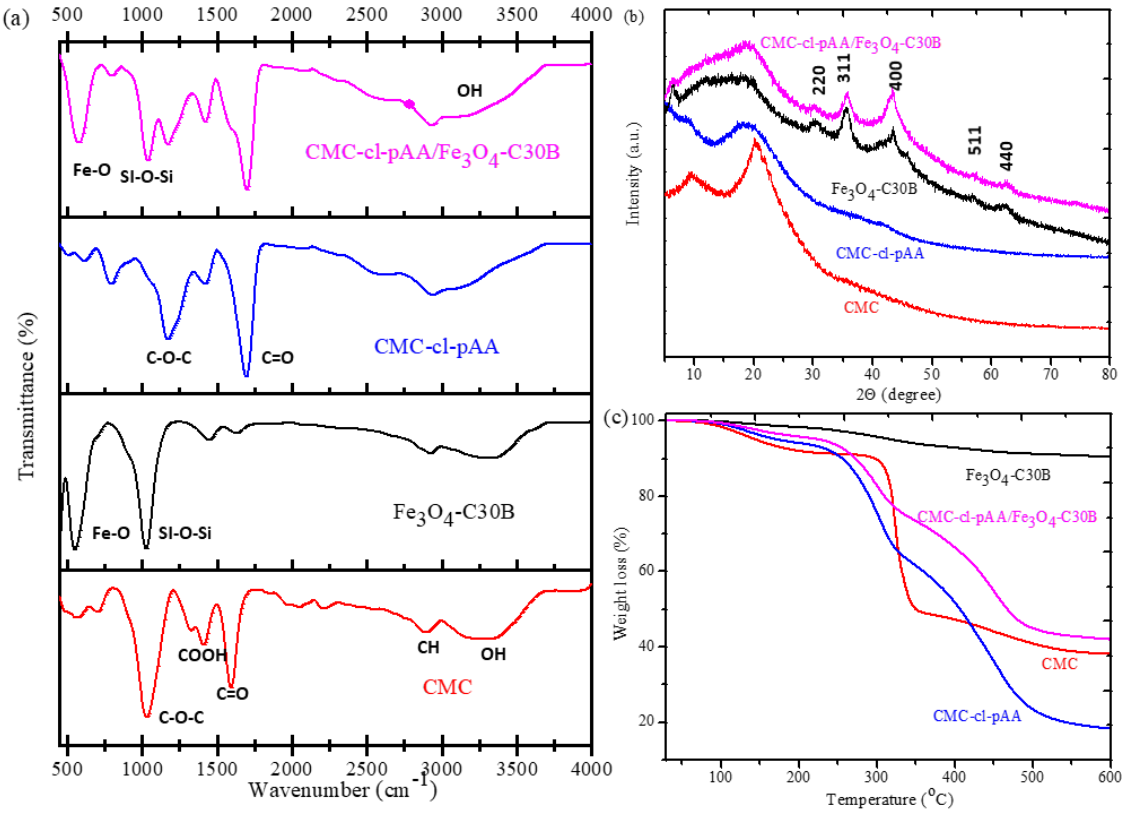

Figure 4. 2:FTIR (a), XRD spectra (b), and TGA of CMC, CMC-cl-pAA hydrogel, Fe_3O_4-C30B, and CMC-cl-pAA/Fe_3O_4-C30B hydrogel nanocomposite.

4.3.2.4. Morphological characterisations

The scanning electron microscopy (SEM) images in Figure 4.3 show the surface morphology of CMC, CMC-cl-pAA hydrogel, Fe_3O_4-C30B, and CMC-cl-pAA/Fe_3O_4-C30B. According to Bao et al., the ability of a hydrogel to retain and absorb water depends on the porosity and the pore size of the material [39]. Therefore, the more microporous the material is, the higher its ability to absorb fluids. On the CMC micrograph in Figure 4.3(a), the structure of CMC was observed to be irregularly shaped with some pores. These results were similar to those obtained by Salama [27]. Upon crosslinking with pAA Figure 4.3(b), the CMC inter-connections were more well-defined, with more irregular shape [40]. The pores formed in the hydrogel are convenient for the penetration of water and dye molecules across the hydrogel composite structure [41]. The image in Figure 4.3(c) showed tiny spherical magnetite

particles on the surface of the clay sheet [1]. In Figure 4.3(d), a structure of well-defined pores with well-defined interconnections was observed. This was due to the presence of C30B clay and Fe_3O_4 which acted as a crosslinker and increased the crosslinking density of the material [34, 39]. Additionally, tiny particles of magnetite were observed on the surface of the irregular-shaped hydrogel, this confirmed the successful synthesis and incorporation of magnetic clay on the hydrogel surface. Furthermore, the existence of Fe_3O_4-C30B in the hydrogel composition was confirmed by EDS analysis Figure 4.3(e). The EDS spectrum showed the oxygen(O) and iron (Fe) peaks of the magnetite nanoparticles, and the silicon (Si), aluminium (Al) and sulphur (S) peaks of C30B clay.

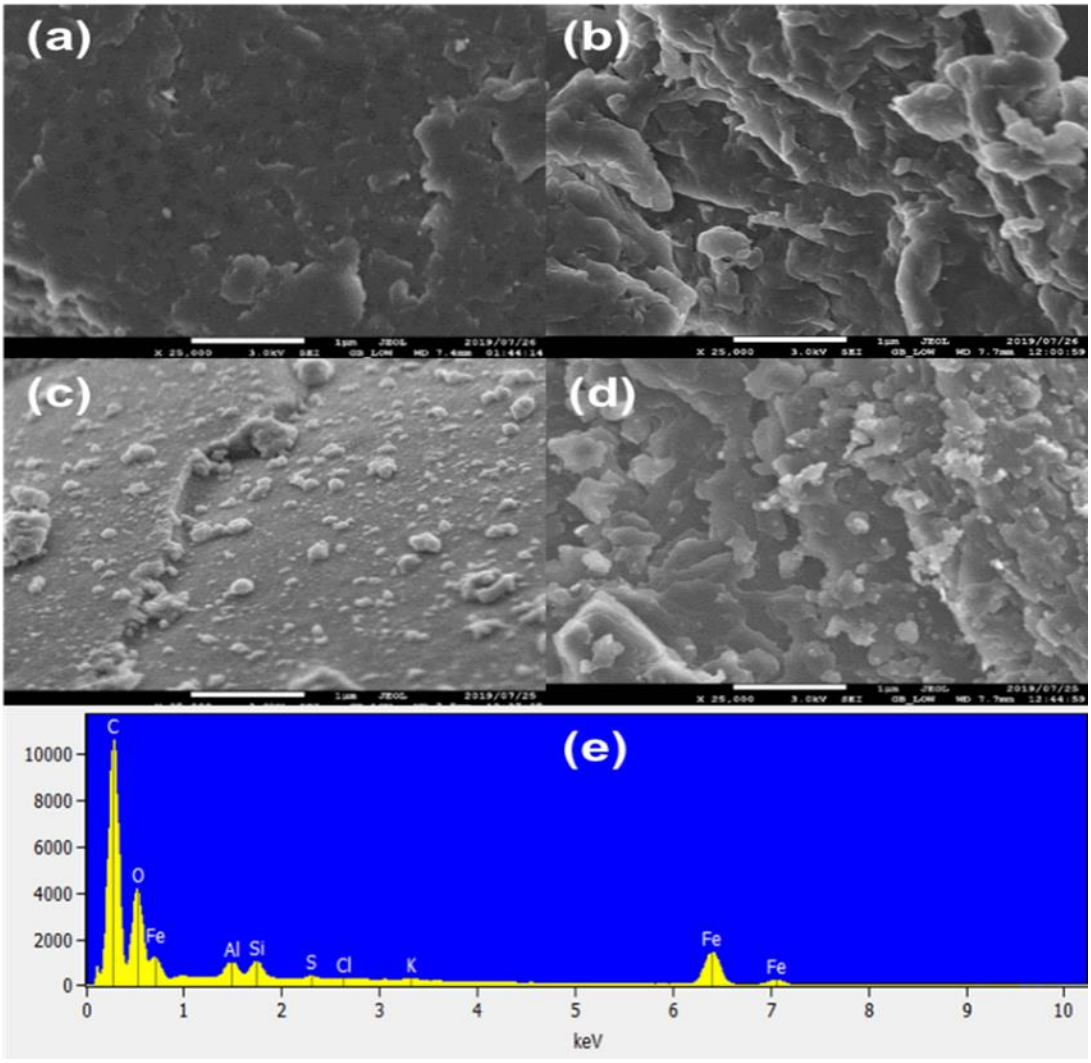

Figure 4. 3: SEM image resolution of 25x of CMC (a), CMC-cl-pAA hydrogel (b), Fe3O4-C30B (c), CMC-cl-pAA/ Fe3O4-C30B (d), and EDS analysis.

Figure 4.4(a) and (b) show the dispersion of spherical shaped magnetic particles over the C30B clay sheets. At some parts of the product, the magnetite particles are clustered together indicating agglomeration [42]. The HRTEM and SAED were employed to further investigate the crystallinity of the Fe_3O_4-C30B nanocomposite. Figure 4.4(c), HRTEM shows the internal crystalline structure of magnetite and a characteristic d-spacing of 0.2505 nm corresponding to the 311 planes of magnetite [44]. From the SAED shown in Figure 4.4(d), a white dash line circle which is characteristic of crystal structures is observed [43]. Furthermore, dotted concentric rings were observed, which occur as a result of the diffraction of particles of different orientations, in this case, the planes of cubic Fe_3O_4 [28]. The scattered white light from the nanoparticles is not very bright compared to the results reported by Sitthichai et al, which could be due to the CMC hydrogel contents [28]. It could, therefore, be confirmed that the material possessed both crystalline and amorphous properties as also observed from XRD results.

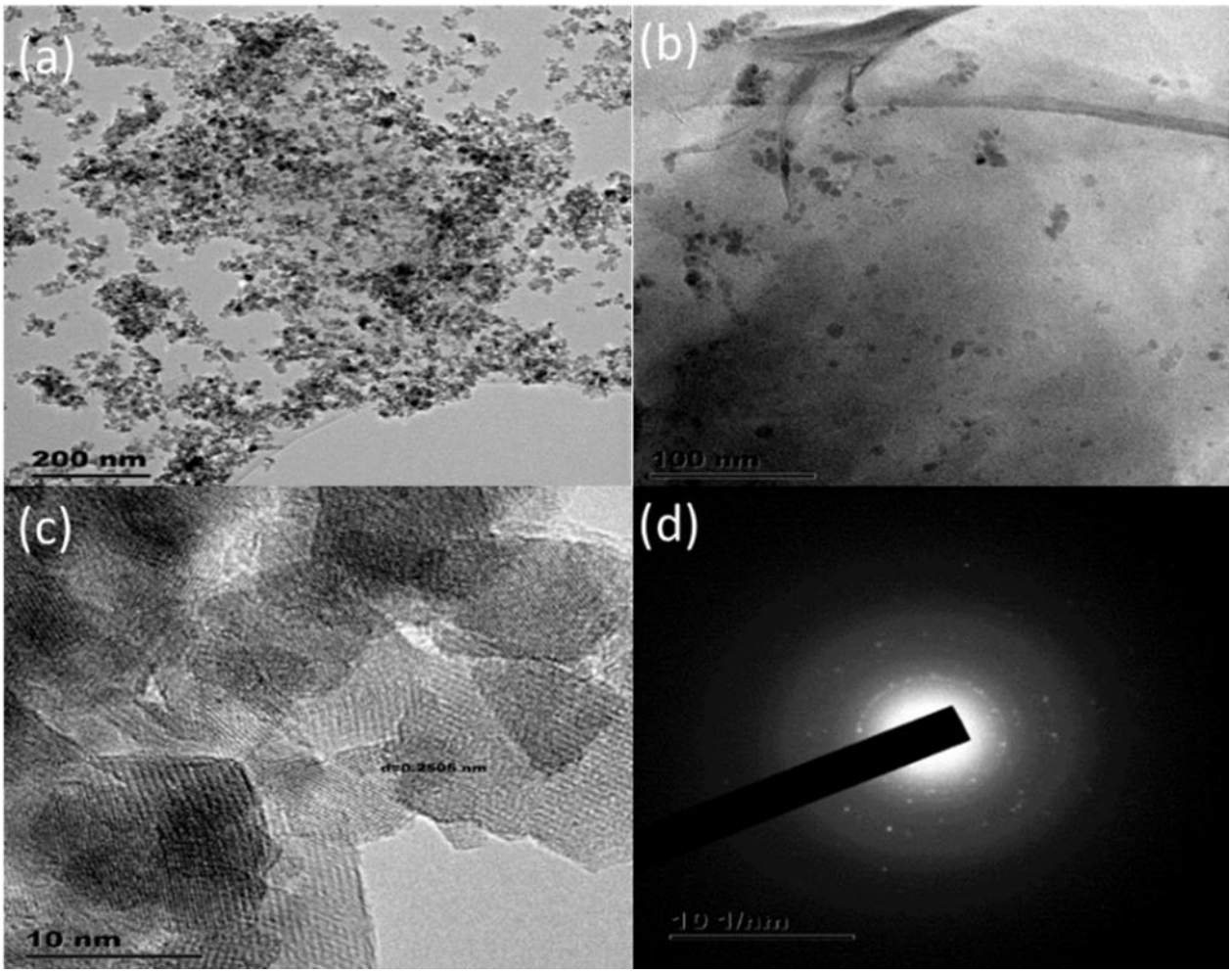

Figure 4. 4: TEM images (a) and (b), HR-TEM image (c), and SAED pattern (d) of CMC-cl-pAA/Fe_3O_4-C30B hydrogel nanocomposite..

4.3.2.5. Mechanical properties

The response of the CMC-cl-pAA/Fe_3O_4-C30B HNC to an oscillatory deformation in tension-torsion mode relative to the temperature was measured using DMA. Figure 4.5 shows the storage (G') and loss (G'') moduli response to the frequency of CMC-cl-pAA hydrogel and CMC-cl-pAA/Fe_3O_4-C30B hydrogel nanocomposites. Upon observation, the storage modulus of the CMC-cl-pAA/Fe_3O_4-C30B HNC was higher than of the CMC-cl-pAA hydrogel, indicating that the HNC can store deformation energy better than the hydrogel [45]. This could be attributed to the highly crosslinked nature of the nanocomposite as a result of crosslinks from the MBA and the ability of iron atoms and

the C30B clay to act as cross-linkers [34]. These findings are in line with the results obtained in a study by Peng et al., of cellulose-MMT hydrogel for removing MB dye [16]. The literature also suggests that the storage modulus is directly propositional to the crosslinking density [46]. These findings suggest that the blending of inorganic components with hydrogel polymer matrices enhance the hydrogel mechanical properties [47]. Enhanced mechanical properties could allow the stability of material when applied in removing the dye in different conditions. The loss modulus as observed in Figure 4.5(b) overlap with each other, this indicates that both the CMC-cl-pAA hydrogel and the CMC-cl-pAA/Fe_3O_4-C30B HNC lose heat energy similarly.

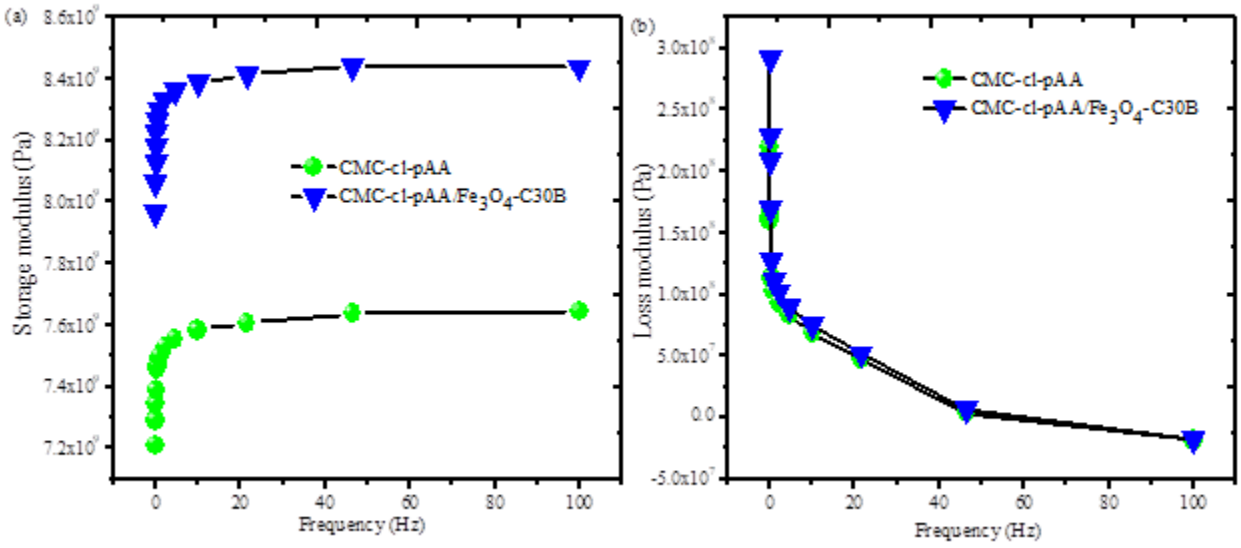

Figure 4. 5: Storage (a), and loss modulus (b) of CMC-cl-pAA hydrogel and CMC-cl-pAA/ Fe_3O_4-C30B hydrogel nanocomposite.

4.3.3. Adsorption studies

4.3.3.1. Factors affecting the adsorption process

4.3.3.1.1 Effect of pH and dose

The effect of solution pH in removing methylene blue (MB) using CMC-cl-pAA hydrogel and CMC-cl-pAA/Fe_3O_4-C30B hydrogel nanocomposite was studied at 25 ^oC (Figure 4.6(a)). The solution pH was controlled in the range of 3.0 to 10.0. CMC and AA contain hydrophilic groups such as the carboxylic (COO^-) group on their surface [17]. At lower pH, the active sites are protonated, resulting in repulsion between the positive adsorbent and the cationic MB dye molecules. When the solution pH was increased from 3.0 to 10.0, the removal capacities of CMC-cl-pAA hydrogel and CMC-cl-pAA/Fe_3O_4-C30B hydrogel nanocomposite increased from 528 to 597 mg/g and 312 to 592 mg/g, respectively. The adsorption equilibrium was obtained from pH 5.0 for the hydrogel and from pH 7.0 for the CMC-cl-pAA/Fe_3O_4-C30B hydrogel nanocomposite.

At higher pH, the active sites become negatively charged which encourage electrostatic attraction with the cationic dye molecules, thus the adsorption capacity is increased in both cases for the CMC-cl-pAA hydrogel and CMC-cl-pAA/Fe_3O_4-C30B hydrogel nanocomposite. Pourjavadi et al. reported similar results in the removal of malachite green dye [49]. The removal capacity of MB for the nanocomposite was observed to be lower than that of the hydrogel. This could be due to the incorporation of Fe_3O_4-C30B clay which promoted more crosslinked networks in the polymer matrix, leading to a decline in the removal capacity [48]. Similar results were also reported by Makhado et al. [21], in the removal of MB using XG-cl-pAA/o-MWCNTs hydrogel nanocomposite.

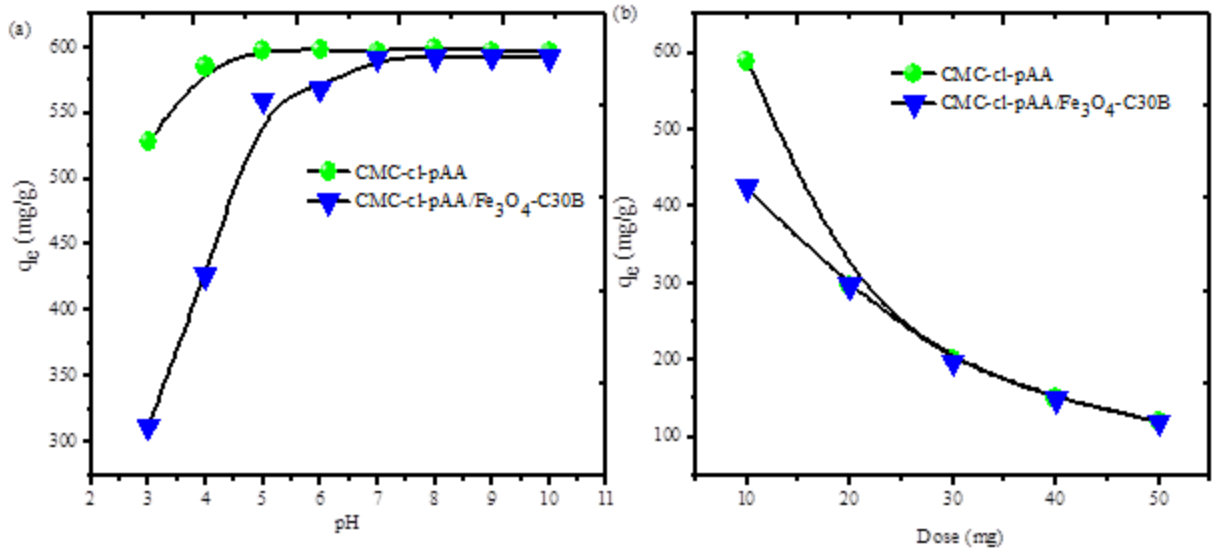

Figure 4. 6: Effect of pH (a) and dose (b) on the removal of MB by CMC-cl-pAA hydrogel and CMC-cl-pAA/Fe_3O_4-C30B HNC.

The adsorbent dose effect was investigated from the range of 10-50 mg. In Figure 4.6(b), it could be seen that the removal capacity of both adsorbents decreased with increasing adsorbent dose. Hu et al., reported that at a lower dose, the active sites fully take part in adsorbing MB, resulting in high removal capacity [50]. However, at high dose, the equilibrium is readily reached owing to the presence of osmotic pressure despite the abundance of active sites. These results are following the result obtained by Makhado et al., where they reported that the agglomeration of the active sites on the adsorbent surface and the heightened diffusion path length could also be responsible for the reduction in adsorption capacity [21]. The removal capacity for the CMC-cl-pAA hydrogel was higher compared to the CMC-cl-pAA/ Fe_3O_4-C30B hydrogel nanocomposite. This could also be attributed to the highly crosslinked structure of the polymer caused by incorporating the nanofillers [48].

4.3.3.1.2 Point of zero-charge

To study the surface charge of CMC-cl-pAA hydrogel and CMC-cl-pAA/Fe_3O_4-C30B hydrogel nanocomposite, the pH_{pzc} was performed and the plot of ΔpH as a function of $pH_{initial}$ is depicted in Fig.4.7 (a,b). The pH_{pzc} of CMC-cl-pAA hydrogel and CMC-cl-pAA/Fe_3O_4-C30B hydrogel nanocomposite are 3.13 and 3.63, respectively. At pH > pHpzc, the surface of adsorbents had a net positive charge, while at pH < pH_{pzc} the surface had a net negative charge. Both adsorbents showed a similar trend throughout the studied pH range. However, CMC-cl-pAA/Fe_3O_4-C30B hydrogel nanocomposite displayed a slightly higher pH_{pzc} than CMC-cl-pAA hydrogel. This surface change confirms the incorporation of Fe_3O_4-C30B nanocomposite on the CMC-cl-pAA hydrogel network. These findings suggest that the change in the pH value during the adsorption process can induce changes in the adsorption pathways. The effect of pH on the adsorption was explained by strong electrostatic attraction between synthesized adsorbents and MB molecules. Makhado et al. [21,22] observed similar trends in the case of xanthan gum-cl-poly acrylic acid/oxidized MWCNTs (XG-cl-pAA/o-MWCNTs) hydrogel nanocomposite.

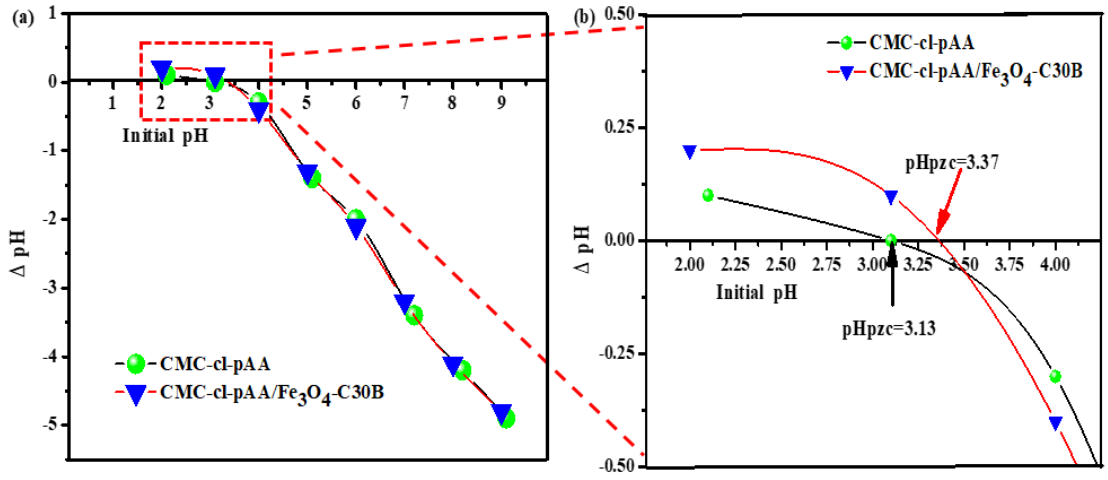

Figure 4. 7: The pHpzc of CMC-cl-pAA hydrogel and CMC-cl-pAA/Fe_3O_4-C30B HNC.

4.3.3.2. Adsorption kinetic studies

Adsorption kinetics rate equation is important for determining the rate of adsorbing MB. In Figure 4.8(a), the dependence of adsorption on contact time was examined and it could be seen that as the contact time increases, the adsorption capacities of CMC-cl-pAA hydrogel and CMC-cl-pAA/Fe_3O_4-C30B hydrogel nanocomposite also increases [8]. This could be due to enough time given for the anionic adsorbent to interact with the cationic MB. The adsorption reached equilibrium after 25 min. Therefore, the optimum time for MB adsorption by the CMC-cl-pAA hydrogel composite was 25 min, which was faster than that of the CMC-cl-pAA/Fe_3O_4-C30B hydrogel nanocomposite. The plots of pseudo-first order (Figure 4.8(a)) and pseudo-second-order (Figure 4.8(b)) kinetics models for the CMC-cl-pAA hydrogel and CMC-cl-pAA/Fe_3O_4-C30B hydrogel nanocomposite were investigated. The obtained data were fitted onto the linearised kinetics equations namely; pseudo-first order (Eq. 4.3) and pseudo-second-order (Eq. 4.4) to study the adsorption rates. From the obtained data tabulated in Table 4.1, the correlation coefficient (R^2) obtained from pseudo-second-order was higher and/or closer to 1 than that of the pseudo-first order. This implies that the surface adsorption is the rate-limiting step and is governed by chemisorption and the physicochemical interactions between two phases. In addition, the experimental q_e values (597.9 mg/g and 537.0 mg/g) were closer to the calculated q_e (598.8 mg/g and 546.4 mg/g) obtained from the pseudo-second-order kinetics for CMC-cl-pAA hydrogel and CMC-cl-pAA/Fe_3O_4-C30B hydrogel nanocomposite, respectively.

$$\log(q_e - q_t) = lnq_e - K_1 t \tag{4.3}$$

$$\frac{t}{q_t} = \frac{1}{K_1' q_e^2} + \frac{t}{q_e} \tag{4.4}$$

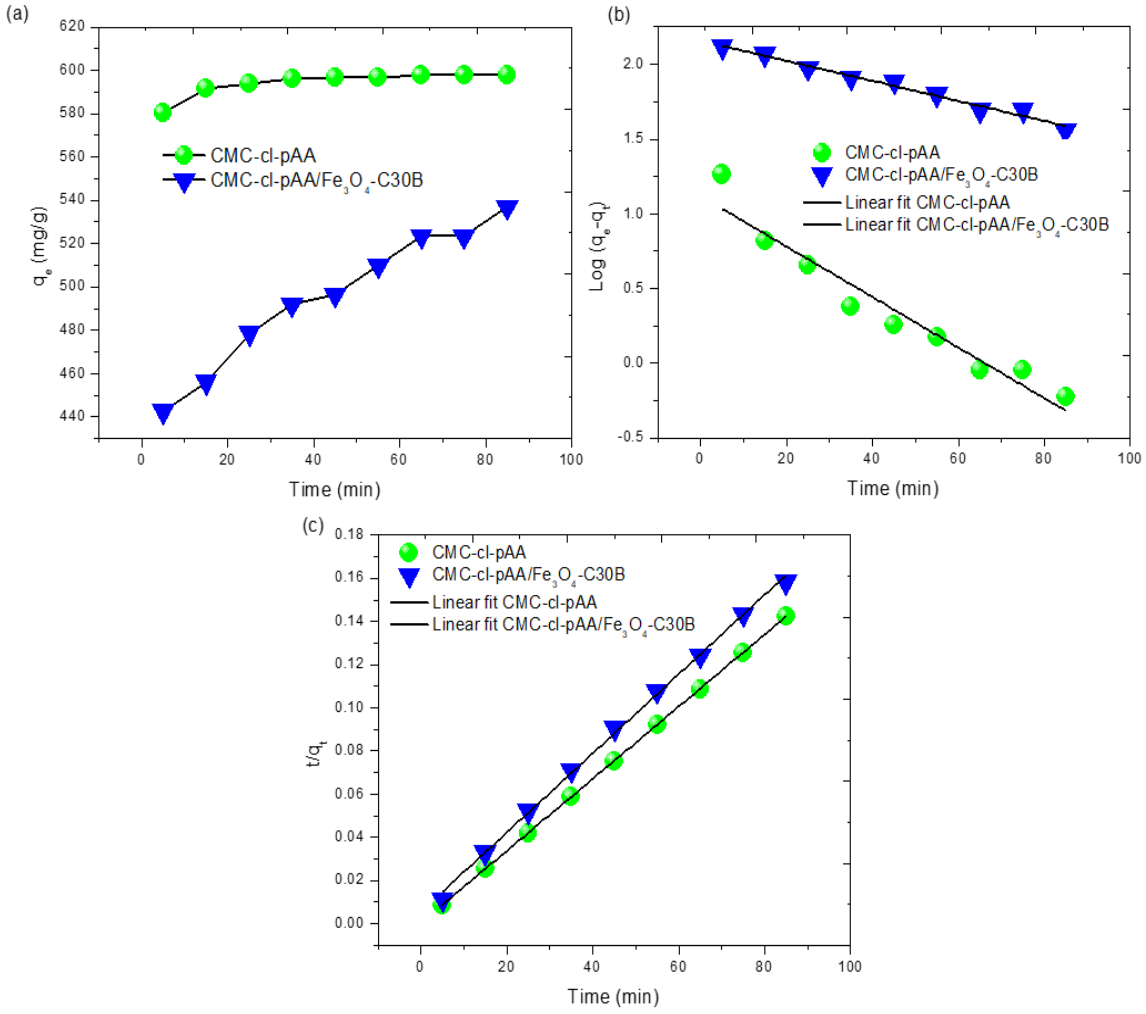

Figure 4. 8: Effect of time (a), pseudo-first order (b), and pseudo-second order (c) kinetics models for CMC-cl-pAA hydrogel and CMC-cl-pAA/ Fe_3O_4-C30B hydrogel nanocomposite.

Table 4.1: Shows pseudo-first order and second-order isotherm models result for CMC-cl-pAA hydrogel and CMC-cl-pAA/Fe_3O_4-C30B hydrogel nanocomposite.

	Pseudo-first-order			Pseudo-second-order		
Parameters	$q_{e\ (cal.)}$ (mg/g)	K_1 (min^{-1})	R^2	$q_{e\ (cal.)}$ (mg/g)	K'_2 (min^{-1})	R^2
CMC-cl-pAA hydrogel	3.063	0.0169	0.929	598.9	5.431	0.999
CMC-cl-pAA/Fe_3O_4-C30B hydrogel nanocomposite	8.648	0.007	0.980	546.4	0.333	0.998

4.3.3.3. Adsorption isotherm studies

From the plot of concentration versus removal capacity Figure 4.9(a), it could be observed that as increasing the concentration of MB solution increased the removal capacity. The sorption equilibriums were reached at 300 mg/L for the CMC-cl-pAA hydrogel and CMC-cl-pAA/Fe_3O_4-C30B hydrogel nanocomposite, respectively. The increase with increasing initial concentration could be ascribed to the rise in the driving force of the concentration gradient [51,52]. Additionally, the diffusion of dye molecules in bulk solution increases towards the CMC-cl-pAA hydrogel and CMC-cl-pAA/Fe_3O_4-C30B hydrogel nanocomposite external surface.

The Langmuir, Freundlich and Temkin adsorption isotherm models were used to study the adsorption mechanism governing the removal of MB. Details of the isotherm models are discussed in the supplementary information. Using the linear regression method, the values of isotherm constants were determined and recorded in Table 4.2. From the data obtained, the calculated values of correlation coefficient (R^2) for each isotherm model were compared for both the hydrogel and the hydrogel nanocomposite, in which the

highest value of R^2 suggested the best fitting model of adsorption. The values of R^2 decreased in the order; Langmuir > Freundlich > Temkin. The Langmuir isotherm model had the highest R^2 values of 0.948 and 0.989 for the CMC-cl-pAA hydrogel and CMC-cl-pAA/Fe_3O_4-C30B HNC, respectively. Therefore, Langmuir isotherm model was favoured, suggesting that adsorption of MB on the surfaces of CMC-cl-pAA hydrogel and CMC-cl-pAA/Fe_3O_4-C30B hydrogel nanocomposite occurred in a monolayer coverage, further implying that the active sites attracted the MB molecules with the same amount of energy such that a single layer of homogeneous sorption was obtained. Similar results were reported by Bhaumik et al. [51], in the removal of hexavalent chromium. The R_L values found in the present study were in the range of 0.12-0.47 and 0.02-0.38 for CMC-cl-pAA hydrogel and CMC-cl-pAA/Fe_3O_4-C30B hydrogel nanocomposite, respectively, indicating that adsorption of MB was favourable ($0 < RL < 1$). These results demonstrate that CMC-cl-pAA/Fe_3O_4-C30B hydrogel nanocomposite is a more efficient adsorbent for removing MB dye from aqueous solution. The adsorption capacity (q_m) obtained in the present study was compared with reported adsorption capacities in the literature (Table 4.3) for the removal of methylene blue. The synthesised CMC-cl-pAA hydrogel and CMC-cl-pAA/Fe_3O_4-C30B hydrogel nanocomposite possessed higher adsorption capacity. This could be attributed to the availability of adsorptive groups resulting from the acrylic acid and the carboxymethylated cellulose backbone.

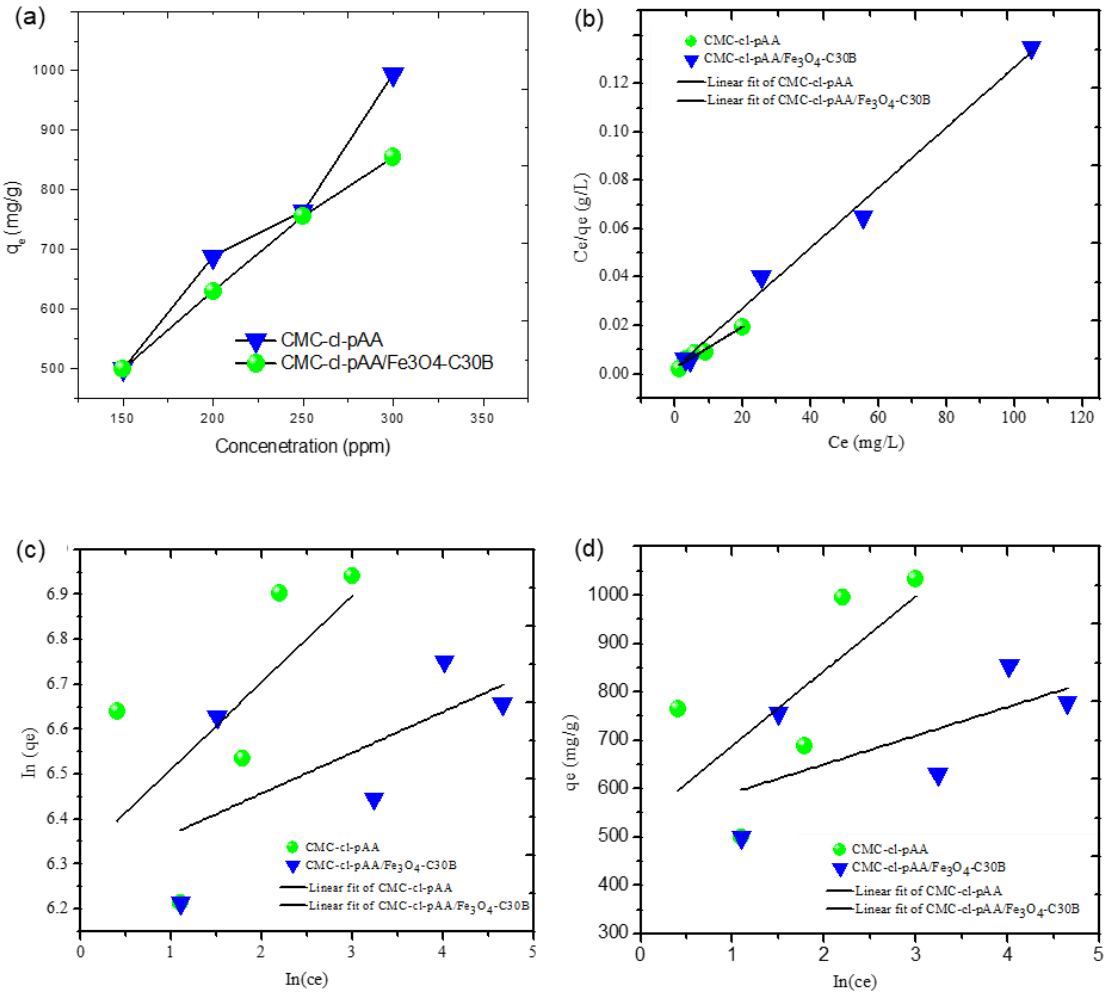

Figure 4. 9: Effect of concentration (a), Langmuir (b), Freundlich (c), and Temkin (d) isotherm models for CMC-cl-pAA hydrogel and CMC-cl-pAA/Fe_3O_4-C30B hydrogel nanocomposite.

Table 4.2: CMC-cl-pAA hydrogel and CMC-cl pAA/Fe_3O_4-C30B HNC for various isotherm models.

sotherm models	**Isotherm constants**	**CMC-cl-pAA hydrogel**	**CMC-cl-pAA/Fe_3O_4-C30B HNC**
Langmuir	q_m(mg/g)	1165	806.5
	b	0.383	0.544
	R_L	0.115-0.465	0.017-03380
	R^2	0.948	0.989
Freundlich	N	5.180	11.01
	K_F	554.7	531.4
	R^2	0.228	0.250
Temkin	A_T (L/g)	31.32	8020
	b_T	16.00	41.90
	β ($J.mol^{-1}$)	154.8	59.81
	R^2	0.314	0.241

Table 4.3: Comparison of adsorption capacities of MB onto different adsorbents.

Adsorbents	Removal capacity (mg/g)	Reference
CMC/PVP hydrogel	83.33	[17]
CMC-based hydrogels beads	82.00	[53]
Regenerated CMC-based hydrogels beads	350.00	[53]
hydroxypropyl cellulose (HPC)/graphene oxide	118.48	[54]
Poly (AA-co-AMPS)/MMT	192.31	[55]
CMC-based hydrogels	5-25.00	[56]
MCA–E/CMC microspheres	998.20	[57]
Magnetic carboxyl functional nano-porous polymer	57.74	[58]
Fe_3O_4/p(Am-co-Na Ac)	635.60	[59]
Xylan/p(acrylic acid) Fe_3O_4	438.60	[60]
CMC/pAA hydrogel	1165.0	Present study
CMC-cl-pAA/Fe_3O_4-C30B hydrogel nanocomposite	806.50	Present study

4.3.3.4. Adsorption thermodynamics

To explore the capacity and thermodynamics during MB removal by the hydrogel and its nanocomposite, experiments were performed at different temperatures. From the plot in Figure 4.10(a), of the CMC-cl-pAA hydrogel it could be observed that as the temperature increases, the removal capacity decreases. According to Pakdel and Peighambardoust, [18], natural hydrogels lack mechanical stability. Hence, they are disrupted when subjected to high-temperature water, leading to a decrease in removal capacity. In contrast, when the temperature is increased for the CMC-cl-pAA/Fe_3O_4-C30B hydrogel nanocomposite, the removal capacity increases. Similar results were reported by Song et al., in the case of chitosan-g-poly (acrylic acid) hydrogel [61].

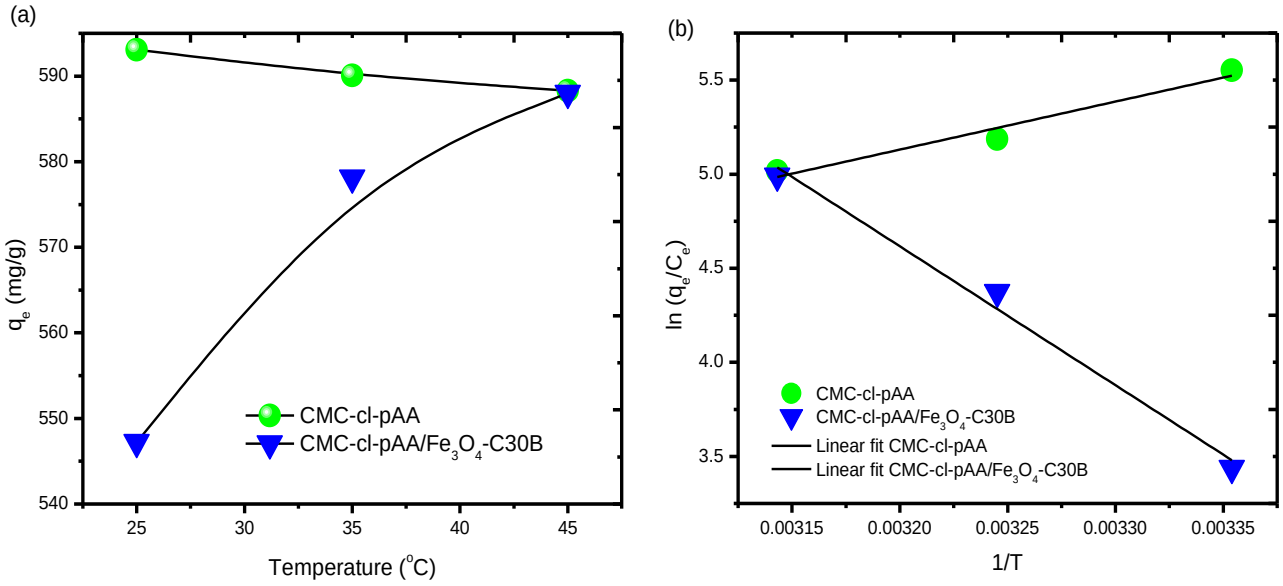

Figure 4. 10: Thermodynamics graph for CMC-cl-pAA hydrogel and CMC-cl-pAA/Fe_3O_4-C30B HNC.

Thermodynamics parameters such as the change in the Gibbs free energy ($\Delta G°$ kJ/mol), enthalpy ($\Delta H°$ kJ/mol), and entropy $\Delta S°$ J/mol K) were determined from the plot of ln (q_e/*Ce*) in Figure 4.10(b) using Eq. S9 and S10 from the supplementary information and recorded in Table 4.4. The obtained values of $\Delta H°$(kJ/mol) and $\Delta S°$ (kJ/mol/K) were -306.98 (kJ/mol) and -0.365 (kJ/mol) for CMC-cl-pAA hydrogel. Indicating an exothermic reaction with less disorder [62]. In contrast, $\Delta H°$ (887.9 kJ/mol) and $\Delta S°$ (3.396 kJ/mol/K) for CMC-cl-pAA/Fe_3O_4-C30B hydrogel nanocomposite were positive, indicating an endothermic reaction with more disorder and randomness [62]. The negative change in Gibbs free energy $\Delta G°$ values for both the hydrogel and the hydrogel nanocomposite indicated a spontaneous reaction. According to the literature, a spontaneous endothermic reaction for CMC-cl-pAA/Fe_3O_4-C30B hydrogel nanocomposite is possible "when the entropy increases by more than the change in enthalpy" [63]. Which usually occurs at high temperatures [61,63]. This confirms the increase in removal capacity as temperature increases. The adsorption of MB by the hydrogel and the hydrogel nanocomposite was dominated by chemisorption since $\Delta G°$ was between -80 and -400 kJ/mol. These results agree with the pseudo-second-order rate law.

Table 4.4: Thermodynamics parameters for CMC-cl-pAA hydrogel and CMC-cl-pAA/Fe_3O_4-C30B hydrogel nanocomposite.

Adsorbent	Temperature (K)	$\Delta G°$ (kJ mol^{-1})	$\Delta H°$ (kJ mol^{-1})	$\Delta S°$ (J mol^{-1} K^{-1})
CMC-cl-pAA hydrogel	298.15	-198.2	-306.9	-0.365
	308.15	-194.5		
	318.15	-190.5		
CMC-cl-pAA/Fe_3O_4-C30B hydrogel nanocomposite	298.15	-124.7	887.9	3.396
	308.15	-158.6		
	318.15	-192.6		

4.3.3.5 Regeneration studies

The practical applicability, stability and reusability play an important role in the adsorption process. Four cycles of adsorption-desorption were carried out to investigate the regeneration of adsorbents (Figure 4.11). The results revealed that both CMC-cl-pAA hydrogel and CMC-cl-pAA/Fe_3O_4-C30B hydrogel nanocomposite maintained high adsorption percentage even after four successive cycles under the same conditions. Nonetheless, CMC-cl-pAA/Fe_3O_4-C30B hydrogel nanocomposite showed that there was no significant reduction in the adsorption percentage, which implied that CMC-cl-pAA/Fe_3O_4-C30B hydrogel nanocomposite was more stable for adsorption of MB in an aqueous solution than CMC-cl-pAA hydrogel. Thus, CMC-cl-pAA/Fe_3O_4-C30B hydrogel nanocomposite holds great potential for remediation of dyes in aqueous solutions.

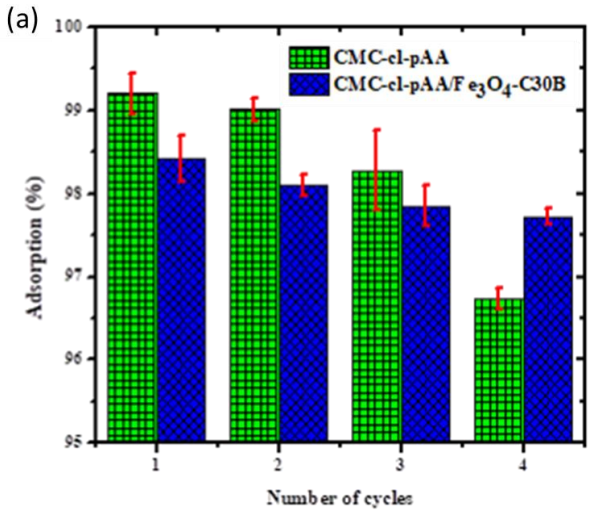

Figure 4. 11: Regeneration of CMC-cl-pAA hydrogel and CMC-cl-pAA/Fe_3O_4-C30B hydrogel nanocomposite for adsorption of MB.

4.3.3.6 Adsorption mechanism

It is well established that the adsorption surface characteristic plays a vital role in the adsorption process [1]. Both adsorbents (CMC-cl-pAA hydrogel and CMC-cl-pAA/Fe_3O_4-C30B hydrogel nanocomposite) contain hydrophilic functional groups on their surface (Scheme 4.1). These functional groups have an influence on MB adsorption processes through factors such as pH, dose, contact time, concentration and temperature. The effect of pH, as well as pH_{pzc} studies, demonstrated that the adsorption between synthesized adsorbents and MB dye depended mainly on the changing pH values. In acidic medium, the adsorption of MB was not favourable because the carboxylic groups on the surface of the adsorbents were protonated. Therefore, electrostatic repulsion occurred between adsorbents and MB dye. At high pH, the carboxylic groups on the surface of the adsorbent were completely ionized as a result strong electrostatic interaction between anionic adsorbents and cationic MB dye as shown in Scheme 4.1 [21]. Furthermore, the adsorption capacity of MB for the CMC-cl-pAA/Fe_3O_4-C30B hydrogel nanocomposite was observed to be comparatively lower than that of the hydrogel. This could be due to the incorporation of Fe_3O_4-C30B

nanocomposite, which could promote more cross-linking networks in the polymer matrix, leading to a decline in the number of active hydrophilic functional groups.

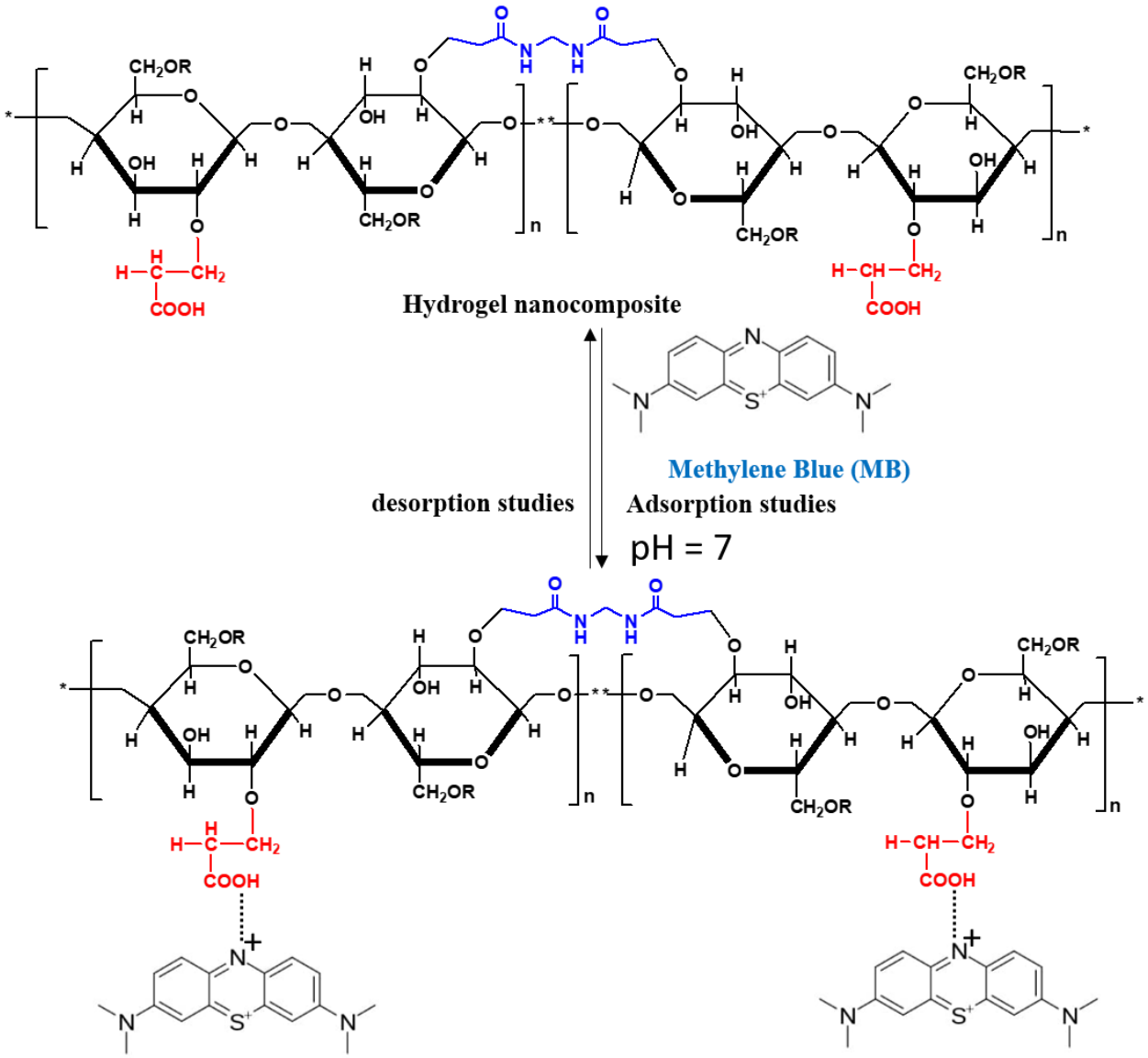

Scheme 4.1. A plausible mechanism for the removal of MB dye from aqueous solution using hydrogel nanocomposite.

4.4. CONCLUSIONS

In this study, CMC-cl-pAA hydrogel and CMC-cl-pAA/Fe_3O_4-C30B hydrogel nanocomposite were successfully synthesised and characterised using various analytical techniques. The TGA and DMA revealed that the thermal stability and mechanical characteristics of the hydrogel were improved after incorporating Fe_3O_4-C30B into the hydrogel polymer matrix. Adsorption studies were performed to evaluate the adsorption capacity and efficiencies of both synthesised materials. The isotherm studies revealed that the CMC-cl-pAA/Fe_3O_4-C30B hydrogel nanocomposite was more efficient in removing MB. The improved physical and chemical properties could aid in the easy recovery of the adsorbent after application and allow removal of contaminants in harsh conditions such as high temperatures. The hydrogel and its nanocomposite removed MB better compared to other adsorbent materials reported. The kinetics followed pseudo-second-order and the thermodynamics showed that the removal of MB was spontaneous.

4.5 REFERENCES

1. Thakur, S., Pandey, S., & Arotiba, O. A. (2016). Development of a sodium alginate-based organic/inorganic superabsorbent composite hydrogel for adsorption of methylene blue. Carbohydrate Polymers, 153, 34–46.
2. Liu, C., Omer, A. M., & Ouyang, X. (2018). Adsorptive removal of cationic methylene blue dye using carboxymethyl cellulose / k-carrageenan / activated montmorillonite composite beads: Isotherm and kinetic studies International Journal of Biological Macromolecules,106, 823–833.
3. Zhang, G., Yi, L., Deng, H., & Sun, P. (2014). Dyes adsorption using a synthetic carboxymethyl cellulose-acrylic acid adsorbent. Journal of Environmental Sciences, 26(5), 1203–1211.
4. Toor, A. T., Verma, A., Jotshi, C. K., Bajpai, P. K., & Singh, V. (2006). Photocatalytic degradation of Direct Yellow 12 dye using UV/TiO2 in a shallow pond slurry reactor. Dyes and Pigments, 68(1), 53–60.

5. Adegoke, K. A., & Bello, O. S. (2015) ‘Dye sequestration using agricultural wastes as adsorbents’, Water Resources and Industry, 12, 8–24.
6. Yagub, M. T., Sen, T. K., Afroze, S., & Ang, H. M. (2014). Dye and its removal from aqueous solution by adsorption, Advances in Colloid and Interface Science, 209, 172–184.
7. Jiang, Y., Liu, B., Xu, J., Pan, K., Hou, H., Hu, J., & Yang, J. (2018). Cross-linked chitosan/β-cyclodextrin composite for selective removal of methyl orange. Carbohydrate Polymers, 182, 106–114.
8. Science, A. (2016). Adsorption of cationic dyes on activated carbon obtained from waste Elaeagnus stone. Adsorption Science & Technology, 34(9–10),512–525.
9. Sulistiyo, Y. A., Andriana, N., Piluharto, B., & Zulfikar, Z. (2017). Silica Gels from Coal Fly Ash as Methylene Blue Adsorbent: Isotherm and Kinetic Studies, Bulletin of Chemical Reaction Engineering & Catalysis, 12 (2), 263-272.
10. Zhao, L., & Yang, S. (2017). Preparation and application of Carboxylated Graphene Oxide Sponge in Dye Removal. International Journal of Environmental Research and Public Health, 14, 1301.
11. Boumediene, M., Benaïssa, H., George, B., Molina, S., & Merlin, A. (2018). Effects of pH and ionic strength on methylene blue removal from synthetic aqueous solutions by sorption onto orange peel and desorption study. Journal of Materials and Environmental Sciences, 9(6), 1700–1711.
12. Chawla, P., Ranjan, S.A., Pandey, P., & Chawla, V. (2014). Hydrogels: A Journey from Diapers to Gene Delivery. Mini Reviews in Medicinal Chemistry, 14(2), 154-167(14).
13. Reza, G., & Adeleh, M. (2013). Synthesis of kappa-carrageenan-g-poly(acrylamide)/ sepiolite nanocomposite hydrogels and adsorption of cationic dye of cationic dye. Polymer Bulletin, 70, 2451–2470.
14. Petri, D. F. S. (2019). Carboxymethyl cellulose/poly (acrylic acid) interpenetrating polymer network hydrogels as multifunctional adsorbents. Cellulose, 26(1), 597–615.
15. Zheng, W.J., Gao, J., Wei, Z., Zhou, J., & Chen, Y.M. (2015). Facile fabrication of self-healing carboxymethyl cellulose hydrogels. European Polymer Journal, 72, 514-522.

16. Peng, N., Hu, D., Zeng, J., Li, Y., Liang, L., & Chang, C. (2016). Superabsorbent cellulose−clay nanocomposite hydrogels for highly efficient removal of dye in water. ACS Sustainable Chemistry and Engineering, 4, 7217−7224.
17. Dai, H., Huang, Y., & Huang, H. (2018). Eco-friendly polyvinyl alcohol/carboxymethyl cellulose hydrogels reinforced with graphene oxide and bentonite for enhanced adsorption of methylene blue. Carbohydrate Polymers, 185, 1–11.
18. Wang, Y., Zhou, P., Luo, S., Liao, X., Wang, B., Shao, Q., & Guo, Z. (2018). Controllable synthesis of monolayer poly (acrylic acid) on the channel surface of mesoporous alumina for Pb (II) Adsorption. Langmuir, 34, 7859–7868.
19. Godiya, C. B., Cheng, X., Li, D., Chen, Z., & Lu, X. (2018). Carboxymethyl cellulose/polyacrylamide composite hydrogel for cascaded treatment/reuse of heavy metal ions in wastewater Carboxymethyl cellulose/polyacrylamide composite hydrogel for cascaded treatment/reuse of heavy metal ions in wastewater. Journal of Hazardous Materials, 364, 28–38.
20. Dai, H., Huang, Y., & Huang, H. (2018). Eco-friendly polyvinyl alcohol/carboxymethyl cellulose hydrogels reinforced with graphene oxide and bentonite for enhanced adsorption of methylene blue. Carbohydrate Polymers, 185(381), 1–11.
21. Makhado, E., Pandey, S., Nomngongo, P. N., & Ramontja, J. (2018). Journal of Colloid and Interface Science Preparation and characterization of xanthan gum-cl-poly (acrylic acid)/ o-MWCNTs hydrogel nanocomposite as highly effective re-usable adsorbent for removal of methylene blue from aqueous solutions. Journal of Colloid and Interface Science, 513, 700–714.
22. Makhado, E., Pandey, S., & Ramontja, J. (2018). International Journal of Biological Macromolecules Microwave-assisted synthesis of xanthan gum-cl-poly (acrylic acid) based-reduced graphene oxide hydrogel composite for adsorption of methylene blue and methyl violet from aqueous solution. International Journal of Biological Macromolecules, 119, 255–269.
23. Hosseinzadeh, H., Sadeghzadeh, M., & Babazadeh, M. (2011). Preparation and Properties of Carrageenan- g -Poly (Acrylic Acid)/ Bentonite Superabsorbent Composite, 2011(July), 311–317.

24. Fekete, T., Borsa, J., Takács, E., & Wojnárovits, L. (2016). Synthesis of cellulose-based superabsorbent hydrogels by high-energy irradiation in the presence of crosslinking agent. Radiation Physics and Chemistry, 118, 114–119.
25. Wang, Z., Ning, A., Xie, P., Gao, G., Xie, L., & Li, X. (2018). Synthesis and swelling behaviours of carboxymethyl cellulose-based superabsorbent resin hybridized with graphene oxide Synthesis and swelling behaviours of carboxymethyl cellulose-based superabsorbent resin hybridized with graphene oxide. Carbohydrate Polymers, 157(September 2016), 48–56.
26. Gao, H., Rao, J., Guan, Y., Li, W., Zhang, M., Shu, T., & Lv, Z. (2018). Investigation of the Thermo-Mechanical Properties of Blend Films Based on Hemicelluloses and Cellulose, 2018.
27. Salama, A. (2015). Carboxymethyl cellulose- g -poly (acrylic acid)/ calcium phosphate composite as a multifunctional hydrogel material. Materials Letters, 157, 243–247.
28. Sitthichai, S., Pilapong, C., & Thongtem, T. (2015). Applied Surface Science CMC-coated Fe 3 O 4 nanoparticles as new MRI probes for hepatocellular carcinoma. Applied Surface Science, 356, 972–977.
29. Fekete, T., Borsa, J., Takács, E., & Wojnárovits, L. (2016). Synthesis of cellulose-based superabsorbent hydrogels by high-energy irradiation in the presence of crosslinking agent. Radiation Physics and Chemistry, 118, 114–119.
30. Yang, F., Li, G., He, Y. G., Ren, F. X., & Wang, G. X. (2009). Synthesis, characterization, and applied properties of carboxymethyl cellulose and polyacrylamide graft copolymer. Carbohydrate Polymers, 78, 95–99.
31. Sand, A., Yadav, M., & Behari, K. (2010). Preparation and characterization of modified sodium carboxymethyl cellulose via free radical graft copolymerization of vinyl sulfonic acid in aqueous media. Carbohydrate Polymers, 81, 97–103.
32. Shen, J., Cui, C., Li, J., & Wang, L. (2018). In situ synthesis of a silver-containing superabsorbent polymer via a greener method based on carboxymethyl celluloses. Molecules, 23, 2483.

33. Loh, K.S., Lee, Y.H., Musa, A., Salmah, A.A., & Zamri, I. (2008). Use of Fe3O4 nanoparticles for enhancement of biosensor response to the herbicide 2,4-dichlorophenoxyacetic acid. Sensors, 8, 5775-5791.
34. Abreu, A. S., Oliveira, M., & Machado, A. V. (2015). Effect of clay mineral addition on properties of bio-based polymer blends. Applied Clay Science, 104, 277–285.
35. Mishra, S., Mukul, A., Sen, G., & Jha, U. (2011). Microwave-assisted synthesis of polyacrylamide grafted starch (St-g-PAM) and its applicability as flocculant for water treatment. International Journal of Biological Macromolecules, 48(1), 106–111.
36. Soliman, F.M., Yang, W., Guo, H., Shinger, M.I., Idris, A.M., & Hassan, E.S. (2016). Preparation of carboxymethyl cellulose-g-poly (acrylic acid - 2-acrylamido-2-methylpropane sulfonic acid)/attapulgite superabsorbent composite. American Journal of Polymer Science and Technology, 2(1), 11-19.
37. Makhado, E., Pandey, S., & Ramontja, J. (2019). Microwave-assisted green synthesis of xanthan gum grafted diethylamino ethyl methacrylate: An efficient adsorption of hexavalent chromium. Carbohydrate Polymers, 222, 114989.
38. Shen, J., Cui, C., Li, J., & Wang, L. (2018). In situ synthesis of a silver-containing superabsorbent polymer via a greener method based on carboxymethyl celluloses. Molecules, 23, 2483.
39. Bao, Y., Ma, J., & Li, N. (2011). Synthesis and swelling behaviours of sodium carboxymethyl cellulose-g-poly (AA-co-AM-co-AMPS)/MMT superabsorbent hydrogel. Carbohydrate Polymers, 84 (1), 76-82.
40. Salama, A. (2018). Preparation of CMC-g-P(SPMA) super adsorbent hydrogels: Exploring their capacity for MB removal from wastewater. International Journal of Biological Macromolecules, 106, 940–946.
41. Li, Y., Du, Q., Liu, T., Peng, X., Wang, J., Sun, J., Xia, L. (2012). Chemical engineering research and design comparative study of methylene blue dye adsorption onto activated carbon, graphene oxide, and carbon nanotubes, 1(July), 361–368.
42. Oun, A. A., & Rhim, J. (2017). Food Hydrocolloids Carrageenan-based hydrogels and films: Effect of ZnO and CuO nanoparticles on the physical, mechanical, and antimicrobial properties. Food Hydrocolloids, 67, 45–53.

43. Acp, C. M. C., Tooth, V., Caries, D., Chen, Z., Cao, S., Wang, H., Deng, X. (2015). Remineralization of Demineralized Dentine Using Scaffold of CMC / ACP Nanocomplexes in an In Vitro Tooth Model of Deep Caries. Plos one 10(1): e0116553. doi:10.1371/ journal. pone.0116553.
44. Chin, S.F., Iyer, K.S., & Raston, C.L. (2008). Fabrication of carbon-nanotubes decorated with ultra-fine super magnetic nano-particles under continuous flow conditions. The Royal Society of Chemistry, Lab Chip, 8, 439-442.
45. Khedmat, S., Momen-Heravi, F., &Pishvaei, M. (2013). A comparison of viscoelastic properties of three root canal sealers. Journal of dentistry, 10(2), 147-154.
46. Smilek, J., Jarábková, S., Velcer, T., & Pekar, M. (2019). Compositional and Temperature effects on the Rheological Properties of Polyelectrolyte–Surfactant Hydrogels. Polymers, 11, 927.
47. Li, X., Rombouts, W., van der Gucht, J., de Vries, R., & Dijksman, J.A. (2019). Mechanics of composite hydrogels approaching phase separation. Plos one, 14 (1), e0211059.
48. Mahdavinia, G., Afzali, A., Etemadi, H., & Hosseinzadeh, H. (2017). Magnetic/ pH-sensitive nanocomposite hydrogel based carboxymethyl cellulose-g-polyacrylamide / montmorillonite for colon targeted drug delivery. Nanomedicine Research Journal, 2(2), 111–122.
49. Chen, Z., Cao, S., Wang, H., Li, Y., Kishen, A., Deng, X., Yang, X., Wang, Y., Cong, C., Wang, H., & Zhang, X. (2015). Biomimetic remineralization of demineralized dentine using scaffold of CMC/ACP nanocomplexes in an in vitro tooth model of deep caries. PLOS one, 10(1), e0116553.
50. Hu, X. (2018). Super-adsorbent hydrogel for removal of methylene blue dye from aqueous solution. Journal of Materials Chemistry A, 6,17612–17624.
51. Bhaumik, M., Maity, A., Srinivasu, V. V., & Onyango, M. S. (2012). Removal of hexavalent chromium from aqueous solution using polypyrrole-polyaniline nanofibers. Chemical Engineering Journal, 181–182, 323–333.
52. Pathania, D., Sharma, S., & Singh, P. (2017). Removal of methylene blue by adsorption onto activated carbon developed from Ficus carica bast. Arabian Journal of Chemistry, 10, S1445–S1451.

53. Benhalima, T., Ferfera-Harrar, H., & Lerari, D. (2017). Optimization of carboxymethyl cellulose hydrogels beads generated by an anionic surfactant micelle templating for cationic dye uptake: Swelling, sorption and reusability studies. International Journal of Biological Macromolecules, 105, 1025–1042.
54. Liu, C., Zhou, Y., Nie, W., Song, L., & Chen, P. (2015). Fabrication of hydrogel of hydroxypropyl cellulose (HPC) composited with graphene oxide and its application for methylene blue removal. Journal of Material Science, 50, 6113–6123.
55. Hosseinzadeh, H., & Khoshnood, N. (2016). Removal of cationic dyes by poly (AA-co-AMPS)/ montmorillonite nanocomposite hydrogel. Desalination Water Treatment, 57 (14), 1–12
56. Nádia S. V. Capanema, Alexandra A. P. Mansur, Herman S. Mansur, Anderson C. de Jesus, Sandhra M. Carvalho, Poliane Chagas & Luiz C. de Oliveira (2018) Eco-friendly and biocompatible cross-linked carboxymethylcellulose hydrogels as adsorbents for the removal of organic dye pollutants for environmental applications, Environmental Technology, 39:22, 2856-2872.
57. Lin, O., Gao, M., Chang, J., & Ma, H. (2017). Highly effective adsorption performance of carboxymethyl cellulose microspheres crosslinked with epichlorohydrin. Journal of Applied Polymer Science 134 (2), 44363.
58. Su, H., Li, W., Han, Y., & Liu, N. (2018). Magnetic carboxyl functional nanoporous polymer: synthesis, characterization and its application for methylene blue adsorption. Scientific Reports, 1–8.
59. Atta, A., Akl, M. A., Youssef, A. M., & Ibraheim, M. A. (2013). Superparamagnetic Core-Shell Polymeric Nanocomposites for Efficient Removal of Methylene Blue from Aqueous Solutions, 3(1), 397–419.
60. Sun, X., Liu, B., Jing, Z., & Wang, H. (2015). Preparation and adsorption property of xylan /poly (acrylic acid) magnetic nanocomposite hydrogel adsorbent. Carbohydrate Polymers, 118, 16–23.
61. Song, W., Gao, B., Xu, X., Xing, L., Han, S., Dua, P., Song, W., & Jia, R. (2016). Adsorption–desorption behaviour of magnetic amine/Fe3O4 functionalized biopolymer resin towards anionic dyes from wastewater. Bioresource Technology, 210,123–130.

62. Melo, B. C., Paulino, F. A. A., Cardoso, V. A., Pereira, A. G. B., Fajardo, A. R., & Rodrigues, F. H. A. (2018). Cellulose Nano whiskers improve the methylene blue adsorption capacity of chitosan-g-poly (acrylic acid) hydrogel. Carbohydrate Polymers, 181, 358–367.
63. https: www.learner.org/courses/chemistry/text/text.html?dis=U&num=Ym5WdEIURS9NQ289&sec=YzjWakIUQS9OU289.
64. Mahmoodi, N. M., Hayati, B., & Arami, M. (2012). Kinetic, equilibrium and thermodynamic studies of ternary system dye removal using a biopolymer. Industrial Crops and Products, 35(1), 295–301.

CHAPTER FIVE

THE SYNTHESIS OF SODIUM ALGINATE HYDROGEL CROSSLINKED WITH ACRYLIC ACID (SA/PAA) AND ITS MODIFICATION WITH ZINC OXIDE (ZnO) FOR THE REMOVAL OF ORGANIC DYE FROM AQUEOUS SOLUTION

CHAPTER SUMMARY

In this study, we report the preparation of graft copolymerisation of sodium alginate (SA) onto acrylic acid (AA) in the presence of ammonium persulfate (APS), MBA and zinc oxide nanoparticles (ZnO NPs), as initiator, cross-linker and nanofiller, respectively. FTIR confirmed the functional groups on the synthesised materials. XRD results confirmed the amorphous structure of the SA/AA hydrogel through the presence of broad peaks. Interestingly the incorporation of ZnO NP's led to increased intensity. Using the scanning electron microscopy and high-resolution transmission electron microscopy, spherical ZnO NP's were observed on the rough surface of SA/AA hydrogel confirming the successful modification with metal oxide nanoparticles. Further analysis from the simultaneous thermal analysis showed thermal stability was improved after incorporating ZnO NP's, further confirming that surface modification was achieved. The dynamic mechanical analysis confirmed the mechanical properties of both the hydrogel and the hydrogel nanocomposite. The influence of initial solution pH, adsorbent loading, contact time, equilibrium concentration and temperature of the dye adsorption were systematically investigated. The assessment of the adsorption kinetic model and isotherms showed that the pseudo-second-order and Langmuir model better fits the experimental data, respectively. The maximum adsorption capacity of 1129.0 and 1529.6 mg/g was achieved at pH 7.0 and 6.0 for hydrogel and hydrogel nanocomposite, respectively. Thermodynamic parameters for SA-cl-pAA hydrogel and SA-cl-pAA/ZnO HNC substantiated the exothermic and endothermic nature of the adsorption processes, respectively. Moreover, SA-cl-pAA/ZnO HNC presented outstanding reusability with relatively better removal efficiencies as compared to SA-cl-pAA hydrogel.

5.1. INTRODUCTION

The existence of organic dyes in water streams originates from several industrial activities through textiles, leather, cosmetics, food processing, paper and pulp, and plastics industries [1]. Dye-containing industrial effluents are highly toxic and carcinogenic due to their complex chemical structure as well as their non-biodegradable nature [2]. Hence, the treatment of dyes in water streams is one of the world's foremost challenges [3]. Numerous traditional technologies are being applied for the removal of organic dyes from aquatic systems. Among various wastewater treatment techniques, the adsorption technique is deemed to be a favourable technique due to its exceptional benefits like low operation cost, simplicity, high removal efficiency and high regeneration [4-8]. In recent years, there is an ongoing search on the preparation of high-affinity adsorbents towards dye removal from industrial wastewater.

Dyes have been adsorbed by various adsorbents such as clays, metal oxides, activated carbons, polymers and their composites [9-12]. Although abovementioned materials are being utilised for adsorption of dyes from wastewater, they have some shortcomings such as low adsorption capacity, poor recyclability and lack of specificity. Currently, significant attention is focused on developing hydrogel-based adsorbents for adsorption of various aquatic contaminants. Hydrogels are considered as ideal adsorbents for the sorption process owing to their unique characteristics including functionality, regeneration as well as reuse of the adsorbents, high sorption ability, and biodegradable nature [13].

Sodium alginate (SA) is a linear anionic polymer, which is biodegradable, low cost, non-toxic, hydrophilic, it can be easily tailored, and it is abundant natural [14-16]. SA is applied in various industries including pharmaceuticals, agriculture, food, and cosmetics [17,18] Recently, Zou and co-workers developed a three-dimensional network structure via emulsion polymerisation of acrylamide and sodium alginate. This material was utilised for methylene blue uptake and hey found that the synthesised material was able to remove about 1070.54 mg/g [19]. Thakur et al. reported the preparation of SA crosslinked acrylic acid (AA) [20]. The as-synthesised material subsequently utilised as an adsorbent in the extraction of dyes from aqueous medium [20]. Although hydrogels

exhibit excellent properties their weak mechanical strength limits their practical use in various applications, as highlighted by in many studies [21]. This hurdle can be overcome by preparing organic-inorganic hybrid polymers. Several studies reported on the incorporation of additional inorganic components in hydrogel matrices and the synthesized hydrogel composites and/or nanocomposites are being used as adsorbents for removing various pollutants from wastewater [22]. This approach proved to be more suitable for enhancing some of the characteristics of hydrogels i.e. specific surface area to volume ratio, sorption capacity, thermomechanical properties, and regeneration ability to some extent [23-26]. Incorporation of inorganic components in hydrogel matrices have outcompeted the conventional adsorbents and could expand their applications in the various field [27].

In recent years, the development of hydrogel-based metal oxide nanoparticles has intensified in wastewater treatment due to their ability to remove various contaminants in water as well as efficient recovery of adsorbents after adsorption processes. Among nano-sized metal oxides, zinc oxide nanoparticles (ZnO NPs) were served as one of the emerging materials for the development of ZnO NPs-based nanocomposites. In this regard, ZnO NPs-based hydrogel has drawn a surge of attention as good materials with enhanced antibacterial activity for wound dressing [18]. The use of ZnO NPs-based hydrogel as adsorbents have not been explored much for removing organic dye from aqueous solution. Recently, Çınar *et al*. [29] reported a facile strategy to prepare chitosan composite beads in the presence of ZnO NPs. In their study, they used nano-ZnO/chitosan composite beads adsorbent to remove Reactive Black 5 from aqueous medium and in their study, they achieved an adsorption capacity of 189.44 mg/g [29]. Tamer *et al.* [30] successfully synthesized zinc oxide using alginate as a polymer template. Their observation revealed that their material was able to adsorb MB from an aqueous medium within a very short period [30]. In another study conducted by Vahidhabanu *et al.* [31] reported the incorporation of ZnO-based sepiolite clay onto alginate hydrogel beads, and subsequently used this material for the uptake of Congo red from aqueous medium. In their study, they reported an adsorption capacity of 546.89 mg/g. Furthermore, as-synthesized hydrogel beads improved regeneration [31].

In the view of above, here we report on the synthesis of ZnO NPs embedded onto sodium alginate crosslinked acrylic acid towards MB removal. Characterisation of as-synthesised SA/AA/ZnO HNC was carried out by HR-TEM, SEM, FITR, XRD, TGA, and DMA. The influence of initial pH, adsorbent dosage, time, equilibrium concentration as well as temperature was carried out in a batch mode. Moreover, adsorption kinetics, isotherms as well as thermodynamics were studied. SA/AA/ZnO HNC was more propitious to adsorb MB than SA/AA hydrogel.

5.2. MATERIALS AND METHODS

5.2.1. Materials

Ammonium persulfate (APS), ammonium carbonate ($(NH_4)_2(CO_3)$), acrylic acid (AA), MBA, MB dye, sodium hydroxide (NaOH), zinc nitrate ($Zn(NO_3)_2$) and the biopolymer, SA having a formula weight of 176.10 g/mg and molecular formula $C_6H_8O_6$ were bought from Sigma-Aldrich (south Africa). HCl and acetone were supplied by Merck (South Africa). Deionised water was utilised in all experiments. Typically, 1 g of MB powder was dissolved in 1000 mL volumetric flask in deionised water, stock solutions were further prepared by diluting as-prepared stock solution for batch experiments.

5.2.2. Preparation of ZnO NPs

In a typical procedure of ZnO NPs preparation, about 1.5 mol/L of $Zn(NO_3)_2$ and 2.25 mol/L of $(NH_4)_2CO_3$ were dissolved in deionised water in separate beakers. Then a solution of $Zn(NO_3)_2$ was added drop-wise into a beaker containing $((NO_4)_2CO_3$ solution with stirring. Then, the precipitates formed from the reaction mixture were filtered washed several times in a large quantity of deionised water and subsequently with ethanol solution. The obtained precursors were vacuum dried at 70 °C then calcined at 550 °C for 2 hrs.

5.2.3. Preparation of SA/AA hydrogel

In this procedure, a biopolymer solution was obtained by dissolving 0.1 g of SA into 10 mL of deionised water. Appropriate amounts of APS (10×10^{-3}M), AA (15×10^{-4}M) as

well as MBA (7.5×10^{-3}M) were dissolved in deionised water and added in the above-mentioned beaker maintaining the overall volume of 30 mL. The beaker was transferred in an oven for 90 min at 70 °C. Finally, SA/AA hydrogel was precipitated with acetone to remove adhered homopolymer. The precipitated SA/AA hydrogel was filleted and vacuum dried at about 60 °C overnight. Using mortar and pestle, SA/AA hydrogel was ground to form a powder sample.

5.2.4. Preparation of SA/AA/ZnO HNC

The synthesis of SA/AA/ZnO HNC was done by following the procedure given in Section 5.2.3 with a slight modification. In brief, 0.1 g of SA powder was liquefied into a beaker containing 10 mL of deionised water. To this beaker, optimum amounts of APS (10×10^{-3}M), AA (15×10^{-4}M) and MBA (7.5×10^{-3}M) were added. Furthermore, 150 mg of ZnO NPs was dispersed into 10 mL deionised water in 10 mL of deionised water, followed by ultrasonication. Then ZnO NPs suspension was added drop-wise into the other reaction mixture. Then, the reaction mixture was stirred and transferred in an oven for 90 min at 70 °C. Finally, SA/AA/ZnO HNC was washed by immersing in acetone followed by stirring several times to remove unreacted materials. The precipitated SA/AA/ZnO HNC was filtered then dried at 60 °C for about 24 hrs. Finally, SA/AA/ZnO HNC was ground to form a powder sample using mortar and pestle. The schematic presentation of the synthesis of SA/AA/ZnO HNC is provided in Scheme 5.1.

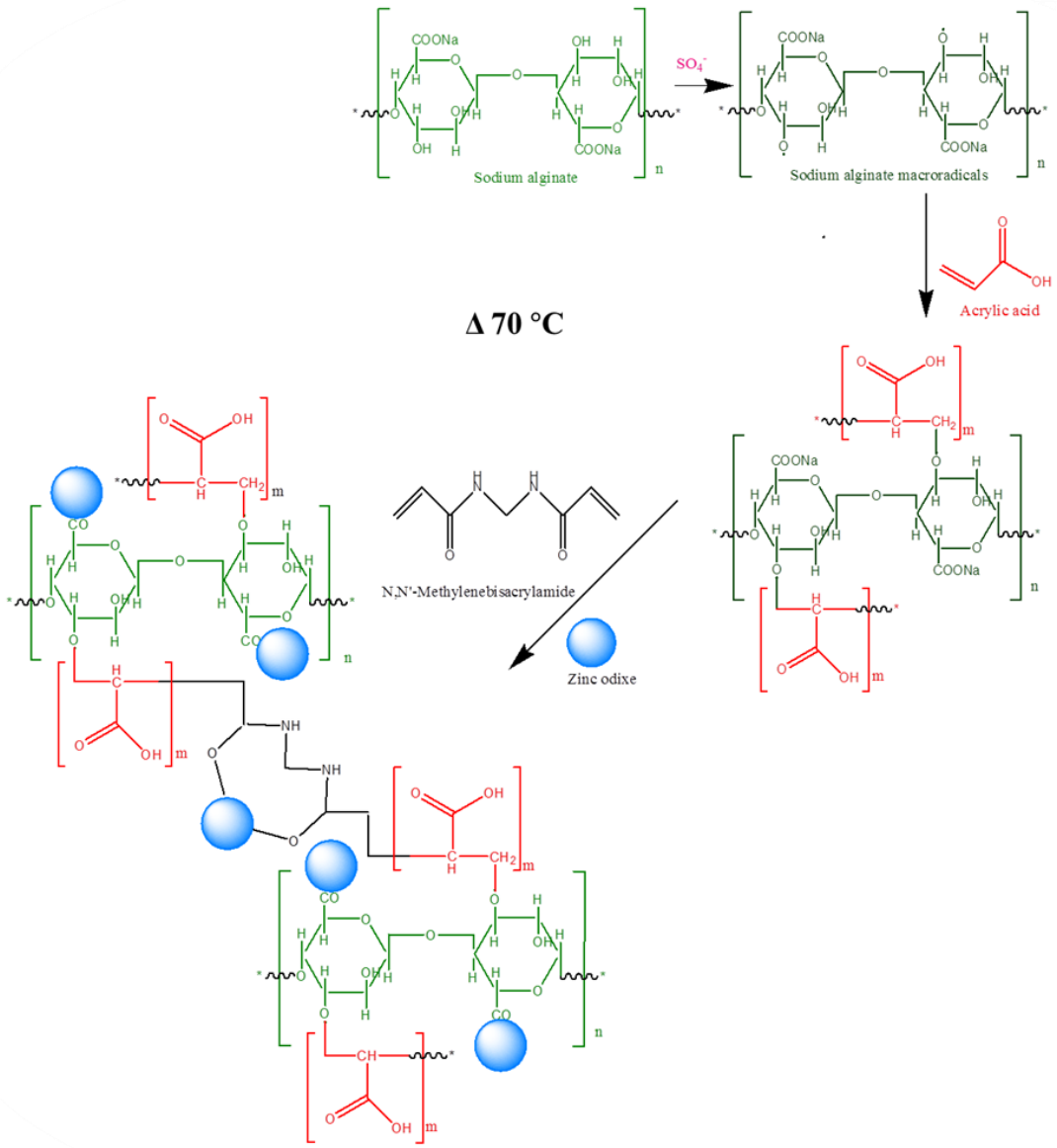

Scheme 5. 1: The schematic representation for the synthesis of the SA-poly(AA)/ZnO HNC.

5.2.5 Characterisation

The techniques used in this study were as discussed in section 4.2.9.

5.2.6. Swelling studies

The equilibrium swelling capacity of samples was investigated by immersing the known amount of sample in deionised water. Typically, 20 mg of samples were soaked in 80 mL of deionised water for 24 hrs. then the swollen sample was taken out of the water and the excess water on the surface was wiped gently and weigh up again to calculate the swelling capacity of samples. The swelling capacity of samples was measured using the following Equation 5.1:

$$\text{Swelling capacity (g/g)} = \frac{W_s - W_d}{W_d} \text{x}100 \qquad (5.1)$$

where *Wd* and *Ws* denote the weight of the initial dry sample and weight of the swollen sample, respectively.

5.2.7. Adsorption studies

The sorption behaviour of MB onto SA/AA hydrogel and SA/AA/ZnO HNC was investigated batch-wise. The adsorption studies were performed in 40 mL of dye solution using 10 mg of adsorbents in a temperature-controlled shaker set at 160 rpm for desired time. The dye solutions after adsorption were withdrawn and filtered with 0.45 m PVDF syringe filters. The concentration of the un-adsorbed dye was measured on a UV-VIS spectrophotometer (Cary 300 Model) at the λmax of 663 nm for MB dye. The percentage adsorption ((%) Adsorption) and adsorption capacity *qe* were calculated using Equation 5.2 and Equation 5.3:

$$(\%)\text{Adsorption} = \frac{Co - Ce}{Co} \times 100 \qquad (5.2)$$

$$q_e = q_t = \frac{Co - C_e}{m} \times V \qquad (5.3)$$

Where *Co* and *Ce* are the initial and equilibrium concentration of MB (mg/L), respectively; is the equilibrium capacity of MB on the adsorbent (mg/g), *qt* denotes the

equilibrium capacity at a defined time (mg/g), *V* is the volume of the MB solution (L); and m is the weight of the adsorbent (g).

5.2.8. Regeneration studies

Reusability of samples was studied through repeated adsorption-desorption experiments. The adsorbents dye loaded were recovered and recycled by rinsing with (0.1 M) of HCL solution, then neutralised with (0.1 M) of NaOH solution. The collected absorbents were further rinsed with deionised water and then dried at 50 °C, ground to a fine powder. Thereafter, the adsorbent was reused for adsorption.

5.2.9 Determination of point of zero charge

The point of zero charge (pH_{pzc}) is simply the pH at which the adsorbent surface has a net charge of zero. The pH_{pzc} is obtained from the difference between the initial and the final pH (ΔpH). To determine the pH_{pzc}, measured amounts of the hydrogel and the hydrogel nanocomposite were immersed in aqueous solutions of pH ranging between 2.0-10.0 and agitated in a shaker (170 rpm, ambient temperature) for 48 hrs. The solution pH was recorded and the pH_{pzc} was calculated as shown from the following Eq. (5.4):

$$\Delta pH = pH_{final} - pH_{initial} \quad (5.4)$$

5.3. RESULTS AND DISCUSSION

5.3.1. Optimisation study for SA/AA hydrogel preparation

The swelling of hydrogels depends on various features such as the presence of functional groups hydrogel, pore size and intermolecular spaces created in the hydrogel network structure [22]. Optimization study of the synthesised hydrogels was based on the swelling ratio. The swelling degree of the hydrogels was carried out by changing the amount of SA from 0.1 to 0.5 g and the equilibrium swelling decreased from 405 to 314 g/g with increasing the mass of SA from 0.1 to 0.5 g, respectively (Figure 5.1(a)). When

the proportion of SA increased, the swelling ratio of SA/AA hydrogel showed a downward trend. The water uptake of SA/AA was studied by varying the concentration of monomer from 3×10^{-4} to 15×10^{-4} M (Figure 5.1(b)). The swelling ratio increased continuously with increasing AA concentration from 3×10^{-4} M to 12.5×10^{-4} M. However, beyond 12.5×10^{-4} M on further increment was noticed with increasing AA concentration. This could be attributed to the -coo- groups which can interact with water molecules via hydrogen bonding [20].

The influence of initiator concentration on the swelling ratio was examined by changing the APS concentration from 10×10^{-3} to 50×10^{-3} M and optimum swelling ratio of 610 g/g was reached at 10×10^{-3} M (Figure 5.1c). Further increase in the APS concentration showed a trend of decreasing the swelling ratio of SA/AA hydrogel. The subsequent decrease in the swelling ratio of SA/AA hydrogel could be attributed to the excess radicals causing termination step reaction via bimolecular collision, thereby enhancing cross-linking density [32,33].

The effect of cross-linker was investigated in the range of 8×10^{-3} to 40×10^{-3} M and the swelling equilibrium ratio was achieved at lower MBA content (Figure 5.1(d)). The equilibrium swelling of SA/AA hydrogel was reduced drastically with increasing the content of crosslinker. More content of crosslinking agent increases the crosslinking density and reduce the space between the copolymer chains [27]. Furthermore, highly cross-linked polymer structure may cause the polymer network to not expand in an aqueous environment, thereby reducing the swelling ratio of SA/AA hydrogel.

The SA/AA hydrogel having the maximum equilibrium swelling capacity was further incorporated with ZnO NP (Figure 5.1(e)). The effect of ZnO NPs on the swelling ratio of SA/AA hydrogel was studied by altering the ZnO NPs content from 0.15 to 0.25 g. SA/AA hydrogel having 0.15 g of ZnO NPs exhibited enhanced swelling capacity than SA/AA hydrogel having 0.2 g and 0.25 g of ZnO NPs. A similar trend was also observed in the sorption of dye, which showed the increase in the percentage adsorption for MB with the incorporation of 0.15 g of ZnO NPs and thereafter the incorporation of ZnO NP exhibited a slight reduction in the percentage sorption of MB (Figure 5.1(f)). Based on

the above results, SA/AA/ZnO HNC formed with 0.15 g of ZnO NPs was selected for subsequent assays and applied for adsorption of MB from aqueous medium.

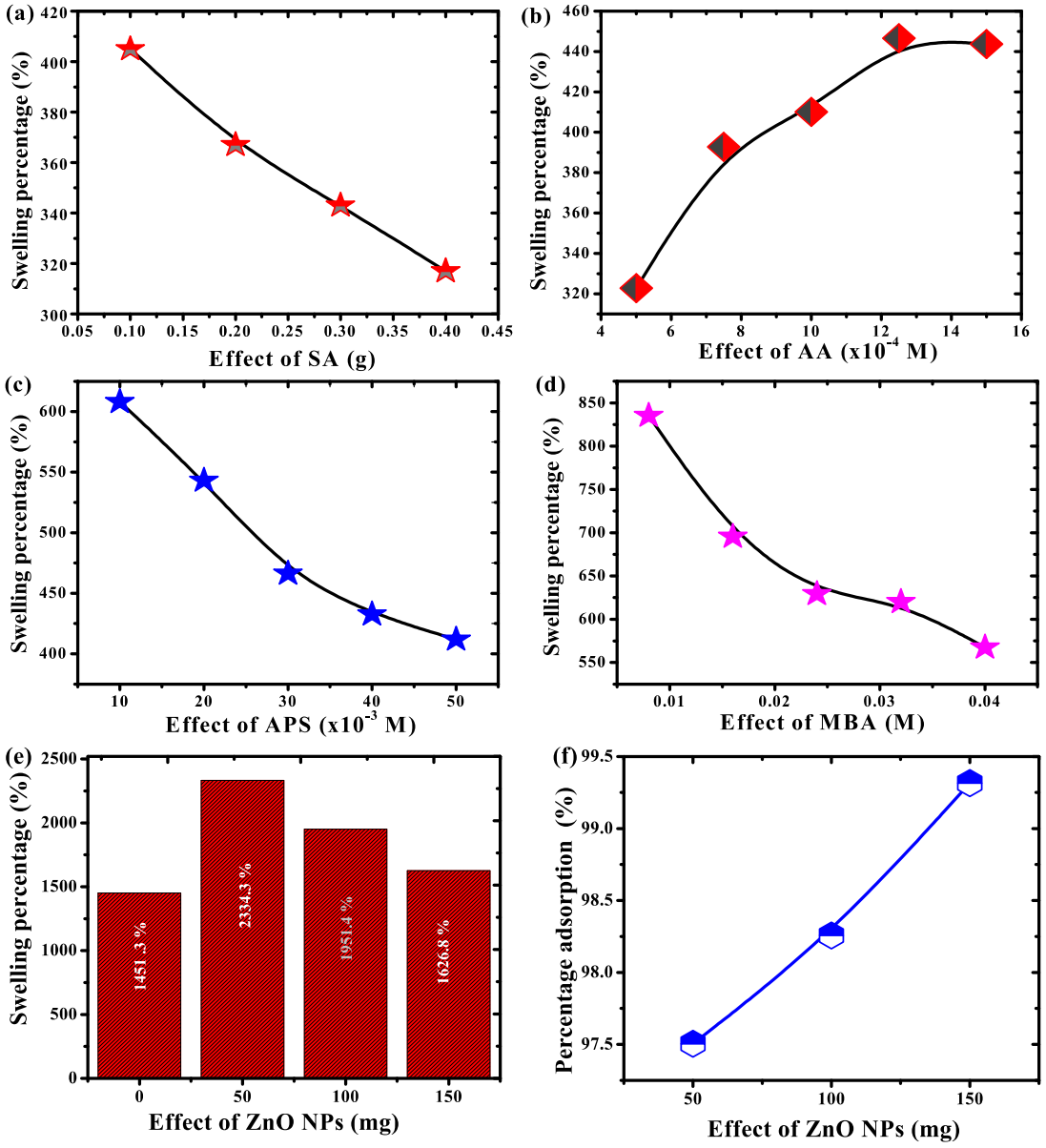

Figure 5. 1: Dependence of equilibrium water adsorption capacity as a function of (a) biopolymer (SA), (b) monomer (AA), (c) initiator (APS), (d) cross-linker (MBA), (e) nanofiller (ZnO NPs) and (f) effect of ZnO NPs on the percentage adsorption.

5.3.2. Characterisation of SA/AA hydrogel and SA/AA/ZnO HNC

5.3.2.1. FTIR analysis

The FTIR spectra of ZnO, SA, SA/AA hydrogel and SA/AA/ZnO HNC are displayed in Figure 5.2(a). Analysing the FTIR spectra for ZnO NPs revealed a peak at 500cm^{-1} was mainly due to the Zn-O stretching. The infrared spectra showed a broad band in the range 3100 to 3620 cm^{-1} assigned to the stretching vibration of the OH group present in the SA polymer chain. The band at about 2925 cm^{-1} may be due to the C-H stretching of the CH_2. Two bands at 1600 and 1418 cm^{-1} were attributed to the COO- groups. The absorption peak at 1017 cm^{-1} was assigned to the C-O stretching frequencies. The characteristic band at 800 cm^{-1} corresponds to the Na-O of the SA [22].

In the FT-IT spectra of SA/AA hydrogel and SA/AA/ZnO HNC, a hump in a broad band between 3620 and 3000 cm^{-1} corresponding to the carboxylic acid O-H stretching vibrations. Both SA/AA hydrogel and its nanocomposite revealed a characteristic peak at about 2941 cm^{-1} indicated the C-H stretching vibration of acrylic acid [11]. As shown in Figure 5.2(a), both hydrogel and its nanocomposite showed a new characteristic peak at about 1701 cm^{-1} was due to the C=O bond associated with carboxylic acid [13]. The peak at 1401 cm^{-1} arose from acrylic acid and was assigned to the symmetric stretching mode of -COO. The band intensity observed at about 1401 cm^{-1} was reduced after the formation of SA/AA hydrogel and its nanocomposite. The appearance of a new band at 1175 cm^{-1} was attributed to the carboxylate groups stretching vibration. Moreover, the intensity of the characteristic peak at 800 cm^{-1} was increased after the formation of both SA/AA hydrogel and SA/AA/ZnO HNC. In the view of the above results, there is evidence for the co-existence of the acrylic acid in the synthesized hydrogel and its nanocomposite. In the view of above data, graft copolymerisation of acrylic acid onto SA backbone was achieved [22].

5.3.2.2. X-ray diffraction analysis

The spectra of ZnO NPs, SA, SA/AA hydrogel and SA/AA/ZnO HNC are illustrated in Figure 5.2(b). The XRD spectra of ZnO NPs revealed several diffraction peaks at 2θ = 31°, 34°, 36°, 47°, 56°, 62° and 67°, which are assigned to (100), (002), (101), (102), (110), (103) and (112), respectively, showing crystal planes of the hexagonal wurtzite

zinc oxide structure (JCPDS Card No. 36-1451) and no characteristic peaks were observed other than ZnO. X-ray diffraction measurements of SA exhibited diffraction peaks at 2θ= 13.8°, 21.5°, and 39.1°, assigned to the (110) plane from polyguluronate unit, (200) plane from polymannuronate and the latter from amorphous halo. The pattern of SA/AA hydrogel showed one broad peak at about 2θ of 20°, corroborating the amorphous nature of the sample. This result confirmed that hydrogel nanocomposite was formed via graft copolymerisation of SA and AA as well as ZnO NPs. Interestingly; SA/AA/ZnO HNC exhibited a very broad peak 2θ of 20°, with increased intensity in comparison to SA/AA hydrogel. This phenomenon implies that there was an interaction between polymeric chains of SA/AA hydrogel and ZnO NPs.

5.3.2.3 Thermal stability

The TGA of the ZnO, SA, SA/AA hydrogel and SA/AA/ZnO HNC are shown in Figure 5.2(c). It was noticed that ZnO NPs exhibited stable degradation temperature in the studied range (30 to 700 ^{o}C). SA presented the initial weight loss below 100 ^{o}C due to loss of adsorbed moisture. The second degradation is the main degradation stage and occurs between 201 to 294 ^{o}C, and in this stage about to 55.5% weight was in the case of SA, which is attributed to the decomposition of SA backbone [20]. The third loss falls at temperatures above 520 ^{o}C, with a mass loss of 59.5% corresponding to the formation of Na_2CO_3 and other carbonaceous materials [34].

The TGA thermograms of SA/AA hydrogel and SA/AA/ZnO HNC exhibited a similar trend throughout the studied temperature; SA/AA/ZnO HNC presented enhanced thermal stability in comparison to its counterpart. The onset decomposition stage for both SA/AA hydrogel and its hydrogel nanocomposite was noticed at above 100 ^{o}C. The second degradation stage lies in between 217 and 350 ^{o}C which could be attributed to the degradation of the residual polymer. For both SA/AA hydrogel and SA/AA/ZnO HNC, the mass loss lying in between 370 and 530 ^{o}C was ascribed to the breakages of carboxyl groups in the acrylic acid chain. In comparison to SA, both SA/AA hydrogel and SA/AA/ZnO HNC showed slower weight loss rate from 30 to 423.6 and 458.5 ^{o}C, respectively. These observations may be due to the graft copolymerisation of AA onto

SA backbone. Based on the above results, it is vividly clear that the thermal stability of SA was enhanced by grafting with AA (30 to 423.6 ^{o}C). Also, incorporation of ZnO NPs into SA-based hydrogel could further enhance the thermal stability (30 to 458.5 ^{o}C).

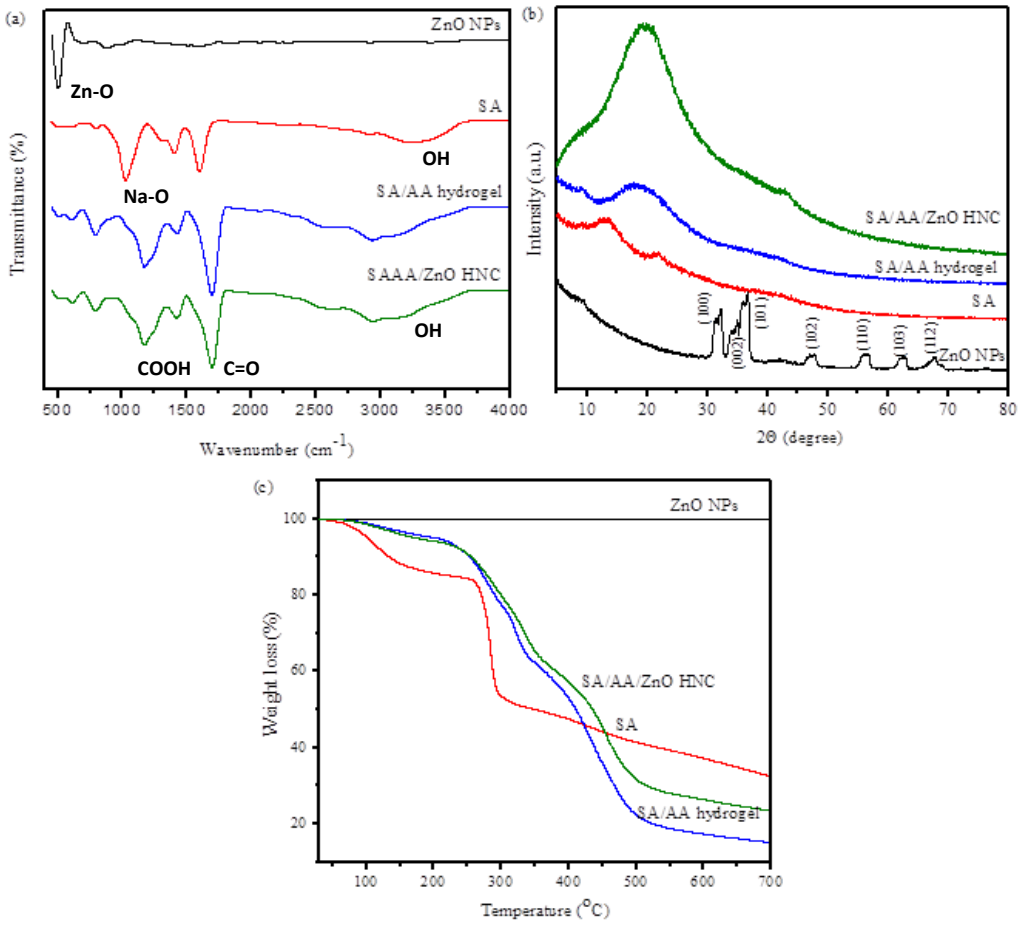

Figure 5. 2: (a) FTIR, (b) XRD, and TGA of ZnO, SA, SA/AA hydrogel and SA/AA/ZnO HNC.

5.3.2.4 Mechanical properties

Viscoelasticity of the SA/AA hydrogel and SA/AA/ZnO HNC was investigated the gel strength. The storage modulus (G'), loss modulus (G"), and tan delta (tan δ) are shown for the as-synthesized SA/AA hydrogel and SA/AA/ZnO HNC as functions of frequency are presented in Figure 5.3. The G′ of both SA/AA hydrogel and SA/AA/ZnO HNC exhibited similar tendency and the G′′increased as the frequency increased (Figure

5.3a). SA/AA hydrogel showed higher G′ values as compared to that of SA/AA/ZnO HNC in the studied frequency range (0.01 to 100 Hz). This behaviour suggested that the SA/AA hydrogel had a higher degree of cross-linking character as compared to its hydrogel nanocomposite. The decrease in G′ could be due to impregnation of ZnO in the SA/AA hydrogel polymer matrix which decreased the cross-linking network density, hence SA/AA/ZnO HNC showed lower G'. The G' values were greater than the G" values throughout the studied frequency range, suggesting the solid-like behaviour. Moreover, G′ values were almost independent of the frequency, which verified the cross-linked hydrogel network. The tan δ is determined by the ratio of G′ and G′′ values. It can be observed that there is no noticeable change in the tan δ for both samples (Figure 5.3(c)).

5.3.2.5. Swelling behaviour

The swelling capacity of SA/AA hydrogel SA/AA/ZnO HNC was examined by varying the solution pH in the range 3.0 to 10.0. As depicted in Figure 5.3(d), SA/AA/ZnO HNC exhibited a high swelling degree than SA/AA hydrogel in the investigated pH range. Both SA/AA hydrogel and SA/AA/ZnO HNC showed that the equilibrium swelling capacity rose from lower pH to neutral pH (pH 3.0 to 7.0). In the acidic medium, carboxylic groups are protonated therefore reduction repulsion of anion-anion leads to a reduced swelling capacity [35]. High swelling capacity was achieved when the solution pH was above neutral; above this pH, carboxylic groups are ionized and can then interact with water molecules, which resulted in greater water adsorption. The incorporation of ZnO NPs led to a decrease in the crosslinking density, which frees the movement of the polymer chains, thus increasing the equilibrium swelling capacity of SA/AA hydrogel. The swelling behaviour of SA/AA hydrogel and SA/AA/ZnO HNC corroborate the obtained result from DMA studies. The water molecules were easily diffused into the SA/AA/ZnO HNC matrix and eventually, a decrement in the storage modulus [36]. The enhancement in the degree of equilibrium swelling changes inversely with the gel strength. The converse results could be attributed to the degree of cross-linking in the polymer matrix.

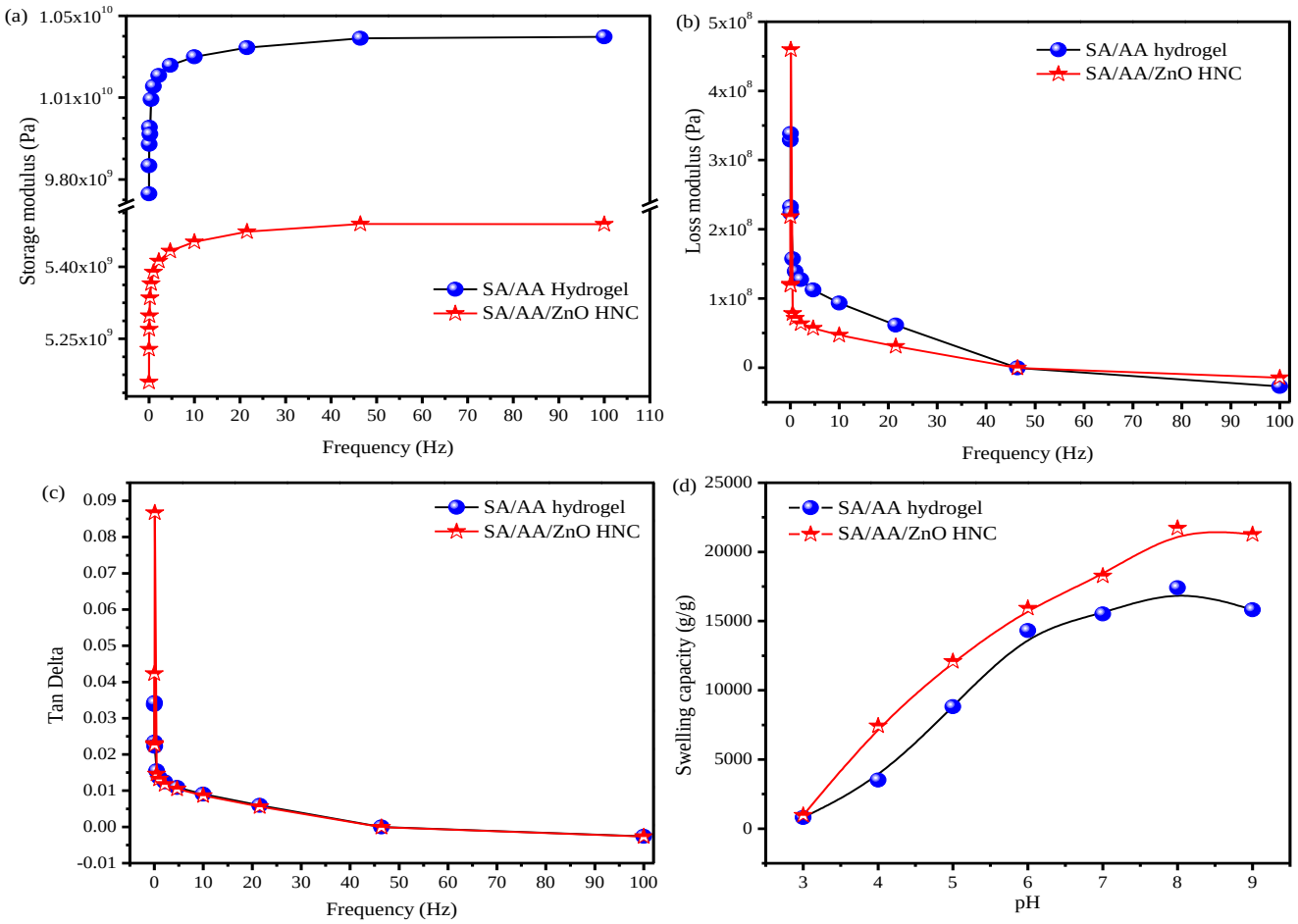

Figure 5. 3: Dynamic mechanical analysis of SA/AA hydrogel, SA/AA/ZnO HNC; (a) storage modulus, (b) loss modulus, (c) tan delta, and (d) equilibrium swelling.

5.3.2.6 Morphological characterisation

To examine the structural features of the SA, SA/AA hydrogel, SA/AA/ZnO HNC and ZnO NPs, SEM and HR-TEM were employed. The SEM image of SA showed a fragment-like loose surface (Figure 5.4(a)). The morphology of as-prepared SA/AA hydrogel exhibited a relatively continuous coarse surface (Figure 5.4(b)), SEM image of SA/AA/ZnO HNC smooth fractured surface morphology with well-dispersed white sphere-shaped ZnO NPs in the polymer matrix (Figure 5.4(c)). Figure 5.4(d and e)

illustrate SEM and TEM micrographs of ZnO NPs, respectively. The SEM results revealed that the ZnO NPs are spherical with a particle size in the range 30-100 nm.

HR-TEM micrograph, selected area electron diffraction pattern (SAED) and the corresponding SAED diffraction intensity profile of ZnO NPs is displayed in (Figure S1). SAED pattern of ZnO NPs demonstrated continuous cycles, which confirm the presences of polycrystalline grains. Additionally, ZnO NPs exhibited an interlayer spacing of about 0.263 nm, which is corresponding to the (002) planes of the ZnO. To further confirm the presence, as well as the distribution of ZnO NPs on the SA/AA hydrogel surface TEM, was employed (Figure 5.4(f)). Furthermore, elemental scanning of SA/AA/ZnO HNC was studied (Figure 5.4(g)), Zn element mapping (Figure 5.4(h)) and O element mapping (Figure 5.4(i)) were found to be uniformly distributed on the SA/AA/ZnO HNC surface. The existence of ZnO NPs in the polymer matrix of SA/AA/ZnO HNC was also confirmed by EDS analysis (Figure 5.4(j)). Table S1 lists the elemental composition of SA/AA/ZnO HNC. The presence of ZnO NPs in the SA/AA/ZnO HNC was about 10% validate the existence of ZnO NPs in the SA/AA hydrogel matrix.

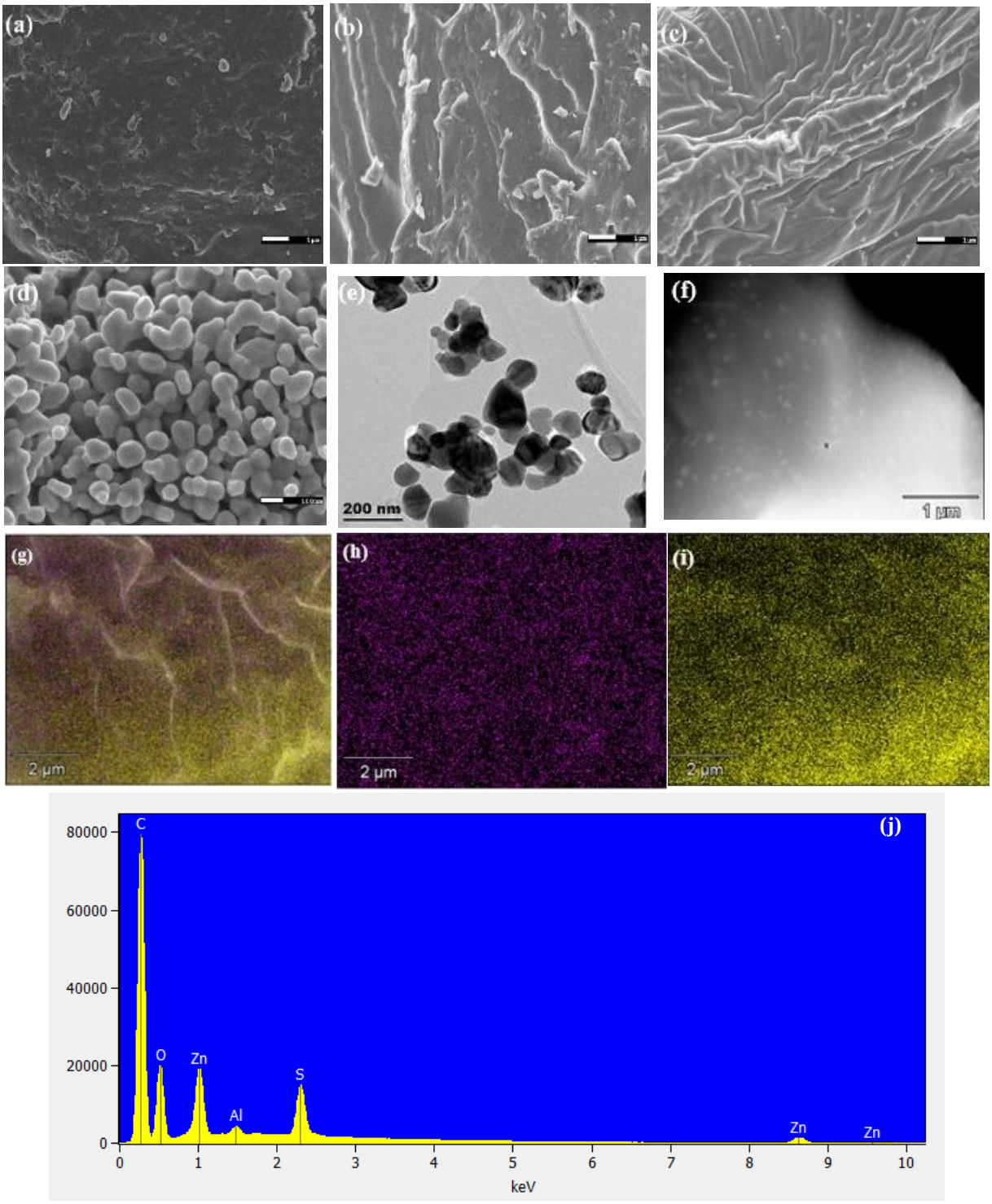

Figure 5. 4: SEM images of (a) SA, (b) SA/AA hydrogel, (c) SA/AA/ZnO HNC, (d) ZnO NPs, (e) TEM image of ZnO NPs, (f) STEM image of SA/AA/ZnO HNC, (g) EDS compositional mapping analysis for SA/AA/ZnO HNC, (h) Zn elemental mapping, (I) O element mapping, and (j) EDS.

5.3.3. Adsorption study of adsorbents for MB

5.3.3.1. Parameters influencing adsorption

5.3.3.1.1 Influence of solution pH and adsorbents dose

The solution pH affects the sorption process to a great extent. The solution pH has been reported to be a vital parameter which governs the electrostatic interaction between adsorbate molecules and adsorbent surface in the sorption process. The sorption experiments of MB on SA/AA hydrogel and SA/AA/ZnO HNC were conducted by varying initial solution pH from 2 to 9 keeping other parameters fixed and the results are displayed in Figure 5.5(a). It was observed that the adsorption capacity of SA/AA hydrogel increased significantly (72.8 to 583.6 mg/g) from (pH 2.0 to 6.0) respectively and thereafter the equilibrium was reached. On the account of SA/AA/ZnO HNC, the experimental results showed that MB sorption was increased as the initial solution pH increased. The high adsorption capacity (q_e) of 579.2 mg/g was achieved at pH 5.0. These results suggest that as the pH approaches neutral most carboxylic groups became ionized, which led to electrostatic interaction between the adsorbents and the MB dye, hence maximum adsorption capacity was achieved at pH above 5.0.

The optimum adsorbent dose was investigated by varying the amount of SA/AA hydrogel and SA/AA/ZnO HNC from (10 to 40 mg) in 200 mg/L in 40 mL of MB dye solution at pH 6.0 and 5.0, respectively. Figure 5.5(b) depicts the influence of dose on the sorption experiments. Both adsorbents exhibited maximum adsorption capacity at low dosage (10 mg). These results may be due to the increased surface area of adsorbents as well as the availability of a large number of active adsorption sites. Further increase in the adsorbents dose (20 to 40 mg) led to a reduction in the adsorption capacity. These results may be as a result of saturation.

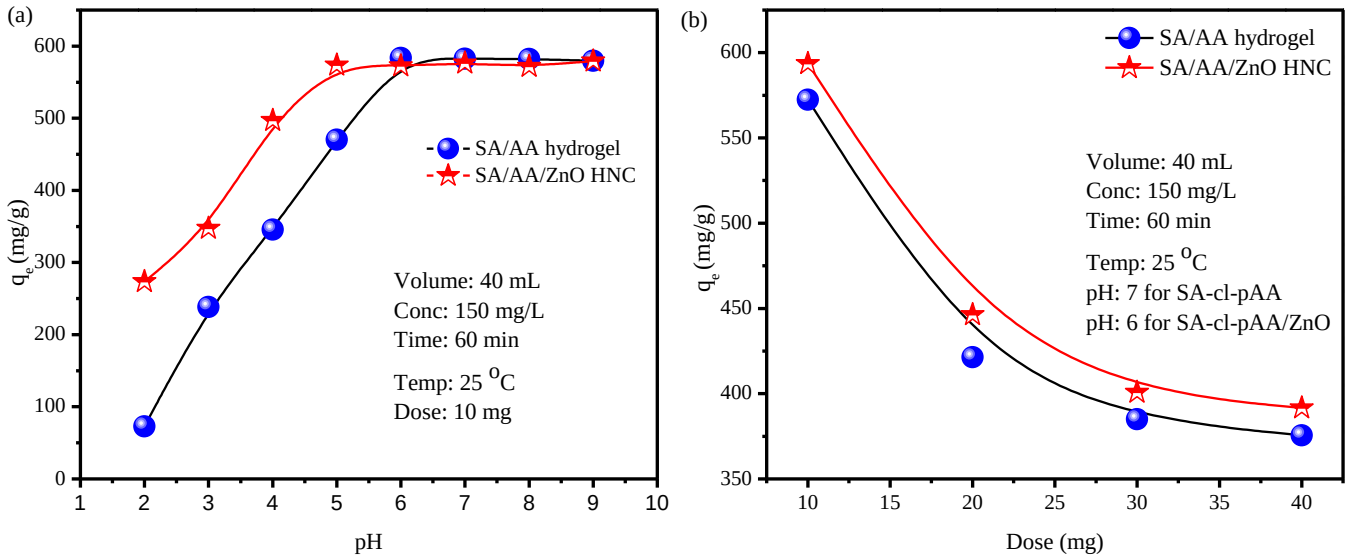

Figure 5. 5: Effect of (a) initial pH and (b) adsorbent dose using SA/AA hydrogel and HNC.

5.3.3.1.2 Point of zero charge

To study the surface charge of SA/AA hydrogel and SA/AA/ZnO HNC, the pH_{pzc} was performed and the plot of ΔpH as a function of $pH_{initial}$ is depicted in Fig. 5.6. “The point of zero charge (pH_{pzc}) is defined as pH of the solution at which charge of the positive surface sites is equal to that of the negative ones, i.e. the adsorbent surface charge has zero value” [37]. As observed in Figure 5.6., pH_{pzc} is obtained at pH 2 for both the SA/AA hydrogel and SA/AA/ZnO HNC. At pH < 2 (pH_{pzc}) the surface charge was positive and at pH > 2 (pH_{pzc}) the surface charge was negative for both adsorbents. Hence for both adsorbents in the effect of pH, the removal capacity was increasing at pH above 2. These findings demonstrated that indeed the overall charge of an adsorbent does affect its adsorption capacity, especially for electrostatic interactions between the adsorbent and the MB dye.

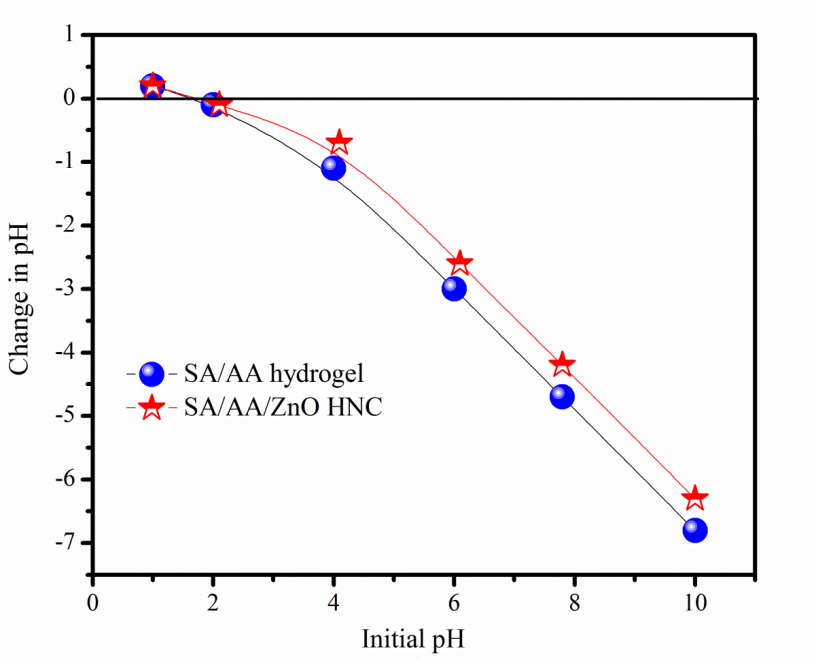

Figure 5. 6: Point of zero charge of the SA/AA hydrogel and its HNC.

5.3.3.2. Adsorption kinetic studies

The effect of time on the adsorption of MB over SA/AA hydrogel and SA/AA/ZnO HNC was investigated to better understand the mechanism of the sorption phenomenon. Pseudo-first-order, pseudo-second-order and intra-particle diffusion kinetic models were applied on the adsorption equilibrium data.

The adsorption kinetics plots of pseudo-first-order, pseudo-second-order, and intra-particle diffusion are presented in (Figure 5.7). The details of the studied adsorption kinetics models (Equations S1-S3) are given in the supplementary information. Moreover, the corresponding kinetics details of the studied models are summarized in Table 5.1. Both SA/AA hydrogel, SA/AA/ZnO HNC showed that the pseudo-second-order was the better fitting model than the pseudo-first-order and intra-particle diffusion kinetics model. Also, the obtained correlation coefficient (R^2) values of the pseudo-second-order were higher, which suggests that chemical adsorption was the rate-controlling step. The experimental points in the intra-particle diffusion model did not

pass through the origin suggesting that the adsorption was not the rate-limiting step and might be jointly controlled by a range of adsorption mechanisms.

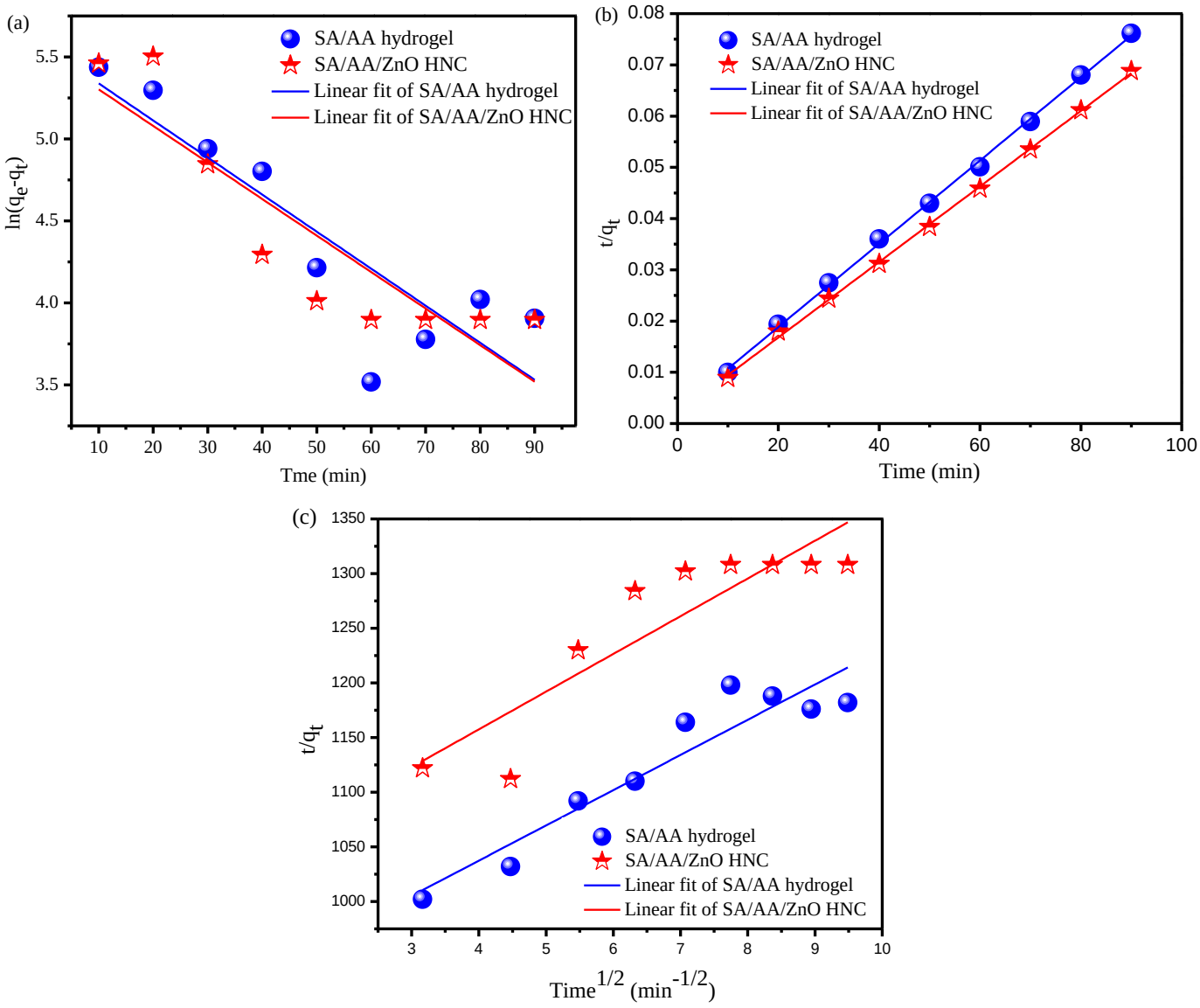

Figure 5. 7: Adsorption kinetic plots for MB onto SA/AA hydrogel, SA/AA/ZnO HNC (a) pseudo-first-order, (b) pseudo-second-order, and (c) second-order model.

Table 5. 1: Adsorption kinetics parameters for the MB dye adsorption.

Temperature (°C)	Pseudo-first-order		Pseudo-second-order			Intra-particle diffusion		
Parameters	K1	R2	K2	qe (cal.)	R2	Ki	C	R2
SA/AA hydrogel	0.052	0.753	2.5×10^{-4}	1230.7	0.998	32.22	908.5	0.878
SA/AA/ZnO HNC	0.051	0.774	2.6×10^{-4}	1357.2	0.999	34.51	1019.5	0.778

5.3.3.3. Adsorption isotherm studies

The equilibrium adsorption is a vital parameter in the sorption process because it aids in determining the adsorption capacity. Adsorption isotherms analysis provides crucial information for the sorption mode between the adsorbent surface and adsorbate molecules. The experimental adsorption data interpreted by commonly used isotherm models namely Langmuir, Freundlich and Temkin models. These adsorption isotherms models were applied to elucidate the affinity and adsorption capacity.

The isotherm models were analysed by fitting the adsorption equilibrium data (Figure 5.8), and all the parameters for the isotherm models were calculated using (Equation S4-S11) given in the isotherm section of the supplementary file and the results are tabulated in Table 5.2. The selection of the obeying adsorption isotherm model was ruled on by R^2 values close to unity. Based on R^2 values, the Langmuir isotherm model is the one which correlated the experimental data. The R^2 values for the Langmuir isotherm model for both SA/AA hydrogel (0.999) and SA/AA/ZnO HNC (0.997) than other studied models (Figure 5.8(a)). These findings authenticate the monolayer adsorption of MB onto both SA/AA hydrogel and SA/AA/ZnO HNC. Furthermore, the values of R_L locate between 0.026 and 0.008 for SA/AA hydrogel, and 0.056 and 0.016 for SA/AA/ZnO HNC. The R_L values of SA/AA hydrogel were negative

and on the account of SA/AA/ZnO HNC R_L values were in the range ($0<R_L<1$) substantiating that the MB sorption was a favourable process. The maximum adsorption capacity obtained from Langmuir was found to be 1129.0 and 1529.6 mg/g for SA/AA hydrogel and SA/AA/ZnO HNC, respectively. To compare the performances of these adsorbents, the maximum adsorption capacity (q_{max}) of both SA/AA hydrogel and SA/AA/ZnO HNC were compared with earlier related reported adsorbents employed for adsorption of MB from aqueous solution [37-43]. A brief list of various adsorbents, including the prepared adsorbents in this study, is presented in Table 5.3.

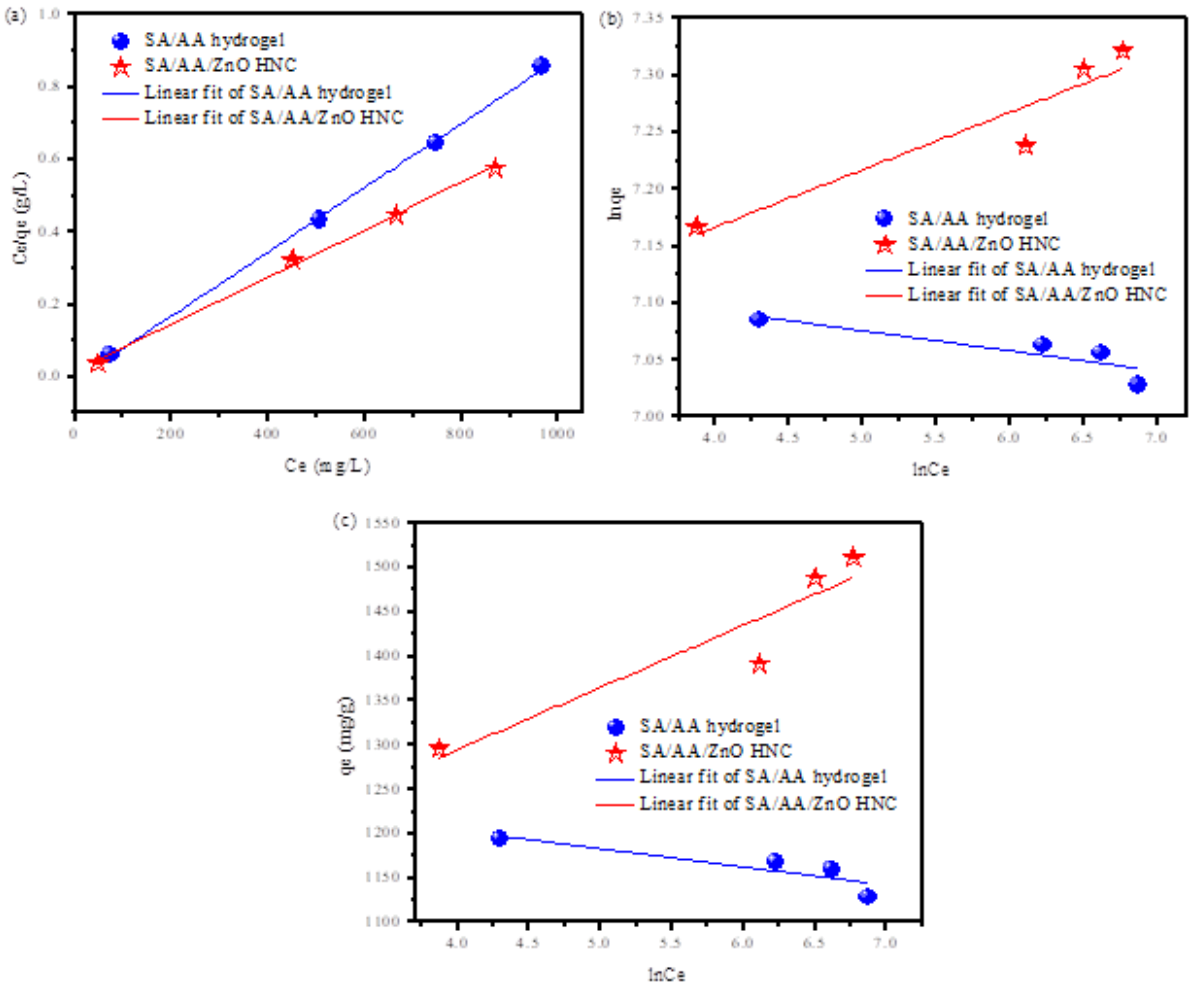

Figure 5. 8: Adsorption isotherm plots for MB onto SA/AA hydrogel, SA/AA/ZnO HNC (a) Langmuir, (b) Freundlich, and (c) Temkin model.

Table 5. 2: Langmuir, Freundlich, and Temkin isotherm models for the MB sorption.

Isotherm models	Isotherm constants	SA/AA hydrogel	SA/AA/ZnO HNC
Langmuir	q_m(mg/g)	1129.0	1529.6
	b	0.100	0.049
	R_L	0.026-0.008	0.052-0.016
	R^2	0.999	0.997
Freundlich	N	-56.82	19.89
	R^2	0.654	0.837
Temkin	A_T (L/g)	6.34×10^{28}	1.98×10^{6}
	b_T	-120.73	35.407
	β ($J.mol^{-1}$)	-20.53	70.01
	R^2	0.667	0.819

Table 5. 3: Comparison of the MB adsorption capacity of adsorbents with other adsorbents.

Adsorbents	q_{max} (mg/g)	Reference
PVP/PCMC/GO/bentonite hydrogel	172.1	[38]
Magnetic PVA/laponite RD hydrogel nanocomposite	251.0	[39]
Chitosan/silica/ZnO nanocomposite	293.3	[40]
Xylan/poly (acrylic acid) magnetic nanocomposite hydrogel	438.6	[41]
TG/CC@EDTA ef-hydrogel nanocomposite	469.0	[42]
TiO_2NP-containing Gg-cl-PAAm composite hydrogel	1305.5	[43]
GK-cl-(PAA-co-AAM)/SiO_2 hydrogel nanocomposite	1408.7	[44]
SA/AA hydrogel	**1129.0**	**Present work**
SA/AA/ZnO HNC	**1529.6**	**Present work**

5.3.3.4. Adsorption thermodynamics studies

Thermodynamics studies give information about the influence of temperature on the sorption process. To evaluate the influence of temperature various parameters such as enthalpy change, (∆H°), entropy change (∆S°), and Gibbs free change (∆G°) were determined using Vant Hoff' equation, which is expressed as shown in Equation 5.4 and 5.5:

$$\Delta G^{o} = \Delta H^{o} - T\Delta S^{o} \tag{5.4}$$

$$\ln\left(\frac{q_e}{C_e}\right) = \frac{\Delta H^{o}}{RT} - \frac{\Delta S^{o}}{R} \tag{5.5}$$

where R is a universal gas constant (8.314 J/mol K), T is the temperature (K) and (qe/ce) is equilibrium constant. The values of ∆H° and ∆S° were calculated from the slope and intercept of the linear plot between In (qe/ce) and 1/T (Figure S2), the values of ∆G° were obtained from equation (5.4) and all thermodynamic parameters are tabulated in Table 5.4. The negative ∆S°, ∆H°, and ∆G° values indicate that the adsorption process was more ordered on the SA poly(AA) hydrogel surface, exothermic and spontaneous, respectively. On the contrary, the positive ∆*S*°, ∆*H*°, and ∆*G*° values show the endothermic nature of the sorption process, disordering, and randomness at the solid-liquid interface for SA-poly(AA)/ZnO HNC. Moreover, the negative ∆*G*° values for SA-poly(AA)/ZnO HNC suggested that the sorption process was spontaneous.

Table 5. 4: Thermodynamic parameter for the sorption of MB onto SA/AA hydrogel, SA/AA/ZnO HNC.

Adsorbent	Temperature (K)	$\Delta G°$ (J mol^{-1})	$\Delta H°$ (kJ mol^{-1})	$\Delta S°$ (kJ mol^{-1} K^{-1})
SA/AA hydrogel	298.15	-1.08	-1.63	-1.84
	308.15	-1.06		
	318.15	-1.05		
SA/AA/ZnO HNC	298.15	-1.99	0.75	9.21
	308.15	-2.08		
	318.15	-2.17		

5.3.3.5. Adsorption/desorption studies

The regeneration of adsorbents is an important index that is decisive to its applicability. Adsorption/desorption experiments were studied to assess the ability of both SA/AA hydrogel, SA/AA/ZnO HNC. Figure 5.9 shows the influence of four regeneration cycles on the adsorption percentage. SA/AA hydrogel exhibited a decrement of 4.2% after the fourth cycle. The percentage (%) adsorption of SA/AA/ZnO HNC showed a slight decrease after the fourth cycle, demonstrating the excellent recycling performance. Based on these results, SA/AA/ZnO HNC can be regeneration and reuse without a significant decrease in MB dye affinity.

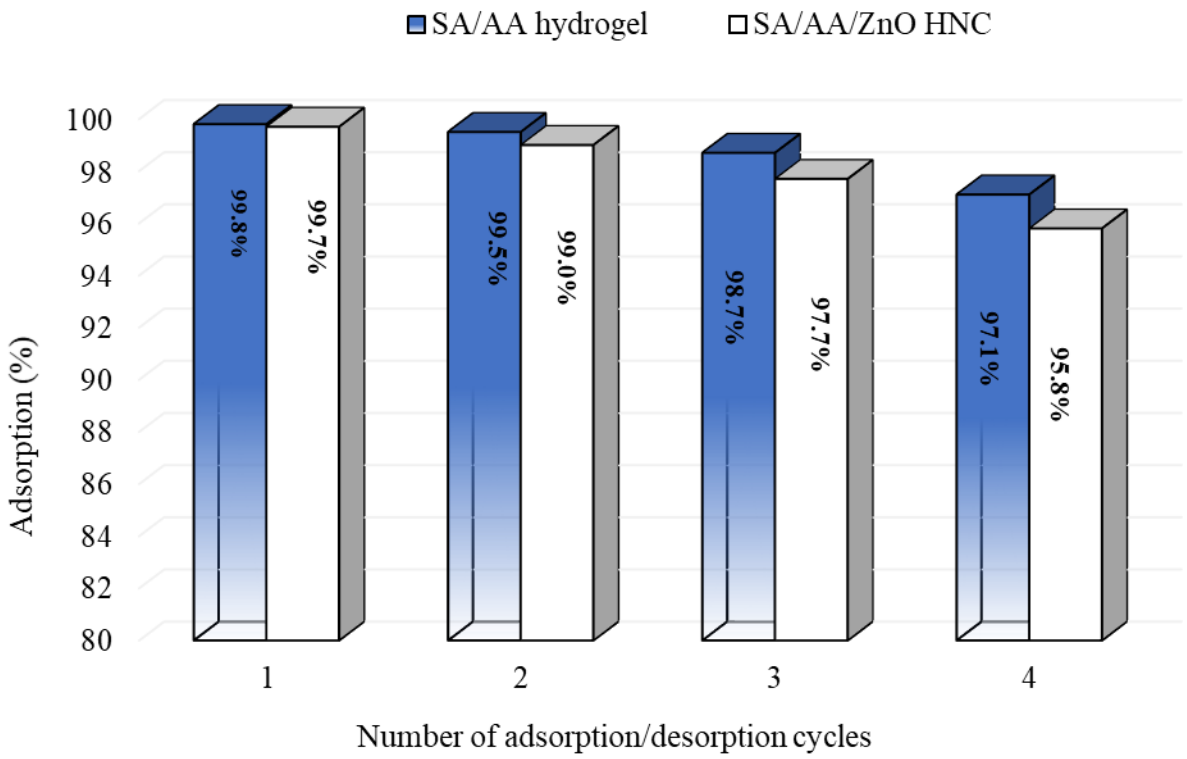

Figure 5. 9: Dye adsorption percentage of adsorbents as a function of the number of adsorption/ desorption cycles.

5.3.3.6 Adsorption mechanism

It is well established that the adsorption surface characteristic plays a vital role in the adsorption process [22,45,46]. The structure of adsorbents was negatively charged due to the presence of carboxylic acid. Based on the adsorption studies (the influence of pH and ionic strength) it can be concluded that the MB dye molecules were attached on the surface of SA-poly(AA)/ZnO HNC through electrostatic interactions. At high pH, the carboxylic groups on the surface of the adsorbents were completely ionized as a result strong electrostatic interaction between anionic adsorbents and cationic MB dye. The SA-poly(AA)/ZnO HNC demonstrated superiority for adsorption of MB in comparison to SA poly(AA) hydrogel. This may be due to the right degrees of ZnO NPs dispersion on

the hydrogel polymer matrix, which may also contribute to the high MB dye adsorption. The most likely mechanism for SA-poly (AA)/ZnO HNC and its interaction with the MB molecules is presented in Scheme 5.2.

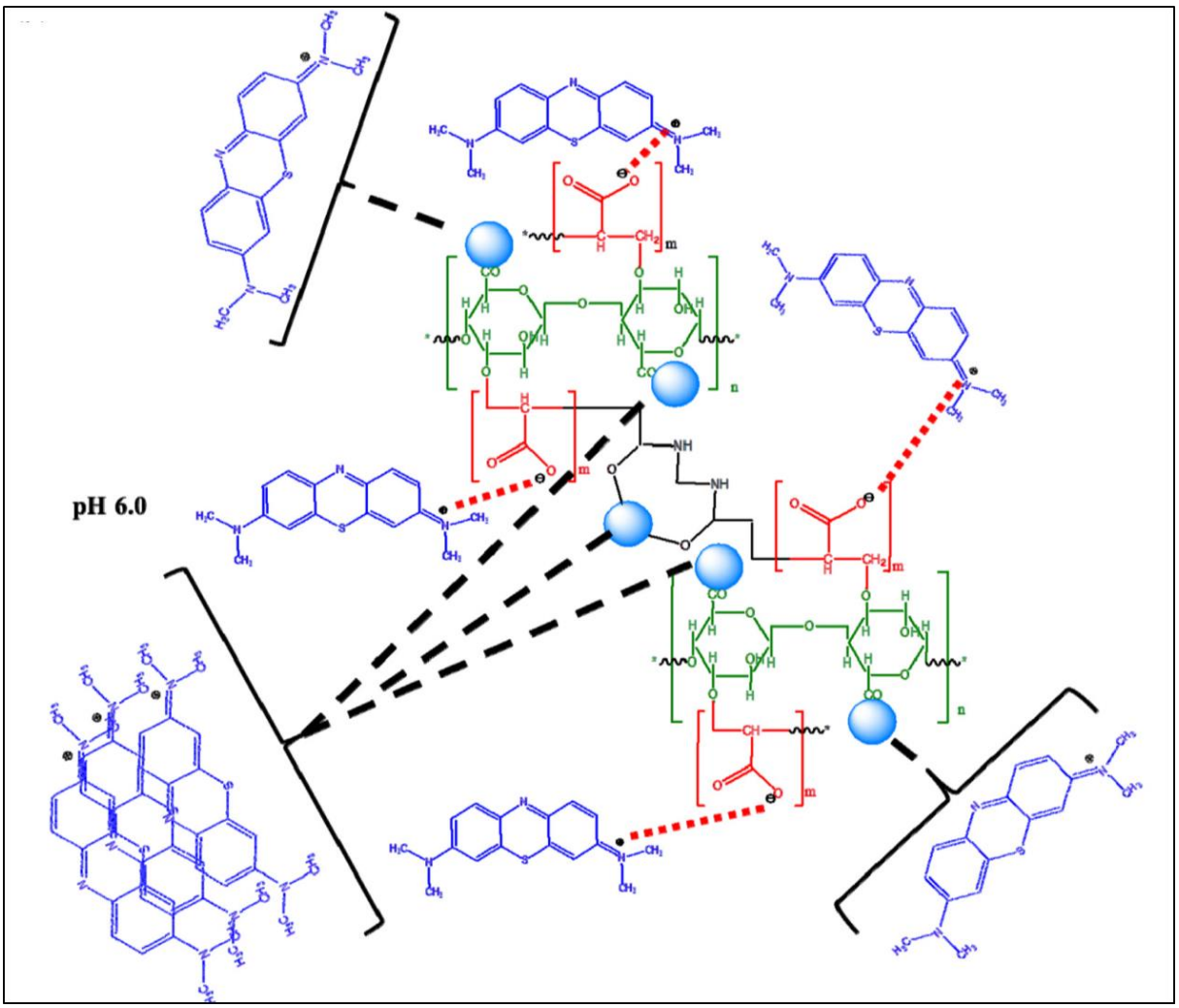

Scheme 5. 2: Plausible mechanism for interaction of MB with SA poly(AA)/ZnO HNC.

5.4. CONCLUSIONS

In this study, SA/AA hydrogel and SA/AA/ZnO HNC were successfully prepared and employed for the removal of MB from an aqueous medium. The as-prepared adsorbents were characterised in more details by XRD, FTIR, TEM, SEM, TGA, and DMA. The incorporation of ZnO NPs in the SA/AA hydrogel matrix increased the water uptake,

which sequentially led to decrement in the gel strength. The swelling ability of hydrogel depends strongly on the crosslinking and charge density of the polymer network. The MB sorption process was influenced by solution pH, adsorbent dosage, time, equilibrium concentration and temperature. The MB dye adsorption process was found to be influenced by parameters such as solution pH, adsorbent dose, contact time, equilibrium concentration and temperature. SA/AA/ZnO HNC showed very good sorption performance for MB in contrast to SA/AA hydrogel. The adsorption kinetics and isotherm modelling data for both SA/AA hydrogel and SA/AA/ZnO HNC were best described by pseudo-second-order rate equation and Langmuir isotherm models, respectively. The maximum adsorption capacity (q_{max}) of SA/AA hydrogel and SA/AA/ZnO HNC were 1129.0 and 1529.6 mg/g, respectively. SA/AA/ZnO HNC demonstrated to be a great adsorbent material for the regeneration of MB dye from aqueous solution. Also, SA/AA/ZnO HNC substantiated the spontaneous nature of the sorption process.

5.5. REFERENCES

[1] K.R. Ramakrishna, T. Viraraghvan. Dye removal using low-cost adsorbents, Water Science and Technology 36 (1997) 189-196.

[2] R. Malik, D.S, Ramteke, S.R. Wate. Adsorption of malachite green on ground nutshell waste-based powdered activated carbon, Waste Management 27 (2007) 1129-1138.

[3] G. Crini. Non-conventional low-cost adsorbents for dye removal: a review, Bioresource Technology 97 (2006) 1061–1085.

[4] K. Song, H. Xu, L. Xu, K. Xie, Y. Yang. Cellulose nanocrystal-reinforced keratin bio-adsorbent for effective removal of dyes from aqueous solution, Bioresource Technology 232 (2017) 254-262.

[5] V.K. Garg, R. Gupta, A.B. Yadav, R. Kumar. Dye removal from aqueous solution by adsorption on treated sawdust, Bioresource Technology 89 (2003) 121–124.

[6] D. Li, Q. Li, D. Mao, N. Bai, H. Dong. A versatile bio-based material for efficiently removing toxic dyes, heavy metal ions and emulsified oil droplets from water simultaneously, Bioresource Technology (2017)245, 649-655.

[7] E. Makhado, S. Pandey, P.N. Nomngongo, J. Ramontja. Xanthan gum-cl-poly(acrylic acid)/reduced graphene oxide hydrogel nanocomposite as adsorbent for dye removal, 9th Int'l Conf. on Advances in Science, Engineering, Technology & Waste Management (ASETWM-17) (2017) 159-164

[8] E. Makhado, S. Pandey, J. Ramontja. Microwave-assisted green synthesis of xanthan gum grafted diethylamino ethyl methacrylate: an efficient adsorption of hexavalent chromium, Carbohydrate Polymers 222 (2019) 114989.

[9] R.Sanghi, B.Bhattacharya, Review on decolorisation of aqueous dye solutions by low-cost adsorbents, Coloration Technology. 118 (2002) 256-269.

[10] M. Nafees, A. Waseem, Organoclays as sorbent material for phenolic compounds: a review, Clean-Soil Air Water. 42 (2014) 1500-1508.

[11] E. Makhado, S. Pandey, P.N. Nomngongo, J. Ramontja, Fast microwave-assisted green synthesis of xanthan gum grafted acrylic acid for enhanced methylene blue dye removal from aqueous solution, Carbohydrate Polymers. 176 (2017) 315–326.

[12] S. De Gisi, G. Lofrano, M. Grassi, M. Notarnicola, Characteristics and adsorption capacities of low-cost sorbents for wastewater treatment: a review, Sustainable Materials and Technologies. 9 (2016) 10–40.

[13] E. Makhado, S. Pandey, J. Ramontja, Microwave-assisted synthesis of xanthan gum-cl-poly (acrylic acid) based-reduced graphene oxide hydrogel composite for adsorption of methylene blue and methyl violet from aqueous solution, International Journal of Biological Macromolecules. 119 (2018) 255-269.

[14] G.T. Grant, E.R. Morris, D.A. Rees, P.J.C. Smith, D. Thom, Biological interactions between polysaccharides and divalent cation: the egg-box model, FEBS Lett.32 (1973) 195–198.

[15] S.K. Bajpai, S. Sharma, Investigation of swelling/degradation behaviour of alginate cross-linked with Ca2+and Ba2+ions, Reactive and Functional Polymers. 59 (2004) 129–140.

[16] J. Chen, G. Li, Q. Liu, J. Ni, W. Wu, Cr(III) ionic imprinted polyvinyl alcohol/sodium alginate (PVA/SA) porous composite membranes for selective adsorption of Cr(III) ions, Chemical Engineering Journal. 165 (2010) 465–473.

[17] L. Agüero, D. Zaldivar-Silva, L. Peña, M. DiasAguero, 2017 Alginate microparticles as oral colon drug delivery device A review, Carbohydrate Polymers. 168 (2017) 32-43.

[18] T. Zehnder, B. Sarker, A.R. Boccaccini, R. Detsch, Evaluation of an alginate-gelatine crosslinked hydrogel for bioplotting, Bio fabrication. 7 (2015) 025001.

[19] X. Zou, H. Zhan, T. Chen, H. Li, C. Meng, Y.Xia, J. Guo. Preparation and characterization of polyacrylamide/sodium alginate microspheres and its adsorption of MB dye, Colloids and Surfaces A: Physicochemical and Engineering Aspects. 567 (2019) 184-192.

[20] S. Thakur, O.A. Arotiba, Synthesis, swelling and adsorption studies of a pH-responsive sodium alginate–poly(acrylic acid) superabsorbent hydrogel, Polymer Bulletin. 75 (2018) 4587–4606.

[21] E. Makhado, S. Pandey, P.N. Nomngongo, J. Ramontja, New Horizons in Wastewaters Management: Emerging Monitoring and Remediation, Hydrogel Nanocomposites: Innovations in Nanotechnology for Water Treatment, Nova science publishers (2019) 87-113.

[22] S. Thakur, S. Pandey, A. Omatayo, Development of a sodium alginate-based organic/inorganic superabsorbent composite hydrogel for adsorption of Methylene blue, Carbohydrate Polymers. 153 (2016) 34–46.

[23] H. Mittal, A. Maity, S.S. Ray, Effective removal of cationic dyes from aqueous solution using gum ghatti-based biodegradable hydrogel, International Journal of Biological Macromolecules. 79 (2015) 8–20.

[24] V.H. Luan, H.N. Tien, S.H. Hur, Fabrication of 3D structured ZnO nanorod/reduced graphene oxide hydrogels and their use for photo-enhanced organic dye removal, Journal of Colloid Interface Science. 437 (2015) 181–186.

[25] K. Gupta, O.P. Khatri, Reduced graphene oxide as an effective adsorbent for removal of malachite green dye: plausible adsorption pathways, Journal of Colloid Interface Science. 501 (2017) 11–21.

[26] Y. Shi, Z. Xue, X. Wang, A.Q.Wang, Removal of methylene blue from aqueous solution by sorption on lignocellulose-g-poly (acrylic acid)/montmorillonite three-dimensional cross-linked polymeric network hydrogels, Polymer Bulletin. 70 (2013)1163–1179.

[27] E. Makhado, S. Pandey, P.N. Nomngongo, J. Ramontja, Preparation and characterization of xanthan gum-cl-poly(acrylic acid)/o-MWCNTs hydrogel nanocomposite as highly effective re-usable adsorbent for removal of methylene blue from aqueous solutions, Journal of Colloid Interface Science. 513 (2018) 700–714.

[28] M. Hashem, S. Sharaf, M.M. Abd El-Hady, A. Hebeish. Synthesis and characterization of novel carboxymethyl cellulose hydrogels and carboxymethyl cellulose-hydrogel-ZnO-nanocomposites, Carbohydrate Polymers. 95 (2013) 421-427.

[29] S. Çınar, Ü.H. Kaynar, T. Aydemir, S.Ç. Kaynar, M. AyvacıklıAn efficient removal of RB5 from aqueous solution by adsorption onto nano-ZnO/chitosan composite beads, International Journal of Biological Macromolecules. 96 (2017) 459-465.

[30] T.M. Tamer, W.M. Abou-Taleb, G.D. Roston, M.S. Mohyeldin, A.M Omer, R.E. Khalifa, A.M. Hafez. Formation of zinc oxide nanoparticles using alginate as a template for purification of wastewater. Environmental Nanotechnology, Monitoring & Management, 10 (2018) 112–121.

[31] S. Vahidhabanu, D. Karuppasamy, A.I. Adeogun, B.R. Babu, Impregnation of zinc oxide modified clay over alginate beads: a novel material for the effective removal of Congo red from wastewater, RSC Advances. 7 (2017) 5669–5678.

[32]Y. Bao, J. Ma, N. Li, Synthesis and swelling behaviors of sodium carboxymethyl cellulose-g-poly(AA-co-AM-co-AMPS)/MMT superabsorbent hydrogel, Carbohydrate Polymers. 84 (2011) 76–82.

[33] Z. Ma, Q. Li, Q. Yue, Synthesis and characterization of a novel super-absorbent based on wheat straw, Bioresource Technology. 102 (2011) 2853–2858.

[34] J.P. Soares, J.E. Santos, G.O. Chierice, E.T.G. Cavalheiro, Thermal behavior of alginic acid and its sodium salt, Eclética Química. 29 (2004) 57–64.

[35] H. Namazi, M. Hasani, M. Yadollahi, Antibacterial oxidized starch/ZnO nanocomposite hydrogel: Synthesis and evaluation of its swelling behaviours in various pHs and salt solutions, International Journal of Biological Macromolecules. 126 (2019) 578–584.

[36] X. Qi, Z. Li, L. Shen, T. Qin, Y. Qian, S. Zhao, J. Shen, Highly efficient dye decontamination via microbial salecan polysaccharide-based gels, Carbohydrate Polymers. 219 (2019) 1-11.

[37] M. Kragović, M. Stojmenović, J. Petrović, J. Loredo, S. Pašalić, A. Nedeljković, I. Ristović, Influence of alginate encapsulation on point of zero charge (pH_{pzc}) and thermodynamic properties of the natural and Fe(III) - modified zeolite, Procedia Manufacturing. 32 (2019) 286–293.

[38] H.J. Dai, Y. Huang, H.H. Huang, Eco-friendly polyvinyl alcohol/carboxymethyl cellulose hydrogels reinforced with graphene oxide and bentonite for enhanced adsorption of methylene blue, Carbohydrate Polymers. 185 (2018) 1-11.

[39] G.R. Mahdavinia, M. Soleymani, M. Sabzi, H. Azimi, Z. Atlasi, Novel magnetic polyvinyl alcohol/laponite RD nanocomposite hydrogels for efficient removal of methylene blue, Journal of Environmental Chemical Engineering. 5 (2017) 2617-2630.

[40] H. Hassan, A.Salama, A.K. El-ziaty, M. El-Sakhawy, New chitosan/silica/zinc oxide nanocomposite as adsorbent for dye removal, International Journal of Biological Macromolecules 313 (2019) 520-526.

[41] X.F. Sun, B.C. Liu, Z.X. Jing, H.H. Wang, Preparation and adsorption property of xylan/poly(acrylic acid) magnetic nanocomposite hydrogel adsorbent, Carbohydrate Polymers. 118 (2015) 16-23.

[42] S. Mallakpour, F. Tabesh, Tragacanth gum-based hydrogel nanocomposites for the adsorption of methylene blue: Comparison of linear and non-linear forms of different adsorption isotherm and kinetics models, International Journal of Biological Macromolecules. 133 (2019) 754-766.

[43] H. Mittal, S.S. Ray, A study on the adsorption of methylene blue onto gum ghatti/TiO2 nanoparticles-based hydrogel nanocomposite, International Journal of Biological Macromolecules. 88 (2016) 66-80.

[44] H.Mittal, A.Maity, S.S.Ray, Synthesis of co-polymer-grafted gum karaya and silica hybrid organic–inorganic hydrogel nanocomposite for the highly effective removal of methylene blue, Chemical Engineering Journal. 279 (2015) 166-179.

[45] S. Pandey, J.Y. Do, J. Kim, M. Kang, Fast and highly efficient removal of dye from aqueous solution using natural locust bean gum based hydrogels as adsorbent, International Journal of Biological Macromolecules. 143 (2020) 60–75.

[46] S. Pandey, A comprehensive review on recent developments in bentonite based materials used as adsorbents for wastewater treatment, Journal of Molecular Liquids. 241 (2017) 1091–1113.

CHAPTER SIX

CONCLUSIONS AND RECOMMENDATIONS

6.1 CONCLUSIONS

This chapter focuses on the general discussion of the results obtained in this work and recommendations for future work regarding the synthesised hydrogel adsorbents. The overall aim of this work was to prepare a hydrogel nanocomposite with exceptional thermal and mechanical properties and high efficiency in removing methylene blue from aqueous solution. The choice of adsorbent material was guided by the fact that biopolymers are cost-effective, non-toxic, insensitive to dye contaminants, biodegradable, able to regenerate and have a high abundance of adsorptive functional groups. Cellulose derivative, carboxymethyl cellulose and sodium alginate offer high abundance in carboxylic and hydroxyl functional groups which are essential in MB dye removal. Acrylic acid (AA) also contains carboxylic functional groups and crosslinks with the biopolymers to create hydrophobic crosslinked 3D networks in the polymer matrix to produce porous hydrogels which are insoluble. This incorporation of AA improves the number of active sites and prevents the biopolymer-based adsorbents from dissolving in water. The incorporation of Fe_3O_4-C30B and ZnO NPs is to improve mechanical properties, thermal stability and the removal capacity.

Chapter one focuses primarily on the introduction of this work, the background of this study, and problem statement. The use of biopolymer hydrogels was briefly identified as the solution to the problem of pollution by organic dyes and the motivation was clearly stated with the aims and objectives of the study outlined. Chapter two covered literature review which was based on the background of water pollution, purification methods and brief discussion of hydrogels and their modifications. Furthermore, hydrogel nanocomposites with metal oxides were discussed in detail. Chapter three focused on the review of analytical techniques, in which structural, microscopic and spectroscopic techniques of characterising the CMC-cl-pAA/Fe_3O_4-C30B and SA/AA/ZnO HNCs and other prepared starting materials such as FTIR, XRD, TGA, DMA, SEM, TEM, and UV-vis were discussed.

The first approach was taken in Chapter four, where it focused on the discussion of the synthesis of carboxymethyl cellulose crosslinked with polyacrylic acid (CMC-cl-pAA) hydrogel modified with magnetic C30B nanocomposite hydrogel. The prepared composite was obtained via in situ free-radical polymerisation technique. The synthesised hydrogel nanocomposite was characterised. From the FTIR, the successful preparation of the hydrogel nanocomposite was confirmed through the presence of the Fe-O (528 cm^{-1}) and Si-O-Si (1080 cm^{-1}) stretches on the hydrogel matrix. The diffractogram from XRD revealed that the hydrogel nanocomposite was semi-crystalline. These results were also observed from the SAED images. Incorporation of magnetic C30B nanoparticles onto the CMC-cl-pAA hydrogel improved the mechanical and thermal stabilities of the adsorbent, enabling it to remove MB even in harsh conditions such as high temperatures. Through batch adsorption studies, the removal efficiency of CMC-cl-pAA/Fe_3O_4-C30B hydrogel nanocomposite for MB dye was investigated. It was observed that the removal efficiency greatly depended on the solution pH, adsorbent dose, time, temperature and dye concentration. The rate kinetics indicated pseudo-second-order rate mechanism was favoured. Further investigation of the mechanism of adsorption indicated a monolayer coverage of MB on the adsorbent surface and that CMC-cl-pAA/Fe_3O_4-C30B hydrogel nanocomposite was more efficient in removing MB from an aqueous solution than most reported hydrogel nanocomposites, including its CMC-cl-pAA hydrogel. Its maximum adsorption was 806.5 mg/g. Thermodynamics studies revealed that the reaction was, highly disordered, endothermic, yet spontaneous. The magnetic property of the hydrogel nanocomposite allowed easy recovery of the material through an external magnetic force.

Chapter 5 focuses on the synthesis of sodium alginate hydrogel crosslinked with acrylic acid (SA/pAA) and its modification with zinc oxide (ZnO) for the removal of methylene blue from aqueous solution. The hydrogel nanocomposite was synthesised via in situ polymerisation technique. All the prepared materials in this study were characterised using various analytical techniques. The successful incorporation of ZnO NP’s onto SA/pAA hydrogel matrix was confirmed structurally by the appearance of the Zn-O (500 cm^{-1}) stretch on the modified SA/AA spectrum. Analysis using the XRD revealed that the SA/AA hydrogel was amorphous, which agreed with the SEM results where it was

observed that the SA/AA has an irregular shape, indicating an amorphous material. The internal morphology of the prepared materials was studied using TEM, in which the tiny spherical ZnO NP's were observed on the surface of the irregular-shaped hydrogel matrix. The prepared hydrogel and its hydrogel nanocomposite were further used for removal of MB from aqueous solution. The experiment was performed in batch mode while investigating the effect of various parameters such as pH, time, solution concentration, dose and temperature. Just as obtained in the study of CMC-cl-pAA/Fe_3O_4-C30B hydrogel nanocomposite, adsorption of MB in this study was greatly influenced by the above-mentioned parameters. The kinetics studies revealed that the pseudo-second-order rate was favoured. The Langmuir isotherm mechanism of adsorption was favoured, indicating monolayer adsorption with removal capacities of 1129.0 and 1529.6 mg/g for SA/AA hydrogel and SA/AA/ZnO HNC, respectively. From these results, it could be concluded that SA/AA/ZnO HNC was a great adsorbent material for the removal of MB dye from aqueous solution. Also, SA/AA/ZnO HNC substantiated the spontaneous nature of the sorption process.

6.2 RECOMMENDATIONS FOR FUTURE WORK

This work was aimed at fabricating alternative highly adsorptive, cost-effective and stable hydrogel nanocomposite adsorbents based on CMC and SA incorporated with metal oxide nanoparticles for adsorption of methylene blue from aqueous solution. In future, Brunauer-Emmett-Teller will be important for use in determining the surface area of the synthesised materials. Furthermore, improvement in the method of synthesising the CMC-pAA hydrogel may be necessary to enhance its regeneration and reusability properties so that it sustains more adsorption cycles making it more cost-effective. More studies are needed to investigate the activity of the prepared nanocomposites towards anionic pollutants and metal ions for simultaneous removal. Even though C30B clay incorporation allowed easy dispersion of the magnetic NPs in the polymer matrix, its incorporation increased crosslinking density which reduced the removal efficiency in exchange for stability, which is a challenge considering the main aim is to be able to remove large amounts of MB from aqueous solution. Because the removal of MB was

done in the lab in batch mode, real-life application of the adsorbent materials using actual industrial effluents would provide come conclusive results on the actual adsorption capacity of the hydrogel nanocomposites. Furthermore, implementation of the CMC-cl-pAA/Fe_3O_4-C30B HNC and SA/AA/ZnO HNC for column studies which is a system that is being used in industries would be of great importance on the potential use of the adsorbents for up-scaled industrial application and therefore potential commercialisation. Nonetheless, the CMC-cl-pAA/Fe_3O_4-C30B and SA/AA/ZnO hydrogel nanocomposites could offer great potential in water treatment and environmental remediation in future.

SUPPORTING INFORMATION

THE SYNTHESIS OF CARBOXYMETHYL CELLULOSE CROSSLINKED WITH POLYACRYLIC ACID (CMC-cl-PAA) HYDROGEL MODIFIED WITH MAGNETIC C30B NANOCOMPOSITE AND ITS ADSORPTION EFFICIENCY TOWARDS MB

Adsorption isotherm studies

The Langmuir isotherm model is based on the monolayer adsorption of adsorbate and assumed that the adsorption takes place at the specific homogeneous adsorbent surface [1], and this is presented in Eq. (1):

$$q_e = \frac{q_m b C_e}{1+bC_e} \quad (1)$$

when linearised, Eq. (2) becomes:

$$\frac{C_e}{q_e} = \frac{1}{q_m b} + \frac{1}{q_m} C_e \quad (2)$$

where qm is the monolayer adsorption capacity per unit of adsorbent (mg/g), qe is the adsorption capacity at equilibrium (mg/g), and b relates the heat of adsorption (L/mg). Ce is the concentration of MB at equilibrium (mg/L). The essential feature of the Langmuir isotherm is known as separation factor (R_L), which can be expressed as the following (3):

$$R_L = \frac{1}{1+bC_o} \quad (3)$$

where R_L value reveals the shape and feasibility of the sorption isotherm. The adsorption isotherm can either be unfavorable ($R_L > 1$), linear ($R_L = 1$), irreversible ($R_L = 0$) or favorable ($0 < R_L < 1$).

The Freundlich isotherm model is valid for the multilayer adsorption of adsorbate at the heterogeneous adsorbent surface [2]. Furthermore, the adsorption capacity depends upon the concentration of adsorbate. The Freundlich isotherm is generally expressed by the following empirical Equation. (4):

$$\ln q_e = \ln K_f + \frac{1}{n} \ln C_e \quad (4)$$

The linear expression takes the following form Equation. (5):

$$q_e = K_f C_e^{\frac{1}{n}} \quad (5)$$

where K_F is the Freundlich equilibrium constant (mg/g(L/mg)$^{1/n}$), C_e is the equilibrium concentration (mg/L), and the parameter 1/n is the adsorption heterogeneity constant (varies with the nature of the adsorbent/adsorbate system) and q_e is the amount of adsorbate adsorbed per unit adsorbent at equilibrium (mg/g).

The Temkin isotherm model considers adsorbate-adsorbate interactions on the adsorbent surface [3]. This model also suggests that the heat of adsorption decreases linearly with the increase in adsorption quantity. The model is provided by Eq. (6-8) as follows:

$$q_e = \frac{RT\ln A_T}{b_T} + \frac{RT}{b}\ln C_e \quad (6)$$

$$b = \frac{RT}{b_T} \quad (7)$$

$$q_e = \beta \ln A_T + \beta \ln C_e \quad (8)$$

where b_T is Temkin isotherm constant, A_T is the Temkin isotherm equilibrium binding constant (L/g), β is constant related to the heat of adsorption (J/mol), R is the universal gas constant (8.314 J/mol/K) and T is the temperature at (273.15 K).

Thermodynamics studies

Thermodynamics parameters such as the change in the Gibbs free energy (ΔG°: kJ/mol), enthalpy (ΔH°: kJ/mol), and entropy ΔS°: J/mol K) can be investigated and determined using the Eq. (9 and 10) below;

$$(\Delta G^\circ = \Delta H^\circ - T\Delta S \quad (9)$$

$$ln\left(\frac{q_e}{C_e}\right) = \left(\frac{\Delta S^\circ}{R}\right) - \left(\frac{\Delta H^\circ}{RT}\right) \quad (10)$$

Where, q_e (mg/g) is the amount of dye adsorbed at equilibrium, and C_e (mg/L) is the concentration of dye at equilibrium, R (8.314 kJ/mol/K) is the universal gas constant. From the plot of ln (q_e/Ce) versus 1/T, the data was fitted on equations 12 and 13. When ∆H°(kJ/mol) is negative the reaction is exothermic, negative $\Delta S°$ (kJ/mol/K) indicates less disorder, and a negative $\Delta G°$ indicates a spontaneous reaction. The opposite. In contrast, when ∆H°(kJ/mol) is positive the reaction is endothermic, positive $\Delta S°$ (kJ/mol/K) indicates more disordered reaction, and a positive $\Delta G°$ indicates a non-spontaneous reaction [4-6]. When $\Delta G°$ ranges between -20 and -80 kJ/mol physisorption are taking place, and when ($\Delta G°$ is between -80 and -400 kJ/mol chemisorption is taking place [7].

References

1. Langmuir, I. (1918). The adsorption of gases on plane surfaces of glass, mica and platinum. Journal of the American Chemical Society, 40, 1361-1403.
2. Freundlich, H.M.F. (1906). Uber die adsorption in losungen. International Journal of Research in Physical Chemistry & Chemical Physics, 57, 385-470.
3. Temkin, M.I. (1941). Adsorption equilibrium and process kinetics on non homogenous surface with interaction between adsorbed molecules. Zhurnal Fizicheskoi Khimii, 15, 296-332.
4. Song, W., Gao, B., Xu, X., Xing, L., Han, S., Dua, P., Song, W., & Jia, R. (2016). Adsorption–desorption behaviour of magnetic amine/Fe3O4 functionalized biopolymer resin towards anionic dyes from wastewater. Bioresource Technology, 210,123–130.
5. Melo, B. C., Paulino, F. A. A., Cardoso, V. A., Pereira, A. G. B., Fajardo, A. R., & Rodrigues, F. H. A. (2018). Cellulose Nano whiskers improve the methylene blue adsorption capacity of chitosan-g-poly (acrylic acid) hydrogel. Carbohydrate Polymers, 181, 358–367.
6. https:www.learner.org/courses/chemistry/text/text.html?dis=U&num=Ym5WdEIURS9NQ289&sec=YzjWakIUQS9OU289

7. Mahmoodi, N. M., Hayati, B., & Arami, M. (2012). Kinetic, equilibrium and thermodynamic studies of ternary system dye removal using a biopolymer. Industrial Crops and Products, 35(1), 295–301.

SUPPORTING INFORMATION

THE SYNTHESIS OF SODIUM ALGINATE HYDROGEL CROSSLINKED WITH ACRYLIC ACID (SA/PAA) AND ITS MODIFICATION WITH ZINC OXIDE (ZnO) FOR THE REMOVAL OF ORGANIC DYES FROM AQUEOUS SOLUTION.

S1: Results

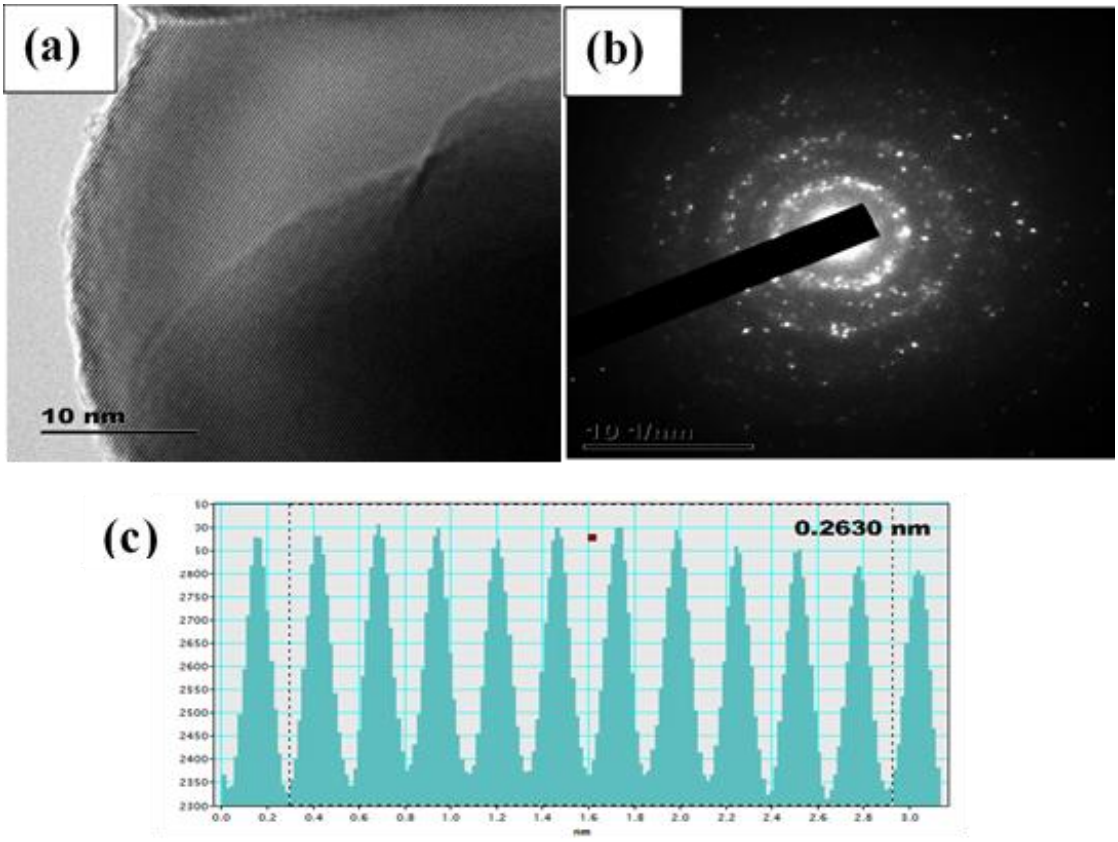

Figure S. 1: HRTEM micrograph of ZnO NPs (a); selected area electron diffraction pattern (SAED) of ZnO NPs; and the corresponding SAED diffraction intensity profile (c).

Figure: S2

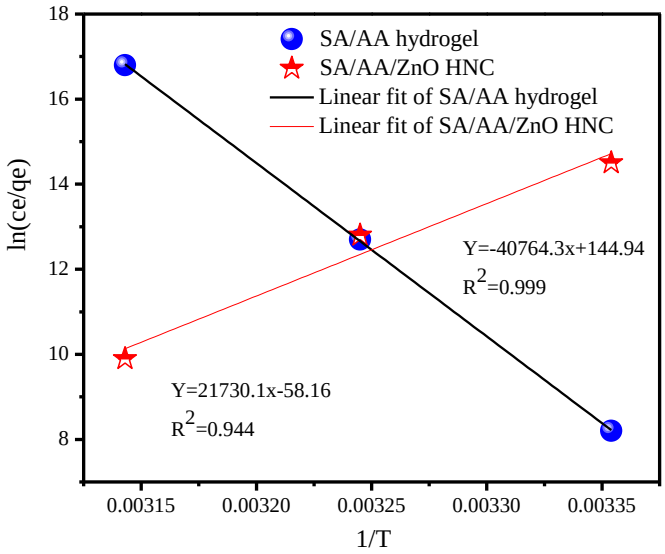

Figure S. 2: Thermodynamic graph between ln(qe/ce) vs 1/T.

Table S. 1: Elemental analysis of SA/AA/ZnO HNC

Element Line	Weight %	Weight % Error	Atom %	Atom % Error
C K	68.27	± 0.29	80.01	± 0.34
O K	18.74	± 0.23	16.49	± 0.20
Al K	0.51	± 0.03	0.26	± 0.02
S K	2.45	± 0.05	1.07	± 0.02
S L	---	---	---	---
Zn K	10.03	± 0.46	2.16	± 0.10
Zn L	---	---	---	---
Total	100.00		100.00	

Adsorption kinetics studies

The kinetic models present the relationship between amounts of dye adsorbed as a function of contact time. Several kinetic models such as pseudo-first-order [1], pseudo-second-order [2,3] and intra-particle diffusion [4] models were introduced to fit the experimental data points. The linear form of pseudo-first-order [1], pseudo-second-order [2,3], and intra-particle diffusion [4] kinetic models are given by the following Eqs.:

$$\ln(q_e - q_t) = \ln q_e - K_1 t \quad \text{(S1)}$$

$$\frac{t}{q_t} = \frac{1}{k' q_e^2} + \frac{t}{q_e} \quad \text{(S2)}$$

$$q_t = k_i t^{0.5} + C \quad \text{(S3)}$$

where qe, qt and t are adsorption capacity at equilibrium (mg/g), the amount adsorbed at defined contact time (mg/g) and the contact time (min), respectively. K_1 denotes the rate constant of the pseudo-first-order (min^{-1}), K_2 is the rate constant of the pseudo-second-order (g mg/min^{-1}) K_i is the intra-particle diffusion rate constant (mg/g $min^{-0.5}$) and C is a constant related to the extent of the boundary layer effect.

Adsorption isotherm studies

The Langmuir isotherm model is based on the monolayer adsorption of adsorbate and assumed that the adsorption takes place at the specific homogeneous adsorbent surface [5], and this is presented in Eq. (S4):

$$q_e = \frac{q_m b C_e}{1 + b C_e} \quad \text{(S4)}$$

when linearized, Eq. (S5) becomes:

$$\frac{C_e}{q_e} = \frac{1}{q_m b} + \frac{1}{q_m} C_e \quad \text{(S5)}$$

where qm is the monolayer adsorption capacity per unit of adsorbent (mg/g), qe is the adsorption capacity at equilibrium (mg/g), and b relates the heat of adsorption (L/mg). Ce is the concentration of MB at equilibrium (mg/L). The essential feature of the

Langmuir isotherm is known as separation factor (R_L), which can be expressed as the following (S6):

$$R_L = \frac{1}{1+bC_o} \quad \text{(S6)}$$

where R_L value reveals the shape and feasibility of the sorption isotherm. The adsorption isotherm can either be unfavorable ($R_L > 1$), linear ($R_L = 1$), irreversible ($R_L = 0$) or favorable ($0 < R_L < 1$).

The Freundlich isotherm model is valid for the multilayer adsorption of adsorbate at the heterogeneous adsorbent surface [6]. Furthermore, the adsorption capacity depends upon the concentration of adsorbate. The Freundlich isotherm is generally expressed by the following empirical Eq. (S7):

$$\ln q_e = \ln K_f + \frac{1}{n}\ln C_e \quad \text{(S7)}$$

The linear expression takes the following from Eq. (S8):

$$q_e = K_f C_e^{\frac{1}{n}} \quad \text{(S8)}$$

where K_F is the Freundlich equilibrium constant ($mg/g(L/mg)^{1/n}$), C_e is the equilibrium concentration (mg/L), and the parameter 1/n is the adsorption heterogeneity constant (varies with the nature of the adsorbent/adsorbate system) and q_e is the amount of adsorbate adsorbed per unit adsorbent at equilibrium (mg/g).

The Temkin isotherm model considers adsorbate-adsorbate interactions on the adsorbent surface [7]. This model also suggests that the heat of adsorption decreases linearly with the increase in adsorption quantity. The model is provided by Eq. (S9-S11) as follows:

$$q_e = \frac{RT\ln A_T}{b_T} + \frac{RT}{b}\ln C_e \quad \text{(S9)}$$

$$b = \frac{RT}{b_T} \quad \text{(S10)}$$

$$q_e = \beta \ln A_T + \beta \ln C_e \quad \text{(S11)}$$

where b_T is Temkin isotherm constant, A_T is the Temkin isotherm equilibrium binding constant (L/g), β is constant related to the heat of adsorption (J/mol), R is the universal gas constant (8.314 J/mol/K) and T is the temperature at (273.15 K).

References

1. S. Lagergren, About the theory of so-called adsorption of soluble substances, Kungliga Svenska Vetenskapsakademiens Handlingar. 24 (1898) 1-39.
2. S.Y. Ho, G. McKay, Sorption of dye from aqueous solution by peat, Chemical Engineering Journal. 70 (1998) 115-124.
3. S.Y. Ho, G. McKay, Pseudo-second order model for sorption processes, Process Biochemistry. 34 (1999) 451–465.
4. W.J. Weber, J.C. Morris, Kinetics of adsorption on carbon from solution, Journal of the Sanitary Engineering Division. 89(1963) 31-60.
5. I. Langmuir, The adsorption of gases on plane surfaces of glass, mica and platinum, Journal of the American Chemical Society 40 (1918) 1361-1403.
6. H.M.F. Freundlich, Uber die adsorption in losungen, International Journal of Research in Physical Chemistry & Chemical Physics 57 (1906) 385-470.
7. M.I. Temkin, Adsorption equilibrium and process kinetics on nonhomogenous surface with interaction between adsorbed molecules, Zhurnal Fizicheskoi Khimii 15 (1941) 296-332.

APPENDIX 1

Help Sitemap

Logged in as modibane84 [Logout]

You can:
Submit and track articles
Update your profile
Change your password

INDERSCIENCE PUBLISHERS
Linking academia, business and industry through research

Home For Authors For Librarians Orders Inderscience *Online*
News

OSPEERS > User > Author > Your Submissions > New Submission
SubmissionID: IJW-275468

Information

Dear Kwena Desmond Modibane,

You have successfully submitted your article "*REMOVAL OF METHYLENE BLUE FROM WASTEWATER USING HYDROGEL NANOCOMPOSITES: A REVIEW*" for the International Journal of Water.
Your submission code is **IJW-276488**
Please use this code when you contact us regarding your submission.

Your article is now being put in the **Screening Process**. You will receive an automatic "Submission Acknowledgement" email within the next two weeks stating when your article has successfully been screened and queued to be peer-reviewed. **If your article is found unsuitable** by our Screening Process, it will be automatically removed and you may **not** receive any submission acknowledgement from us. If your article is withdrawn or rejected, any author copyright agreement(s) will be destroyed.

FAQs

- **How long will take to review my article?**
  This depends on the journal. Please contact the journal editor for more precise information. However, if you haven't received any communication from the editor after six months of submission, you can contact us at submissions@inderscience.com

- **What happens during the Screening Process?**
  All new submissions are screened by the staff at the Editorial Office to filter out incomplete articles and unsuitable or malicious information. It also removes authors' identifications found in submissions, to preserve the blind peer-review policy. Our staff verifies the details of your nominated experts (if required). The Screening Process also removes or flags duplicate submissions. Your manuscript will automatically be

removed if it is found to be a malicious or below standards submission. In this case you will not receive any acknowledgment from the Editorial Office.

- **How I can know if my article is being reviewed?**
  You can monitor the review progress of your submission by periodically logging in to http://www.inderscience.com and from **http://www.indersolenoe.com/ospeers/admin/user** following the menu links:
  Author -> Track -> View Review Progress
  The editor will notify you by email when the first round of review has been completed.

- **If I don't receive email messages from the Editor, can I assume that nothing is happening?**
  No. Because there are chances that our emails never arrive to you due anti-spam protections, we strongly advise you to log in to http://www.inderscience.com at least once a week and from *Author -> Track -> View Review Progress* find and click the "Editor/Author Comments" link to see if there is a new message for you from the editor.

- **Do I have to pay to publish my article, once accepted?**
  NO. There are no charges for publishing with Inderscience, UNLESS you clearly require us to make your article an Open Access (OA) article. If you receive an email requesting payment in relation to your article (for example for editing or reviewing services), then you should ignore and delete the email; it is not a legitimate Inderscience email. If you are unsure, you can check with us at: editor@inderscience.com. If you are considering publishing an Open Access article with us, remember that we will never request payment before your paper has been accepted. OA requests and payment are handled only by the Editorial Office of Inderscience and not by anyone else.

We thank you for submitting your article and for your interest in the International Journal of Water (IJW).

Help is available by email at submissions@inderscience.com.

Sign Out